AN OPTICAL ALIGNMENT TRANSFER SYSTEM

FOR TRACKING DIM TARGETS

by

Robert Lawrence Gilgen

Submitted to the
DEPARTMENT OF ELECTRICAL ENGINEERING AND COMPUTER SCIENCE
in Partial Fulfillment of the Requirements for the Degrees of

BACHELOR OF SCIENCE

and

MASTER OF SCIENCE

at the

MASSACHUSETTS INSTITUTE OF TECHNOLOGY

June, 1987

Signature of Author:_____

Department of Electrical Engineering
and Computer Science, June, 1987

Certified by:_____

Jeffrey H. Lang
Thesis Supervisor

Approved by:_____

Peter A. Welling
Technical Supervisor,
The Charles Stark Draper Laboratory, Inc.

Accepted by:_____

Arthur C. Smith, Chairman,
Departmental Committee on Graduate Students

AN OPTICAL ALIGNMENT TRANSFER SYSTEM
FOR TRACKING DIM TARGETS

by
Robert L. Gilgen

Submitted to the Department of Electrical Engineering and Computer Science in June, 1987 in partial fulfillment of the requirements for the Degrees of Master of Science and Bachelor of Science in Electrical Engineering and Computer Science.

ABSTRACT

This thesis studies the problem of aligning an optical signal laser with a dim target. Of particular interest is the problem of tracking the target in the presence of disturbances of the structure which supports the sensor. The need for an inertial reference to measure sensor structure vibrations and to track the target line-of-sight for signal point ahead angle calculations are discussed. A pseudo star is selected as the appropriate inertial reference.

Two methods of implementing a pseudo star in a tracker are presented, and first-pass designs of the optics for both methods are discussed; target motion is limited to the horizontal plane in both designs. The indirect projection method projects the pseudo star through the tracking telescope front aperture via an extended corner cube. Because the pseudo star and target image follow the same optical path to the sensor, nulling the pseudo star on the sensor has the effect of nulling the disturbances which affect the target image. The direct projection method projects the pseudo star directly onto the sensor platform. Vibrational disturbances are measured by pseudo star displacement on the sensor, and then subtracted from the target image. Because of a large aperture size mismatch and a heat dissapation problem with the indirect projection method, the direct projection method is selected as the better of the two designs.

A simplified laboratory experiment is constructed to demonstrate the direct projection method. Despite simplification, the experiment exhibits the significant features of an optical tracker. The simplified tracker dynamics are decoupled into three independent control loops by the appropriate choice of actuator pointing errors, and a tracking controller is designed. The controller is implemented in a microprocessor.

Five experiments are run on the laboratory system. The first three test the individual control loops. The characteristics of each loop are nearly identical to those expected from their designs. The fourth experiment closes all three loops together; the tracker remains stable and a tracking error as low as ± 7 μrad is recorded. The last experiment measures the response with three loops closed to a step in target position. Here loop cross coupling, probably due to sensor non-linearities, is seen to lower the relative stability of the system.

Thesis Supervisor: Jeffrey H. Lang
Title: Associate Professor of Electrical Engineering

ACKNOWLEGEMENTS

I would like to thank Bill Johnson, my project supervisor at The Charles Stark Draper Laboratory, for finding this project for me and for his enthusiastic support of my work. I also thank Professor Jeff Lang, my thesis advisor at MIT, for patiently reading this thesis, and Pete Welling, my advisor at Draper, for sharing his circuit design and writing skills with me.

I thank Bob Zak, without whose software support the laboratory experiment would never have taken place, and Mike Luniewicz, for his encouragement, advice, and insight. And I thank Dianne Silva for her endless encouragement and her refusal to take me seriously. I am especially grateful to Kelly Riordan for her help in preparing the figures in this thesis, and for being there when I needed her.

This research was done at The Charles Stark Draper Laboratory, Inc. under IR&D #18262

TABLE OF CONTENTS

LIST OF FIGURES

List of Figures

List of Figures

List of Figures

List of Figures

INTRODUCTION

Applications are now evolving in which a large telescope and its associated optics are required to track a dim target and to point a communication beam at that target. This tracking and pointing must be accomplished in spite of vibrational disturbances which may be present on the telescope. To achieve this tracking and pointing, the angle of the target must first be measured in inertial space, and this angle must next be transferred to, and maintained by, the telescope. An inertial reference unit (IRU) can provide a reference for measuring the angle of the target over time with respect to inertial space, and for measuring the telescope disturbances. Since the angle of the target is measured by an optical sensor, a convenient output for the IRU would be an optical beam whose angular position in inertial space is accurately known. The optical signals from the target and from the IRU must be used within an optical alignment transfer system, which utilizes optics and a closed loop electrical controller to measure the position of the target with respect to the output of the IRU. These signals must allow the system to maintain the target in the telescope field of view, and to compensate for mechanical disturbances. This thesis examines such an alignment transfer system, both theoretically and experimentally.

The design of the optical alignment transfer system depends on the characteristics of the telescope and of the IRU. The telescope must be large enough to collect sufficient light from a dim target. An aperture at the primary of 5 meters is assumed in this thesis. This thesis also assumes the availability of an inertially stabilized IRU capable of maintaining an orientation in inertial space with the accuracy to which the target angular position must be known. The IRU must also be capable

of slewing, upon electrical command, to a different orientation while maintaining accuracy throughout the slew. In addition to the assumptions made about the telescope and IRU, it is assumed in this thesis that some means for measuring the range from the telescope to the target is available. The target range is necessary if the communication beam is to lead the target properly.

As discussed above, this thesis investigates the design of an optical alignment transfer system. To begin, two candidate systems are outlined, and their relative strengths and weaknesses are discussed. These two systems differ only in how the optical inertial reference, or pseudo star, reaches the platform which holds the optical sensor. In one of the systems, the pseudo star is projected onto the sensor platform through the front aperture of the telescope, and the other sytem projects the pseudo star directly onto the sensor platform. In order to make a relative comparison managable, the systems are to track target motions and reject mechanical disturbances only in the horizontal plane. One of these systems, the system using the direct pseudo star projection method, is then selected for an experimental study.

The experimental study is based on a scaled alignment transfer experiment (SATE). The SATE is designed using laboratory optics and mounted on an optical bench. The issue of directing a communication beam to the target is not explicitly addressed in this experiment. Rather, the focus is on the tracking aspects of the system. Alignment lasers are used to represent the target, the optical inertial reference, and another optical alignment signal. The signals from these sources are focussed on an optical sensor with an array of 32x32 pixels, and appear on the sensor as spots. The sensor is sampled at 1100 samples per second, and the target spot is integrated over 109 samples to provide time for a dim target to be sensed. The three outputs of the optical sensor are combined within a digital controller. The controller drives three actuators, two of which are implemented with electronically movable mirrors, and one which is a movable telescope, to align the spots as desired. The control loops are simultaneously closed, and the positions of the alignment spots

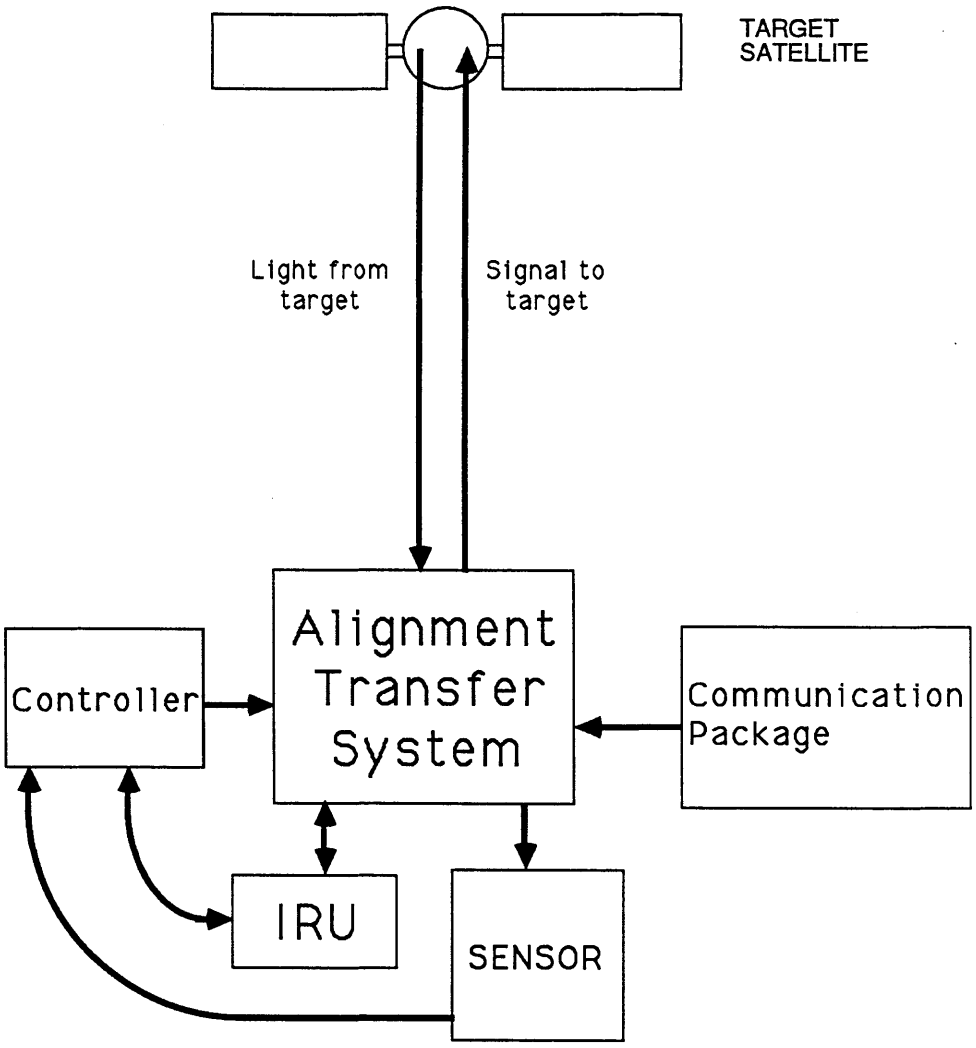

Figure 0.0.0-1 Functional Schematic of An Optical Alignment Transfer System

positions are measured, allowing the system to be characterized. Limitations associated with the sensor, the actuators, and the laboratory environment are also explored. It is shown that the direct projection method can track a target very accurately. A minimum tracking error of ±7 μrad is calculated for the system tracking a stationary target. However, the system is also shown to be very sensitive to sensor non-linearities and modelling errors.

The need for an inertial reference mentioned above, and the use of a pseudo star as an optical inertial reference are discussed in Chapter 1. Also in the first chapter, the optical paths for a tracker which projects the pseudo star onto the sensor platform through the front aperture of the tracking telescope is designed. After the first tracker topology is designed, a second tracker is designed which projects the pseudo star directly onto the sensor platform. Finally, the two pseudo star projection methods are compared, and one of the systems, the system utilizing the direct pseudo star projection method, is chosen to be scaled and simplified so that it can be tested in the laboratory.

In Chapter 2, the optical paths of the system using the direct projection method are simplified and scaled to permit the construction of a laboratory tracker. Here, the pointing function of the system is dropped in favor of concentrating on the tracking functions of the system. Dynamic models for the actuators which are used in the experimental tracker are developed, and the magnification factor of the telescope and the sensor gain are characterized. Finally, a controller is designed which will allow the system to track targets moving in the horizontal plane. The controller is to have good low frequency tracking characteristics and good stability robustness properties. It must also be kept simple so that it can be run at a fast speed on a microprocessor, and it must be robust to the finite word lengths to which it will be limited by the processor.

In Chapter 3, laboratory experiments and their results are presented. These experiments characterize the bandwidth and relative stability of the three control loops individually and simultaneously. A

lower bound on the scaled system tracking error and the effects of sensor non-linearities and other parameters which are poorly modelled are investigated. Finally, suggestions for further experiments on the scaled system are suggested, which would test the disturbance rejection properties of the tracker. These experiments are primarily concerned with measuring the disturbance rejection properties of the system, which could not be tested in this thesis due to hardware constraints, and with attempting to linearize the sensor with a lookup table.

Chapter 4 contains a summary of the results of the experiments, conclusions, and suggestions for further research.

Chapter 1
ANALYSIS OF THE PSEUDO STAR

1.0 INTRODUCTION

Designing a space-based optical tracker which is to track a dim target is a very complex task. A single thesis could not hope to address all of the issues posed by such a design problem. However, this chapter presents a first-pass at a design which will track a dim optical target and allow a communications beam to be aligned with the target.

This chapter begins by describing the need for an inertial reference in a tracking system, and how an optical inertial reference, or pseudo star, is particularly suited to an optical tracker. After the pseudo star concept is introduced, two methods of using a pseudo star in an optical tracker are discussed, and a first-pass design for each of the methods is made. Finally, the two trackers are compared, and one of the systems is chosen for a scaled laboratory experiment which is intended to prove the concept.

1.1 THE PSEUDO STAR CONCEPT

1.1.0 Introduction

There are many reasons why a precision pointing and tracking system requires an inertial reference. The uses of an inertial reference range from locating a target acquisition window, to handing over target position information to other systems, to making measurements necessary to point the signal laser in the right direction. In addition, an inertial reference can be used to measure sensor platform disturbances which may

interfere with target position measurements.

Section 1.1.1 explains how an inertial reference can be used to stabilize the image of a target on the sensor when the sensor platform is subject to disturbances. Section 1.1.2 explains why it is necessary to track the line of sight (LOS) to the target, and why the inertial rate of the LOS must be measured. Finally, the advantages of implementing the inertial reference as an optical pseudo star are discussed in Section 1.1.3.

1.1.1 Stabilizing the Target Spot

The objective of the tracking and pointing system which is to be designed is to track a target with a high degree of precision and place a communications beam on it. Since structural vibrational disturbances will exist within the system, these disturbances will have to be filtered out of the target position measurements. The easiest way to realize this filtering process is by including steering mirrors in the optical paths which can compensate for the vibrational disturbances.

If the target were very bright, compensating for the vibrational disturbances would be relatively easy. The vibrations which are expected in the system will be in the range of 0.1 Hz to 100 Hz. To compensate for these disturbances by using target image motion as a measurement of the disturbances, the target image position on the mosaic array sensor would have to be measured at a sampling rate of over 2000 samples per second. This fast sampling rate would not be a problem if the target were very bright because the sampling period would be long compared with the average photon arrival rate. However, the position of a dim target measured at this fast sampling rate might not be measured accurately because the sampling period would be short compared with the average photon arrival rate. This measurement degradation occurs because photons in a spot have an arrival radius (distance from the center of the spot) which is a random process with approximately Gaussian distribution, and the angular position

of these arrivals is a uniformly distributed random process. Averaged over a large number of arrivals, the expected value of the radial distance of the center of mass of the arrivals will be close to the actual center of the spot. The fewer the number of arrivals used in calculating the center of mass, the less accurately the center of the spot can be calculated. This can be seen more clearly in an example.

Figures 1.1.1-1 and 1.1.1-2 show photon arrival distributions for a circular gaussian spot with unit radius where the radius is defined to be one standard deviation of the Gaussian from the center of the spot. Figure 1.1.1-1 shows the case where the accumulation time is significantly longer than the average time between photon arrivals. The window in the upper right of the figure shows the distribution of the distance of photon arrivals from the actual center of the spot. The gaussian nature of this distribution can easily be recognized. With 1200 photon arrivals, the center of mass, or centroid location, is calculated to be (-0.006063,0.017350), where the center of the spot is at (0.0,0.0). The radial error of the calculated centroid is 1.84% of one standard deviation of the Gaussian distribution.

The accumulation time is much shorter in Figure 1.1.1-2, where only 10 photon arrivals occur during the sample period. The distribution graph shows little resemblance to the gaussian nature of the actual stochastic distribution of the photon arrivals. The centroid location is calculated to be (0.228592,0.160019), where the center of the spot is once again (0.0,0.0). Here the error is 27.9% of the radius of the spot. In short, to get an accurate distribution of photons in the target spot, the photons must be accumulated over a time period which is long compared with the average time between photon arrivals. The stochastic problem of calculating the centroid of a dim spot with a perfect sensor is addressed on Appendix A.

For a dim target then, it may be necessary to slow down the sampling rate to as low as 50 to 100 samples per second. With a sampling rate this slow, it would be impossible to filter out the low intensity

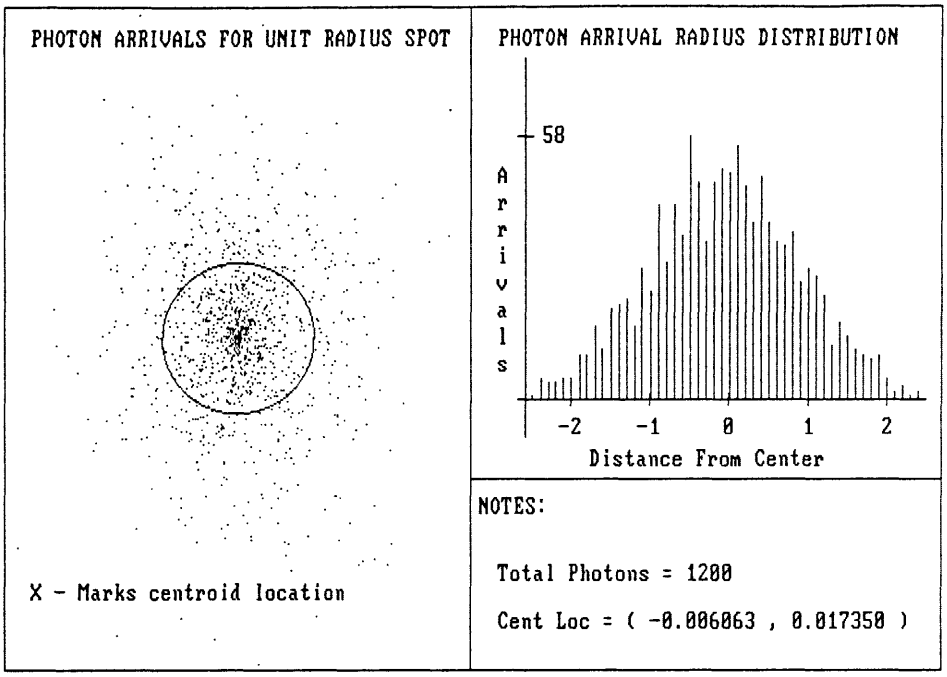

Figure 1.1.1-1 Photon Distribution of Gaussian Spot With 1200 Photon Arrivals

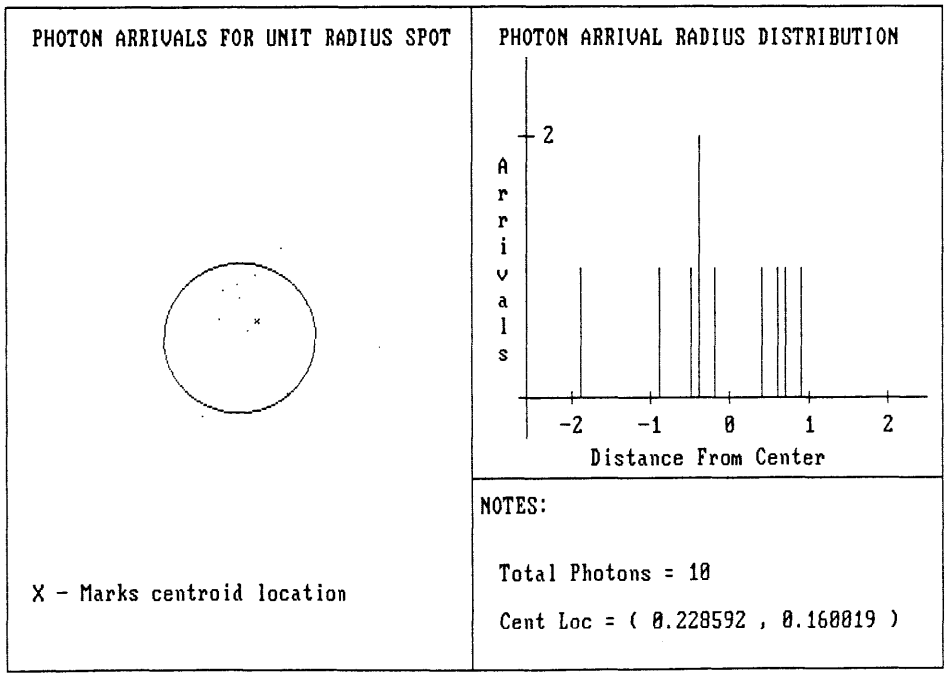

Figure 1.1.1-2 Photon Distribution of Gaussian Spot With 10 Photon Arrivals

target spot will not allow a sampling rate high enough the vibration noise, which has a spectrum from 0.1 Hz to 100 Hz. Since to filter out the vibration noise, another method must be found.

In order to filter the vibration disturbance from the image of the target it is necessary to measure the disturbance at high sampling rates. Doing this optically necessitates using a light source which is isolated from the vibrational disturbances on the satellite. The vibrations will cause a relative angular displacement of the reference beam which can be measured on the optical sensor. If a steering mirror is placed in the path of the target spot, the vibrational disturbance could be subtracted from the target image.

An example of a suitable inertial reference is a star. Since the star is "fixed" in inertial space, it will maintain a fixed direction from the tracker even with the presence of structural vibration disturbances on the satellite. If light from the star could be made to fall on the sensor, then the disturbance angle could be measured, and the steering mirror could subtract the disturbance from the target spot. Better yet, if the star could enter the tracking telescope with the target, and itself be steered by the steering mirror, then a feedback loop could be closed around the steering mirror using the position of the star on the sensor as feedback. As long as the position of the star is kept centered, the effect of the disturbance has been successfully subtracted from the image of the star and of the target.

Although a star is an ideal inertial reference, it is not ideally suited to the task at hand. First, not all stars have the ideal brightness for tracking. If the chosen reference star is too dim, the same measurement rate restrictions apply to the reference as to the target, and the reference has not helped the disturbance problem. If the star is too bright, back scattering in the sensor can cause inaccurate measurements of the position of the star, and increase the stray light noise level on the sensor. Second, because there are not very many stars which meet the intensity criterion, there may not be a reference star close enough to the target to place it in the field of view of the

tracker. Consequently, to measure vibration disturbances on the satellite, some form of artificial inertial reference, a pseudo star, will be needed.

1.1.2 Tracking the Target Line Of Sight

An inertial reference has another very important function besides providing a reference for vibration noise rejection. This is to track the line of sight (LOS) to the target. If a laser is to be pointed at the target, the tracker must know the angle to the target. This can be accomplished by using the measurements of the target position made by the optical sensor. However, because of the finite speed of light, there is a delay between the time when light is emitted by the target and the time the sensor receives the light. There is also a finite delay between the time when light is emitted by the signal laser and the time when the target receives the signal. During this time, of course, the target may be moving. So, some algorithm is required to point the signal laser ahead of the LOS so that the light will reach the target at an advanced position. The reason that an inertial reference is needed to calculate the point ahead angle can best be explained by an example.

Assume that the tracking satellite is moving crossrange at velocity v_{targ} as shown in Figure 1.1.2-1. For small angles, the range to the target will remain constant, and will be x_{targ}, which will be measured by some other system. We can define the time for light emitted by the target to reach the tracker as

$$T_D = x_{targ}/c \qquad (1.1.2\text{-}1)$$

where c is the speed of light.

At time t=0, the target is located at position 0 in the figure. At this time, light is emitted by the target, and begins to travel toward the tracker.

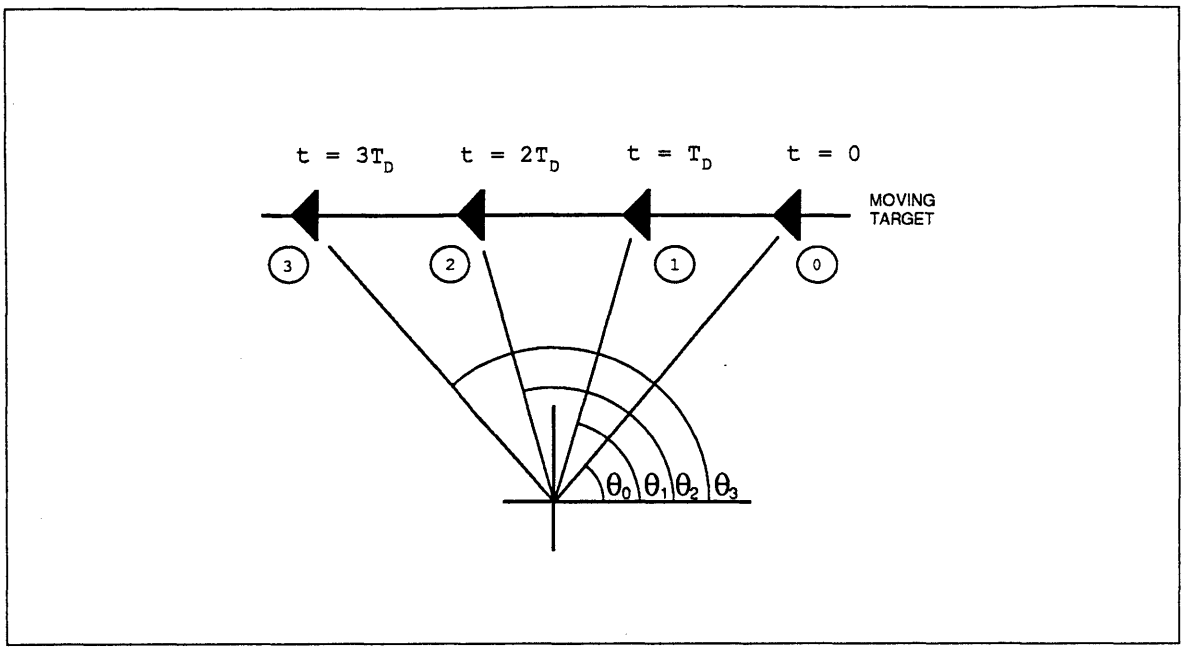

Figure 1.1.2-1 Target Line of Sight at Discrete Time Intervals

At time $t=T_D$, the target has moved to position 1 in the figure. Now, the light which left the target at t=0 reaches the tracker, which measures the LOS angle to be θ_0. Because only one LOS measurement has been taken, the target velocity cannot yet be estimated. As a result, the tracker does not yet have an estimate of where the target is at this time, nor where it will be at any future time.

At time $t=2T_D$, the target has moved to position 2 in the figure. Now light which left the target at time $t=T_D$ has reached the tracker, which again measures the LOS to the target, θ_1. Because the tracker now has two measurement points, a first order approximation can be made as to where the target is at the present time. The angular velocity can be estimated as

$$\frac{d\theta}{dt} \approx \frac{\theta_1 - \theta_0}{T_D} \qquad (1.1.2\text{-}2)$$

The actual present position of the target can be estimated as

$$\theta_2 = \theta_1 + (\theta_1 - \theta_0) \qquad (1.1.2\text{-}3)$$

If the motion is extrapolated one time delay further, the angle to the target at $t=3T_d$ can be estimated to be

$$\theta_3 = \theta_1 + 2(\theta_1 - \theta_0) \qquad (1.1.2\text{-}4)$$

If the signal is sent at $t=2T_D$ in the direction θ_3, it will travel the distance to the target in T_D seconds, and will reach position 3 in the figure just as the target reaches the same position.

In order to measure these angles properly, an inertial reference is needed. It is not good enough to measure the angles with respect to a local coordinate system fixed to the tracker, because the local coordinate system will in general be rotating. This means that measurements of the target position will be made in an accelerating frame. In order to measure the LOS and LOS rate, the acceleration of the sensor platform must be measured, thus requiring an inertial reference.

1.1.3 The Pseudo Star

As discussed above, a good reference for measuring disturbances would be a star. Its good qualities were that it was inertially stable, and its output was optical. A similar reference, a pseudo star, can be made by placing a laser on an inertially stabilized platform. The laser beam would be an optical reference to inertial space, as was the light from the star. Unlike the star reference, the brightness of the pseudo star can be controlled by changing the power to the laser or by including neutral density filters in the path of the pseudo star. Also, the IRU can be torqued to keep the pseudo star near the image of the target on the

sensor, so that the pseudo star is always visible to the sensor as the target is tracked.

At the present time, The Charles Stark Draper Laboratory is developing an Advanced Inertial Reference Unit (AIRU) [1][2] which will allow an optical payload to be mounted on its stable member. It also provides optical paths to the stable member from outside the case of the unit.

The pseudo star just described has met three requirements. First, it allows satellite vibration motion to be measured by providing an inertial reference to the tracker. Second, it can be torqued to track the target, thus allowing the target absolute LOS angle and LOS angular rate to be measured. Third, the output is optical, and the intensity of the output can be set at an optimal level. Unfortunately, there are several factors which may make this pseudo star difficult to implement.

The problem is that the laser is mounted on the stable member of the AIRU. In order to get power to the laser, large high voltage leads would have to be attached to the stable member. The large flexible leads would be fairly stiff, and would allow vibrations from the satellite to disturb the platform. If transformers were used to provide power to the stable member, then electromechanical coupling would allow external vibrations to affect the stable member. Also, modern lasers are very inefficient (about 5 watts of electrical power is required to get a 1 mW beam), which means that a large amount of heat would have to be removed from the stable platform. Since the stable member would be magnetically suspended in a vacuum to avoid frictional forces and to isolate the platform from disturbances, there would be no fluid to carry away heat by convection. Finally, in order to get a high quality pseudo star beam, a fairly large laser would be required. However it is desirable to have a small inertial reference unit so that power requirements are not too high, and weight is kept minimal. It would be nice if the laser on the AIRU could be replaced by a passive component such as a mirror.

An example will show the effect of replacing the pseudo star laser with a mirror. Figure 1.1.3-1 shows a laser mounted on a platform. The

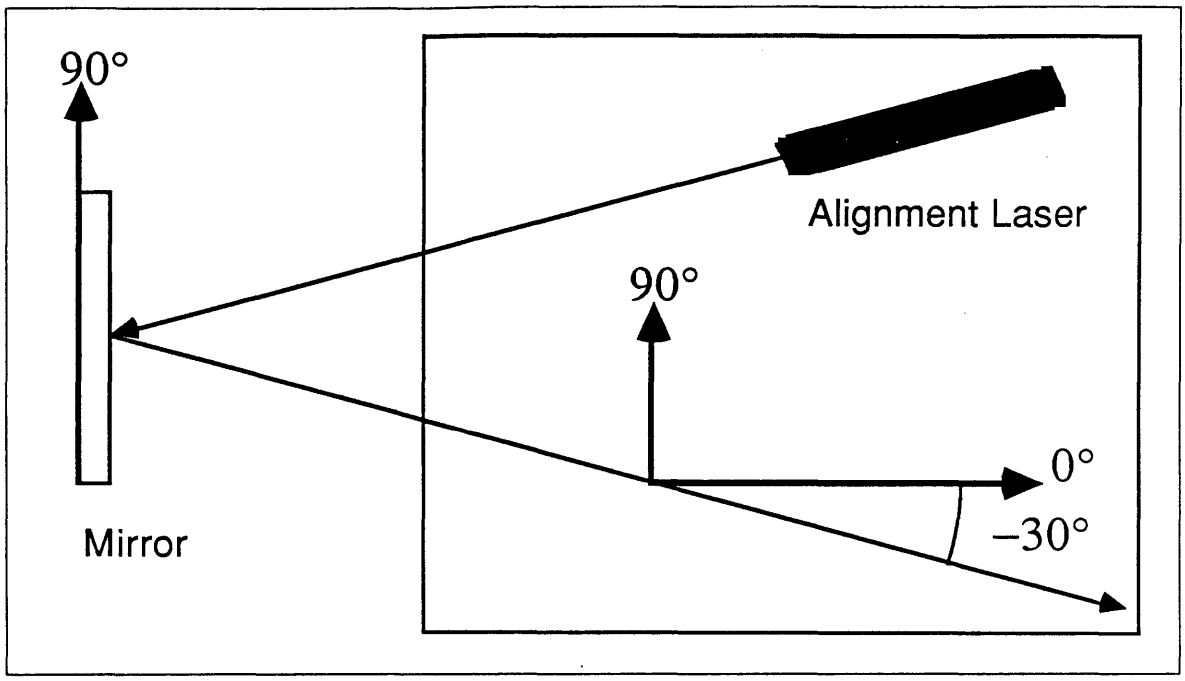

Figure 1.1.3-1 Laser Beam Return Angle for Undisturbed Platform

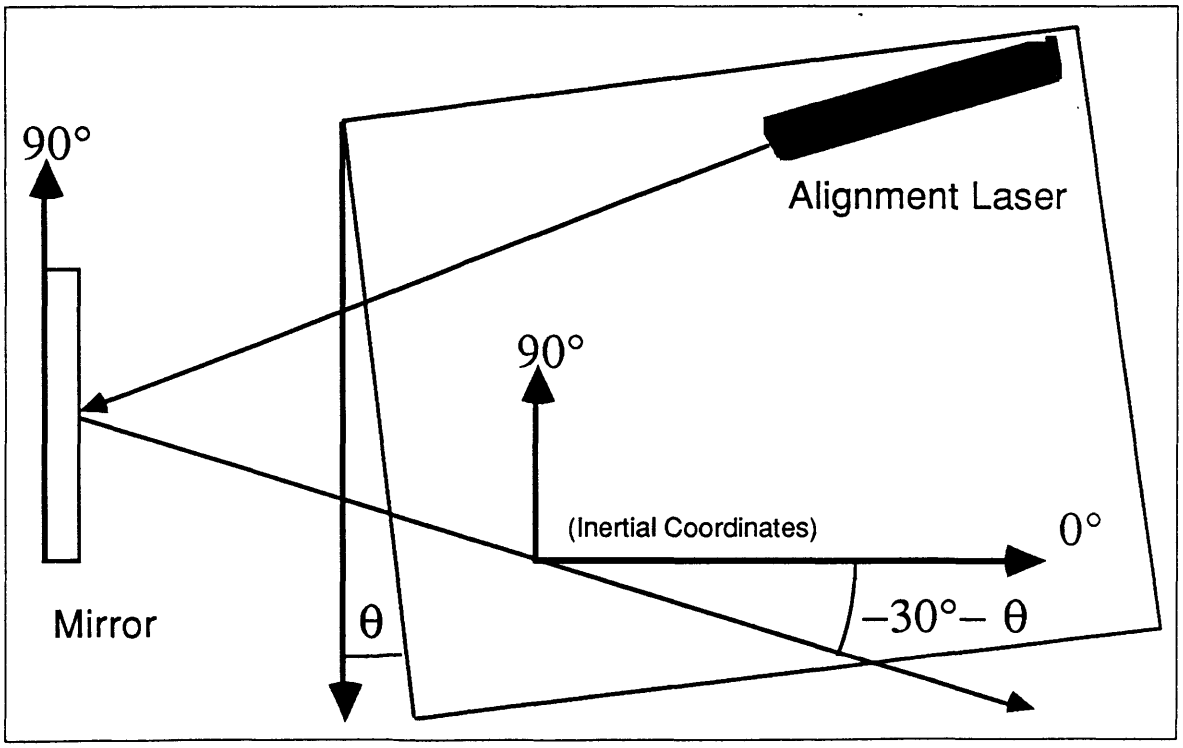

Figure 1.1.3-2 Laser Beam Return for Disturbed Platform (Inertial Coords)

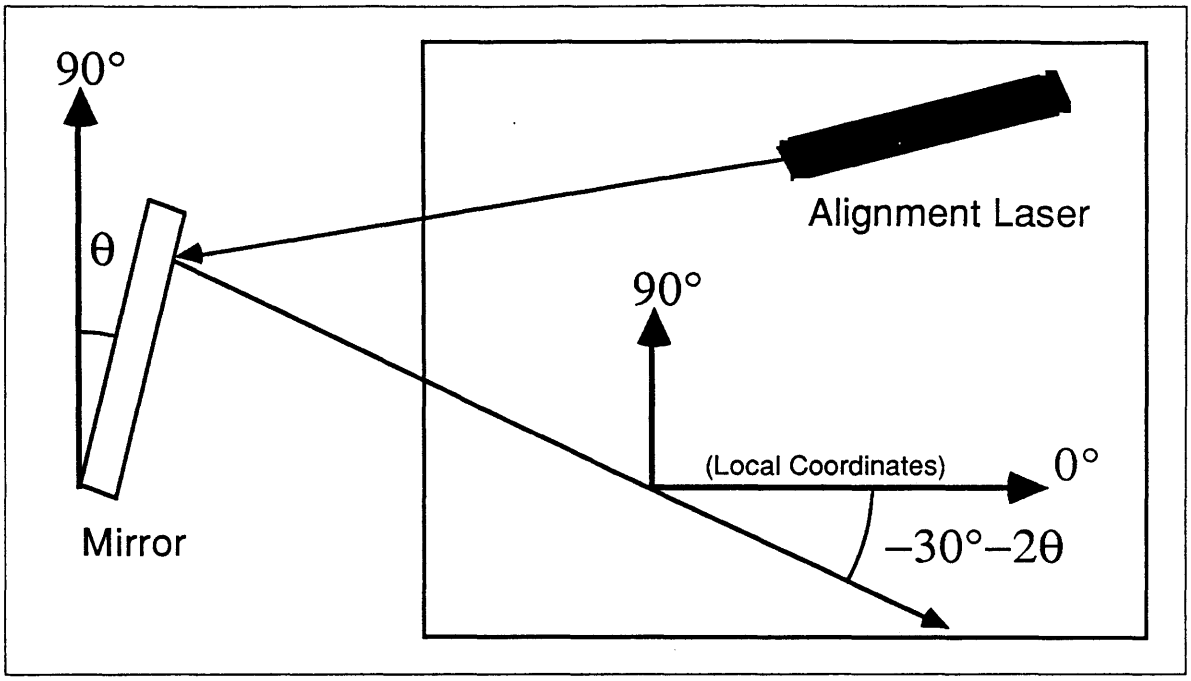

Figure 1.1.3-3 Laser Beam Return for Disturbed Platform (Local Coords)

beam from the laser reflects from a stationary mirror, and then returns to the platform. Consider rotating the platform through an angle θ as shown in Figure 1.1.3-2. In a coordinate plane which is attached to the platform, as in Figure 1.1.3-3, the mirror appears to have rotated through an angle $-\theta$. So, when the laser beam returns to the platform after being reflected from the mirror, it will be shifted from its original direction by an angle -2θ. Thus, if the mirror were fixed in inertial space, the angular motion of the platform could be calculated by scaling the angle of the return beam by a factor of -1/2.

The purpose of an artificial reference is to be able to measure the motion of the space platform so that action may be taken to compensate for this motion. By placing a mirror on the stable member of the AIRU and by placing an alignment laser on the sensor platform, the vibrational motion of the platform could be measured by the sensor on the platform. Since the mirror on the AIRU needs no power, generates essentially no heat, and can be made small and light, it is much more suitable for

mounting on the stable member of the AIRU. Also, the alignment laser can be moved to the platform, where its size, power consumption, and heat dissipation constraints are less stringent. The price that is paid is that the angular motion of the platform is scaled by a factor of two.

There is one problem which must be solved before the noise can be filtered from the target image. The inertial reference beam (pseudo star) must be made to fall on the sensor if it is to be useful in filtering vibration noise from the target image. Two methods are being considered for projecting the pseudo star image onto the sensor. In both methods, the AIRU would be mounted behind and beside the sensor, and the pseudo star image would be projected onto the sensor through an aperture which is shared with the image of the target.

The first pseudo star projection method which will be examined will be the projection of the pseudo star through the front aperture of the tracking telescope, and will be referred to as the indirect projection method. The second method to be examined will be the projection of the pseudo star image directly onto the sensor without passing through the tracking telescope optics, and will be called the direct projection method. Next, the two pseudo star projection methods will be evaluated and compared. Finally, the pseudo star projection method to be used in the scaled alignment transfer experiment (SATE) will be chosen, and the optical paths for the experiment will be designed.

1.2 Indirect Projection of the Pseudo Star

1.2.0 Introduction

In this section the method of projecting the pseudo star onto the sensor platform through the front aperture of the tracking telescope is

discussed. It is shown that the optical paths required to track the target precisely are simple, and that the control system required is also simple. This section also shows that there are problems with the indirect projection method, as this method is called. This section begins by describing the optical paths of the indirect projection method. It then covers some of the control system considerations of this method. Finally, implementation problems which make this method unattractive are discussed.

1.2.1 Optical Path Description

The three primary units in the indirect projection method are the same as those found in most precision tracking systems. They are the tracking telescope, the inertial reference unit, and the sensor platform. The tracking telescope can be either a focussing telescope, where the telescope has a finite focal length, or a beam compressor. The present indirect projection method will use a beam compressor as the tracking telescope. Attached to the telescope is the sensor platform. During the discussion of the indirect projection method the sensor platform will be assumed to be mounted rigidly to the back of the primary mirror of the telescope, and that there is no relative motion between the two. The inertial reference unit will be separated from the telescope and the sensor platform, and will have an inertially stabilized platform, with a laser on the stable member.

Figure 1.2.1-1 shows a simplified sketch of the indirect projection method. The pseudo star can be seen to originate at an alignment laser on the AIRU. It is reflected from one end of an extended corner cube, off all three orthogonal faces, and then onto the primary mirror of the tracking telescope. From the primary mirror, the pseudo star reflects to the secondary mirror, and then onto a flat mirror. The pseudo star is then reflected from the fast steering mirror, which is

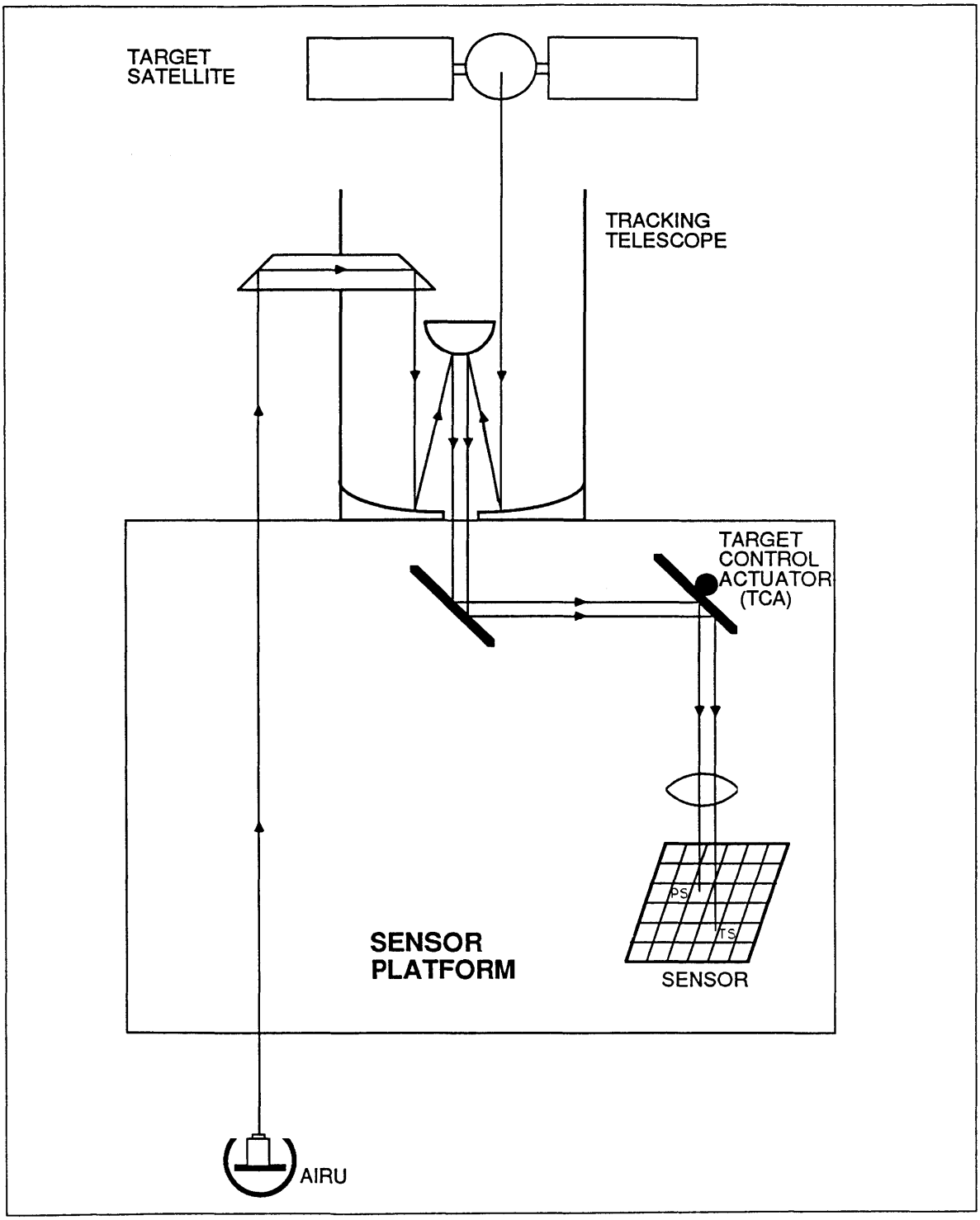

Figure 1.2.1-1 Simplified Optical Paths for the Indirect Projection Method

called the Target Control Actuator (TCA), through a lens to the sensor.

One of the properties of the extended corner cube, which is shown in Figure 1.2.1-2, is that a beam entering the cube at an absolute angle θ, will exit the cube at the same angle, travelling in the opposite direction. Thus, if the beam is travelling exactly parallel to the optical axis of the telescope when it originates, then it will travel parallel to the optical axis of the telescope after leaving the extended corner cube. Moreover, the properties of the corner cube allow the corner cube to be disturbed by vibrational noise without disturbing the angle of the pseudo star beam at the primary mirror. To an observer sitting on the primary mirror, then, the pseudo star is indistinguishable from a point source of light an infinite distance from the telescope, even in the presence of vibrational noise on the telescope.

The great advantage of routing the pseudo star through the front aperture of the tracking telescope is that the pseudo star follows the same optical paths which the target spot follows once it reaches the telescope. Hence, all of the vibrational noise which is seen by the target is also seen by the pseudo star. Thus, any tilt or decentering motion of the secondary mirror and any tilt of the primary mirror will be reflected in the motion of the pseudo star on the optical sensor.

The pseudo star spot on the sensor will be a bright spot, and its position can be measured at a fast sampling rate. When the pseudo star spot moves due to vibration disturbances, the TCA can be used to drive the pseudo star spot back to its nulled position. The TCA is used to subtract the vibrations of the sensor platform from the position of the pseudo star spot, thus transferring the alignment of the pseudo star spot into the coordinate frame of the sensor platform.

Once the target light reaches the tracking telescope, this light follows the same optical paths that the pseudo star spot follows. Thus, any disturbances which are seen in the pseudo star spot are also seen in the target spot. Since the target spot also sees the TCA steering mirror, the vibrational noise which was subtracted from the pseudo star spot by the TCA will also be subtracted from the target spot.

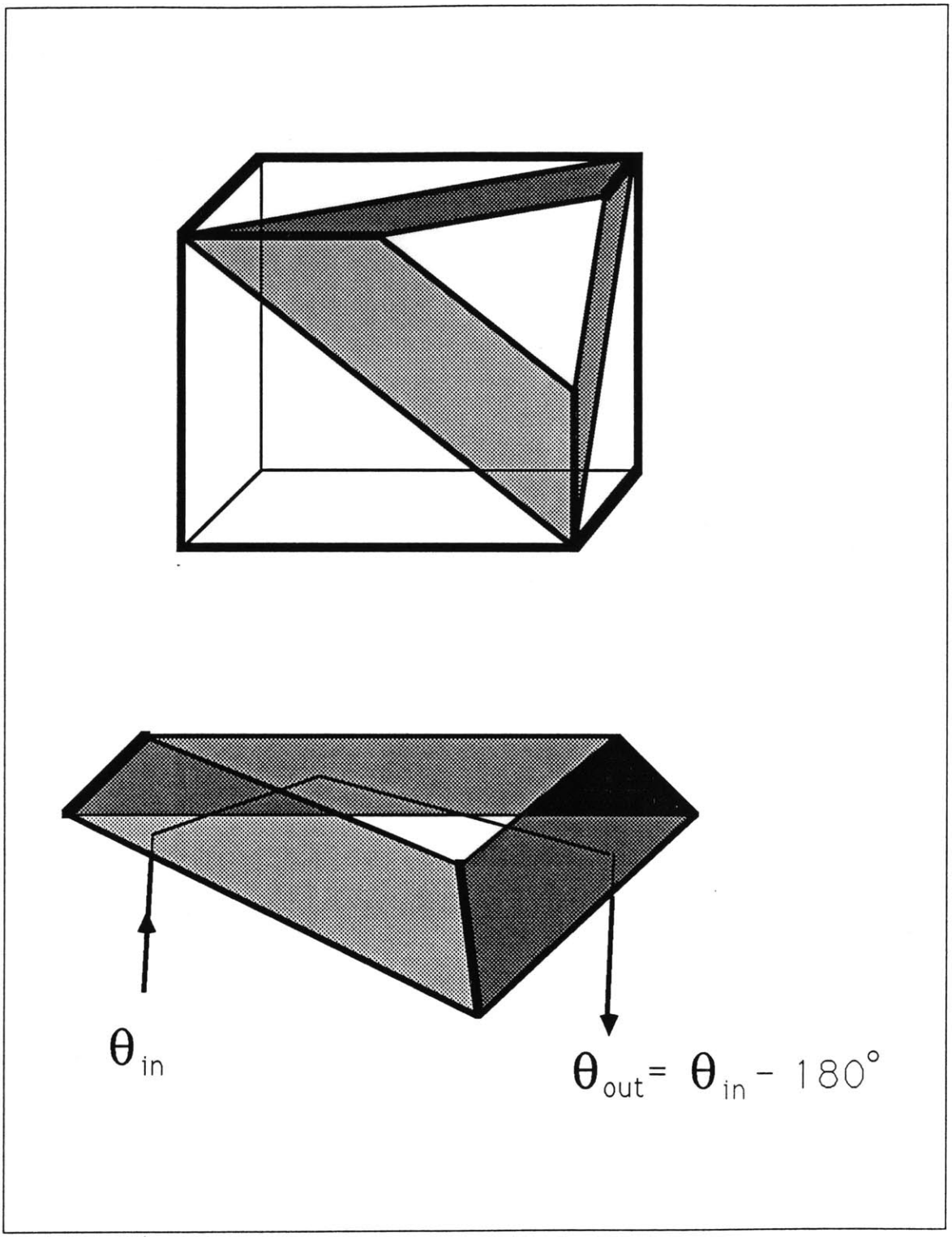

Figure 1.2.1-2 Retroreflection From An Extended Corner Cube

The optical paths just described allow the position of the dim target spot to be tracked in the presence of high frequency disturbances. However, because this is a tracker for an optical communications system, knowing where the target is located is only half of the problem. It remains to be shown how the indirect projection method can point the communications beam at the target.

Figure 1.2.1-3 shows the components which appear on the sensor platform of the indirect projection method tracker. It can be seen that the requirement to measure the angular position of the outgoing signal beam causes the optical paths to be more complicated. To see how this system works, the optical paths of all of the alignment spots will be described individually.

The target spot (TS) enters the system at the front aperture of the tracking telescope; see Figure 1.2.1-4. When the light exits the telescope, it reflects from beam splitter BS2, over to the TCA. From the TCA, the target spot transmits through beam splitter BS1, and is then focussed on the sensor by focussing lens L1. Because the target spot will be dim, the attenuation within the target spot path must be kept to a minimum. For this reason, the beam splitter BS1 will have a reflectivity of only 10%, and BS2 will have a reflectivity of 90%. This results in 81% of the target light which reaches the telescope to reach the sensor.

Figure 1.2.1-4 also shows the path of the pseudo star spot, PS1. This spot originates at a laser on the inertial reference unit. It then transmits through beam splitter BS3 to the extended corner cube. After retroreflection from the corner cube, the pseudo star spot follows the same path which the target spot follows.

A third spot, the secondary pseudo star spot PS2, also reaches the sensor after originating at the laser on the inertial reference unit, as shown in Figure 1.2.1-5. This spot is reflected by BS3, through neutral density filter ND1, and then transmits through BS2 to the TCA. After reflecting from the TCA, it transmits through BS1 and is focussed on the sensor by L1. The reason that this spot is necessary is that the original pseudo star PS1 does not allow the vibrations which disturb the sensor

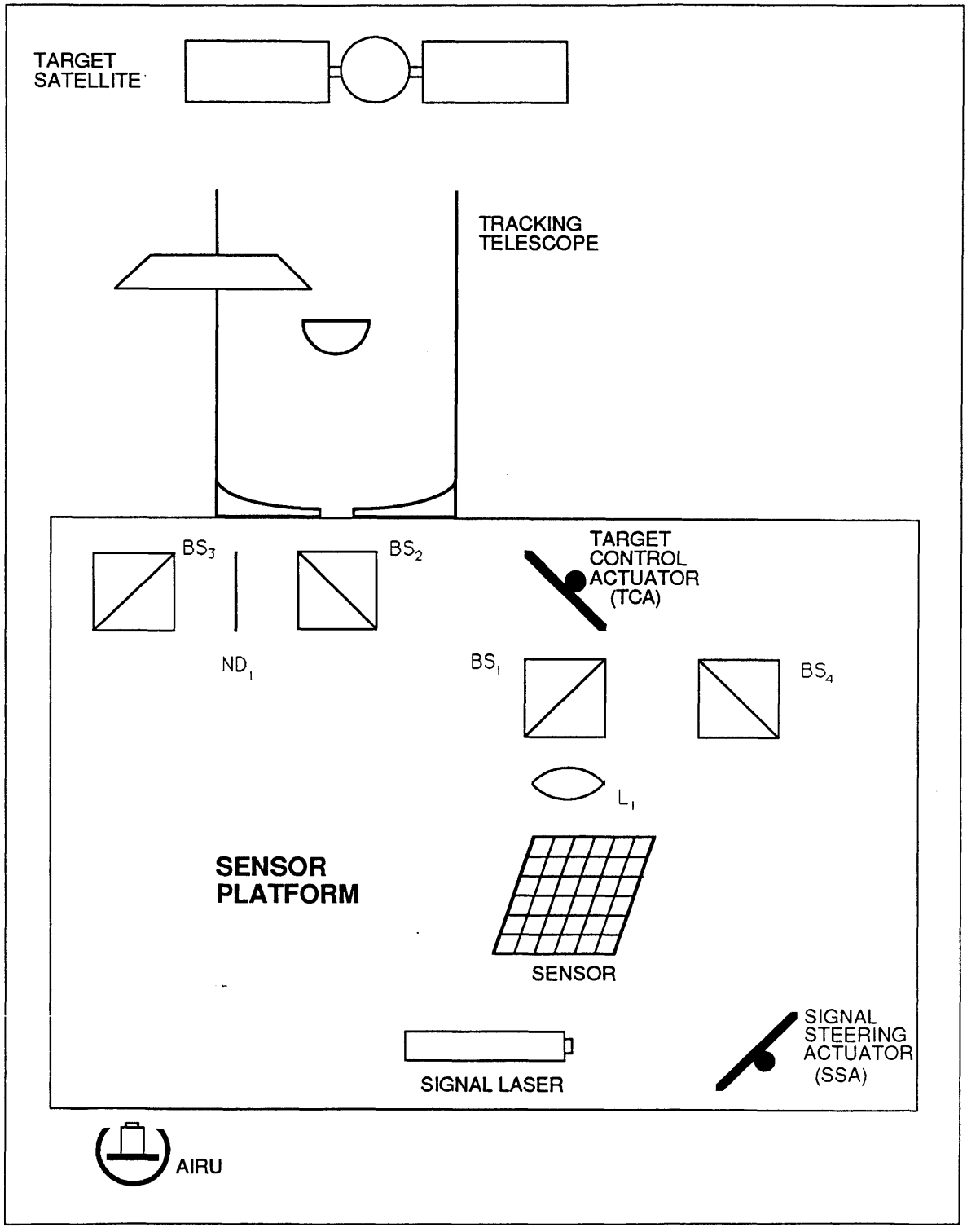

Figure 1.2.1-3 Indirect Projection Method Sensor Platform Optics

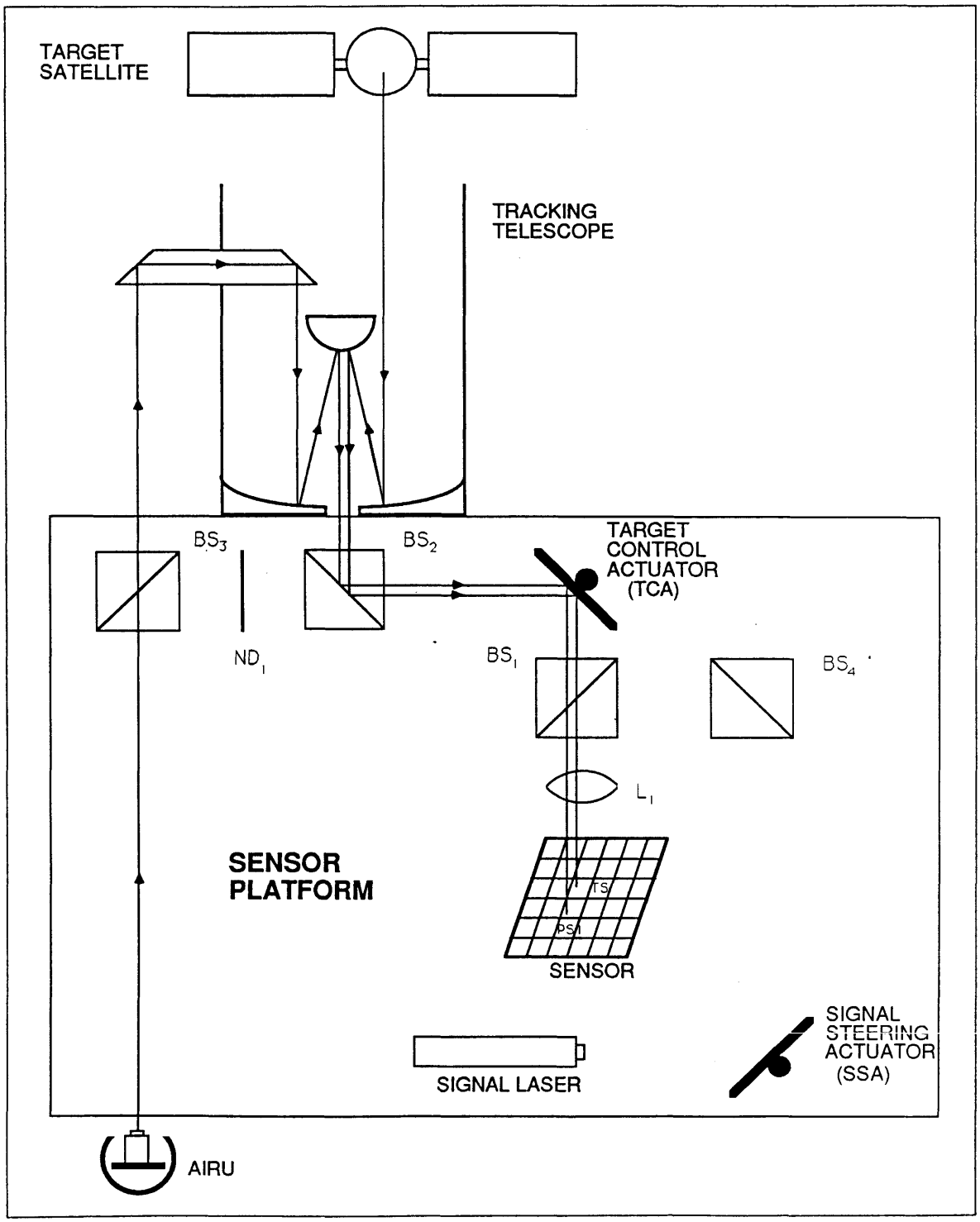

Figure 1.2.1-4 Indirect Projection Method Target and Pseudo Star Optical Paths

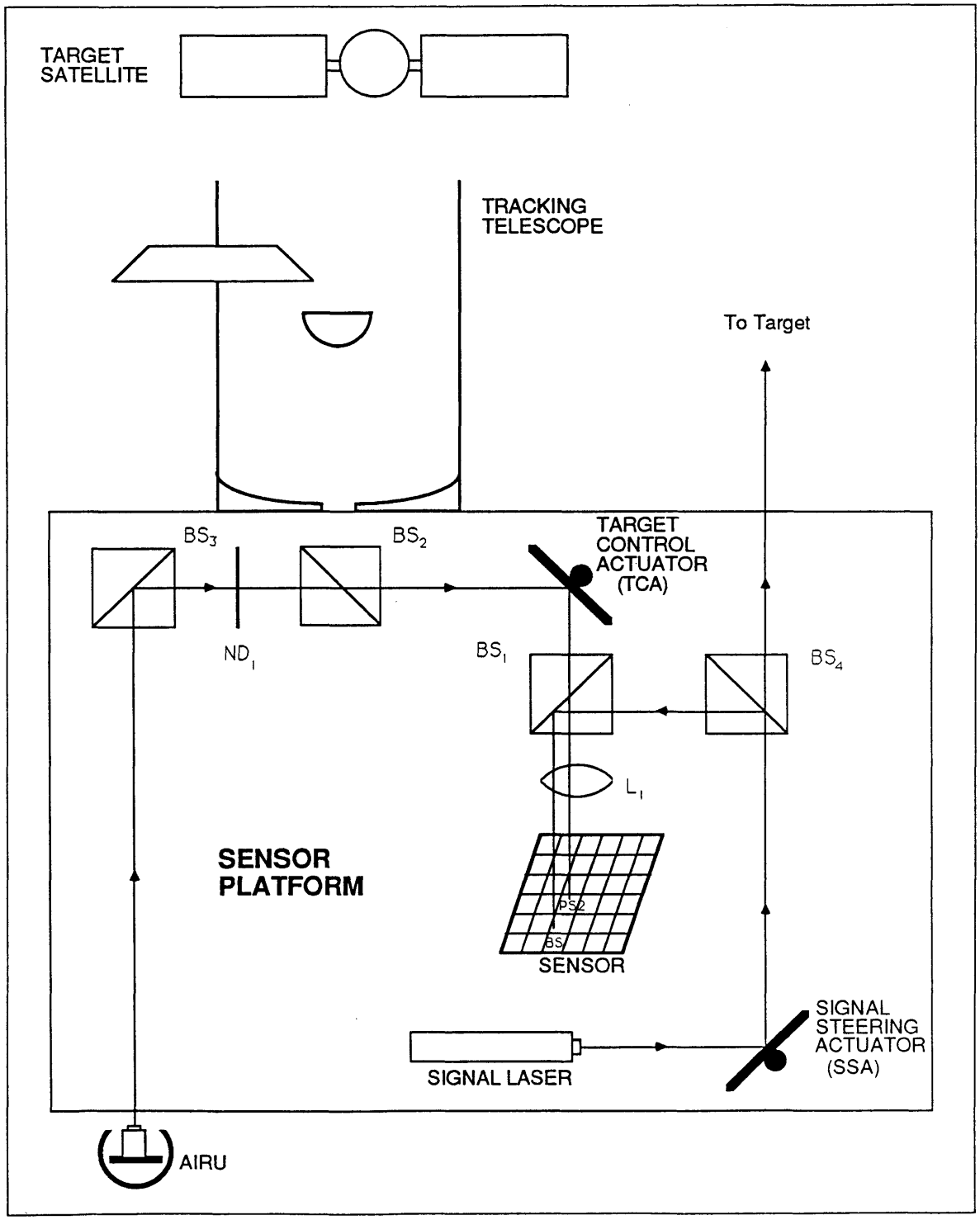

Figure 1.2.1-5 Indirect Projection Method Beacon and Secondary Pseudo Star Optical Paths

platform to be explicitly measured. The motion of PS2 on the sensor is directly proportional to a linear combination of the platform disturbance, and and the motion of the TCA. Because the motions of PS1 and PS2 are proportional to different linear combinations of platform disturbance and TCA motion, these two linear equations can be solved to find both the disturbance angle, and the TCA angle.

The reflectivity of BS3 is chosen to be 0.1, which allows the intensity of PS1 and PS2 to be matched on the sensor. It is not obvious at first that this is the case. However, the laser on the inertial reference unit must be kept small due to the size constraints of the stable member of the IRU. This will limit the pseudo star beam to a maximum aperture of approximately 5cm. When the pseudo star spot is compressed by the tracking telescope, its aperture will be 100 times smaller than the aperture of the secondary pseudo star spot. When the two spots are focussed on the sensor, the pseudo star spot will have an area 10000 times larger than the area of the secondary pseudo star spot. The energy in PS2 is made 81 times smaller than the energy in PS1 by the beam splitter reflectivities, and the neutral density filter ND1 further reduces the energy in PS2 by a factor of 100. This allows the intensities to be matched to within 20%.

The final spot which the system requires is the spot from the outgoing signal beam. This is called the beacon spot, or BS, and its path is shown in Figure 1.2.1-5. This spot originates at the signal laser, and is reflected from the Signal Steering Actuator (SSA), which is a fast steering mirror similar to the TCA. From the TCA, the signal transmits through BS4 to the target. However, BS4 reflects some of the signal over to BS1. After reflecting from BS1, the beacon spot is focussed on the sensor by L1. The reflectivity of BS4 will be a function of how much power is required to communicate with the target satellite, and the intensities of PS1 and PS2, which must be matched by the intensity of the Beacon Spot on the sensor.

The optical paths which were just described are quite simple. There are no unwanted stray spots due to internal reflections which reach

the sensor, and there is no need for a system of compensation lenses which will be required by the direct pseudo star projection method discussed in Section 1.3. Next, the control system considerations for the indirect projection method will also be shown to be simple.

1.2.2 Control System Considerations

There are four actuators which must be controlled in the indirect projection method, namely the TCA, AIRU, telescope, and SSA. The TCA will be used to subtract high frequency disturbances from the target spot. To do this, it will use a measurement of the position of PS1 on the sensor, and drive it to a null position. Thus, the movement of the target spot from its null position will be due only to target motion. The AIRU actuator will be used to cause the stable member of the inertial reference unit to track the target. This loop will use the difference between the positions of the target spot and PS1 to drive the AIRU actuator to move PS1 to the same position as the target spot. The telescope actuator will be driven to track the low frequency components of the TCA motion. If the TCA loop is functioning properly, its low frequency motion will be compensating for telescope pointing error. This error must be nulled by moving the telescope. The last loop is the loop around the SSA. It uses the positions of PS1, PS2, and BS to drive the signal beam toward the same direction in which the AIRU is pointing. If the AIRU loop is working properly, the AIRU will be tracking the target, and the SSA will direct the signal beam toward the target.

Just before the light from each of the four spots reaches the focussing lens L1, the light will be travelling at an angle with respect the the local coordinate system of the sensor. If light travelling toward the sensor parallel to the optical axis of L1, this light will be said to have an angle of zero. The angles of each of the spots are given by

$$\begin{aligned}
\phi_{TS} &= M(\theta_{TARG} - \theta_{TEL}) + 2\theta_{TCA} \\
\phi_{PS1} &= M(\theta_{AIRU} - \theta_{TEL}) + 2\theta_{TCA} \\
\phi_{PS2} &= \theta_{AIRU} - \theta_{TEL} + 2\theta_{TCA} \\
\phi_{BS} &= 2\theta_{SSA}
\end{aligned} \qquad (1.2.2\text{-}1)$$

The angles designated as θ are the angles of the different components of the system. θ_{TARG} is the angle of the target from the sensor, measured in an absolute inertial coordinate frame. θ_{TEL} is the angle at which the telescope is pointing, and is also measured in the absolute coordinate frame. The angle at which the stable member of the AIRU is pointing is labelled θ_{AIRU}, and is also measured in the absolute frame. θ_{TCA} and θ_{SSA} are the angles of the TCA and SSA, and are measured with respect to their resting angles in the local coordinate frame of the sensor platform. Finally, M is the beam compression ratio of the tracking telescope, which is discussed in Section 1.3.1.

In matrix form, Equations (1.2.2-1) become

$$\begin{bmatrix} \phi_{TS} \\ \phi_{PS1} \\ \phi_{PS2} \\ \phi_{BS} \end{bmatrix} = \begin{bmatrix} -M & 0 & 2 & 0 \\ -M & M & 2 & 0 \\ -1 & 1 & 2 & 0 \\ 0 & 0 & 0 & 2 \end{bmatrix} \begin{bmatrix} \theta_{TEL} \\ \theta_{AIRU} \\ \theta_{TCA} \\ \theta_{SSA} \end{bmatrix} + \begin{bmatrix} M \\ 0 \\ 0 \\ 0 \end{bmatrix} \theta_{TARG}$$

or

$$\underline{\phi} = C_1\underline{\theta}_A + \underline{L}_1\theta_{TARG} \qquad (1.2.2\text{-}2)$$

The physical outputs of the system will be the spot angles as seen through the sensor. The sensor will be a source of gain, and a source of additive noise, so the physical outputs will be

$$\underline{y}_P = g_s\underline{\phi} + \underline{N}_s \qquad (1.2.2\text{-}3)$$

A block diagram of the physical system is shown in Figure 1.2.2-1.

The physical outputs are not quite what would be desired to close the loops around the four actuators. It would be best to close the loops with outputs which measure pointing errors, so that regulators could keep the actuators pointing in the proper direction. A list of pointing errors required for the system is given by

TCA POINTING ERROR: $\epsilon_1 = \phi_{PS1} = M(\theta_{AIRU}-\theta_{TEL}) + 2\theta_{TCA}$

AIRU POINTING ERROR: $\epsilon_2 = \phi_{TS} - \phi_{PS1} = M(\theta_{TARG}-\theta_{AIRU})$

TELESCOPE POINTING ERROR: $\epsilon_3 = \phi_{TS} + \phi_{PS1}/(M-1) - M\phi_{PS2}/(M-1) = M(\theta_{TARG}-\theta_{TEL})$

SSA POINTING ERROR: $\epsilon_4 = \phi_{PS2}-\phi_{PS1}+\phi_{BS}(M-1) = (M-1)(2\theta_{SSA}+\theta_{TEL}-\theta_{AIRU})$

(1.2.2-4)

Note that each error is defined to within a multiplicative constant. It can be seen that the pointing errors, which are the outputs desired for closing the control loops, can be found directly from the physical outputs. That is,

$$\underline{y}_D = \begin{bmatrix}\epsilon_1\\ \epsilon_2\\ \epsilon_3\\ \epsilon_4\end{bmatrix} = \begin{bmatrix} 0 & 1 & 0 & 0\\ 1 & -1 & 0 & 0\\ 1 & 1/(M-1) & -M/(M-1) & 0\\ 0 & -1 & 1 & (M-1)\end{bmatrix}\begin{bmatrix}\phi_{TS}\\ \phi_{PS1}\\ \phi_{PS2}\\ \phi_{BS}\end{bmatrix}$$

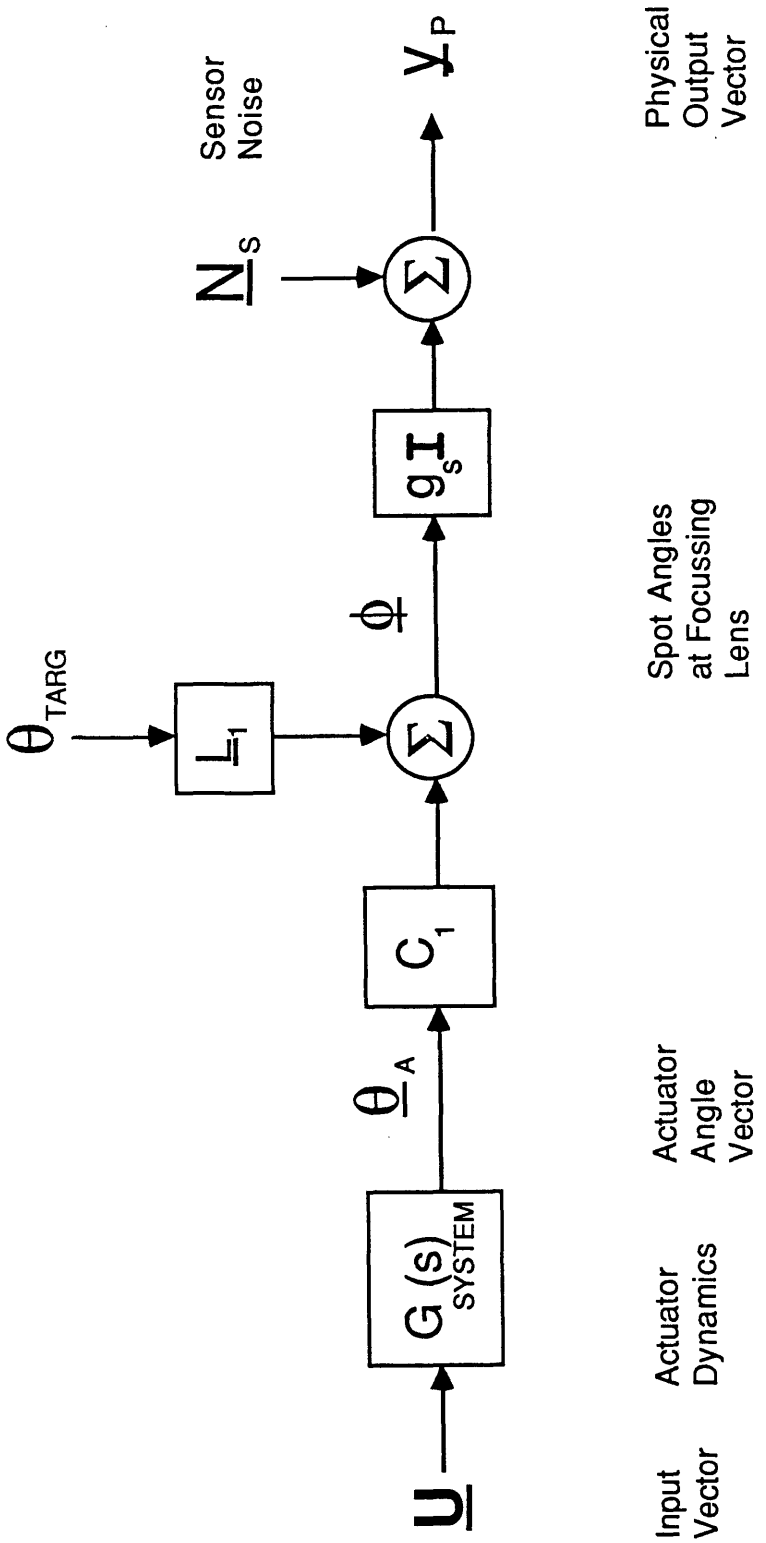

Figure 1.2.2-1 Block Diagram of Indirect Projection Method Physical Plant

or

$$\underline{y}_D = A\underline{\phi} \qquad (1.2.2\text{-}5)$$

The desired outputs from the system are represented by y_D in Equation (1.2.2-5). Since the desired outputs are realizable from the physical outputs, the only other requirement for the system is for the states of the system to be observable from the desired outputs. From Equations (1.2.2-4), the desired outputs can be derived from the actuator angles and the angular position of the target according to

$$\underline{y}_D = \begin{bmatrix} -M & M & 2 & 0 \\ 0 & -M & 0 & 0 \\ -M & 0 & 0 & 0 \\ (M-1) & (1-M) & 0 & 2(M-1) \end{bmatrix} \begin{bmatrix} \theta_{TEL} \\ \theta_{AIRU} \\ \theta_{TCA} \\ \theta_{SSA} \end{bmatrix} + \begin{bmatrix} 0 \\ M \\ M \\ 0 \end{bmatrix} \theta_{TARG}$$

or

$$\underline{y}_D = B\underline{\theta} + \underline{C}\theta_{TARG} \qquad (1.2.2\text{-}6)$$

Equation (1.2.2-6) shows how the desired outputs are dependent upon the actuator output angles $\underline{\theta}$. Because the matrix B in this equation is invertible, the actuator outputs are observable from the desired outputs. This means that the system will be observable from the desired outputs if and only if the actuator states are observable from the actuator output angles.

1.2.3 Implementation Problems

The optical paths which were discussed in Section 1.2.1 are very simple. They require only four beam splitters and a single lens on the sensor platform with the sensor, two fast steering mirrors, and the signal laser. The components which reside on the sensor platform can be made small, and very rigid, so that relative motions between these optical components can be made to be negligible. The one component of the optical paths which does not reside on the sensor platform is the extended corner cube.

As was noted before, the direction which light travels out of an ideal corner cube is a function only of the direction of the incoming light, and is independent of the orientation of the corner cube. The corner cube cannot be made perfect, however, and the large size of the cube will allow the cube to flex. In order to keep all three faces of the cube as nearly perpendicular as possible, the structure of the cube must be made strong, which will add weight to the tracking system. To keep the cube from warping due to uneven heating, it must be shielded from sunlight, and kept in a temperature-controlled environment. These issues concerning the corner cube can be resolved, but they add a cost in increased weight and complexity to the tracking system.

A second problem is that the pseudo star which this method uses requires that a laser be mounted on the stable member of the AIRU. Because of size and stability constraints on the AIRU design, this might not be practical. First, power must be channelled to the stable member, which means that there will be some sort of mechanical or electro-mechanical linkage between the AIRU stable member and its outer case. This allows more of the vibrations which will be shaking the case to disturb the stable member. Second, since lasers are very inefficient, the waste heat from the laser will cause temperature gradients which will be harmful to the operation of the AIRU. Even without the laser, cooling is a major concern in the design of the AIRU, and the laser will compound the

problem. Third, the quality of the beam tends to be better with larger lasers. In order to calculate the centroid of the pseudo star spots accurately enough, the necessary beam quality may dictate that a large laser be used. This would force the size requirements of the AIRU stable member to be prohibitively large and expensive. Fourth, since the beam from any laser tends to diverge, the beam from the alignment laser must be conditioned by going through a beam expander to increase its diameter, and reduce its divergence angle. This beam expander will also add to the size requirements of the AIRU stable member.

The corner cube and pseudo star laser are serious problems faced by the implementation of this method. However, the one problem which appears unresolvable is that the system has a severe aperture size mismatch between the pseudo star spot and the target spot when they enter the telescope. Because the target spot will use the full five meter aperture size, and the pseudo star spot will be only five centimeters when it enters the telescope, the pseudo star spot will be 100 times larger in diameter than the other spots when it reaches the sensor. In order to calculate the centroids of the three small spots accurately, their diameters on the sensor will be about three pixel widths [D]. This means that the pseudo star spot will cover an area of approximately 65,000 square pixels! Not only would it take extraordinary computing power to calculate this centroid at a rate of 10,000 centroids per second, but it would require a prohibitively large sensor.

For these reasons it now becomes a requirement that the method of projecting the pseudo star onto the sensor not project the pseudo star through the telescope, and that it not require a laser to be mounted on the AIRU. The next section will describe just such a system.

1.3 DIRECT PROJECTION OF THE PSEUDO STAR

1.3.0 Introduction

In Section 1.2 the indirect method of projecting the pseudo star onto the sensor platform was discussed. There were several problems associated with the direct projection method to be addressed in the design of a tracker for an optical communications system. First, there is no actual measurement of the sensor platform disturbances. Second, it requires a laser on the stable member of the inertial reference unit. Finally, the sizes of the spots which reach the sensor are mismatched by two orders of magnitude, making centroid calculations inaccurate and very time consuming. In the design of the tracker using the direct projection method an attempt will be made to address all three of these problems.

This section will begin by describing the optical paths of the direct projection method tracker, noting how spot intensities and sizes are matched when they reach the sensor. Then the design will be checked for observability and controllability properties, to see if a compensator can be designed to control the optics. Finally, some of the possible implementation problems and technological advances required for system operation will be discussed.

1.3.1 Optical Path Description

The direct method of projecting the pseudo star onto the optical sensor differs dramatically from the indirect projection method described in the last section. First, the pseudo star path does not enter the tracking telescope. Instead, it shares an aperture with the target image after the target image has exited the telescope. The tracking telescope does not focus incoming light, but rather acts as a beam compressor. This means that the nearly collimated light which enters the front aperture

will exit the beam compressor nearly collimated but compressed. So the collimated beam which exits the tracking telescope will have to be focussed on the sensor.

A different type of pseudo star is used in this configuration than in the configuration of the last section. This type of pseudo star uses a mirror on the AIRU and an alignment laser on the sensor platform. The advantages of removing the laser from the AIRU were outlined in Section 1.1.3. As in the previous section, the sensor platform is assumed to be rigidly mounted to the primary mirror of the tracking telescope.

An interesting property of the beam compressor tracking telescope is that it magnifies angles by the compression ratio of the beam compressor (see Figure 1.3.1-1). For example, if the tracking telescope has a front aperture of 5 meters, and an exit aperture of 5 centimeters, the compression ratio is

$$M = 5m / 0.05m = 100 \qquad (1.3.1\text{-}1)$$

So, a beam entering the front aperture of the compressor at an angle θ will exit the beam compressor at an angle of $M\theta$. Conversely, if an error measuring the angle to the target $d\theta_m$ is made at the sensor, the actual angular measurement error, when projected back to the target, will be divided by the compression ratio. The actual measurement error is

$$d\theta_{ACTUAL} = d\theta_m / M \qquad (1.3.1\text{-}2)$$

This is particularly useful for rejecting round off errors associated with digitized spot position measurements.

Figure 1.3.1-2 shows that there are sixteen optical components on the sensor platform. These are needed to achieve several goals of the system. First, since the target will be very dim, the path of the target spot (TS) must contain as little attenuation as possible. This is done by including as few optical components as possible in the target spot path. A steering mirror must be in the target spot path in order to subtract out

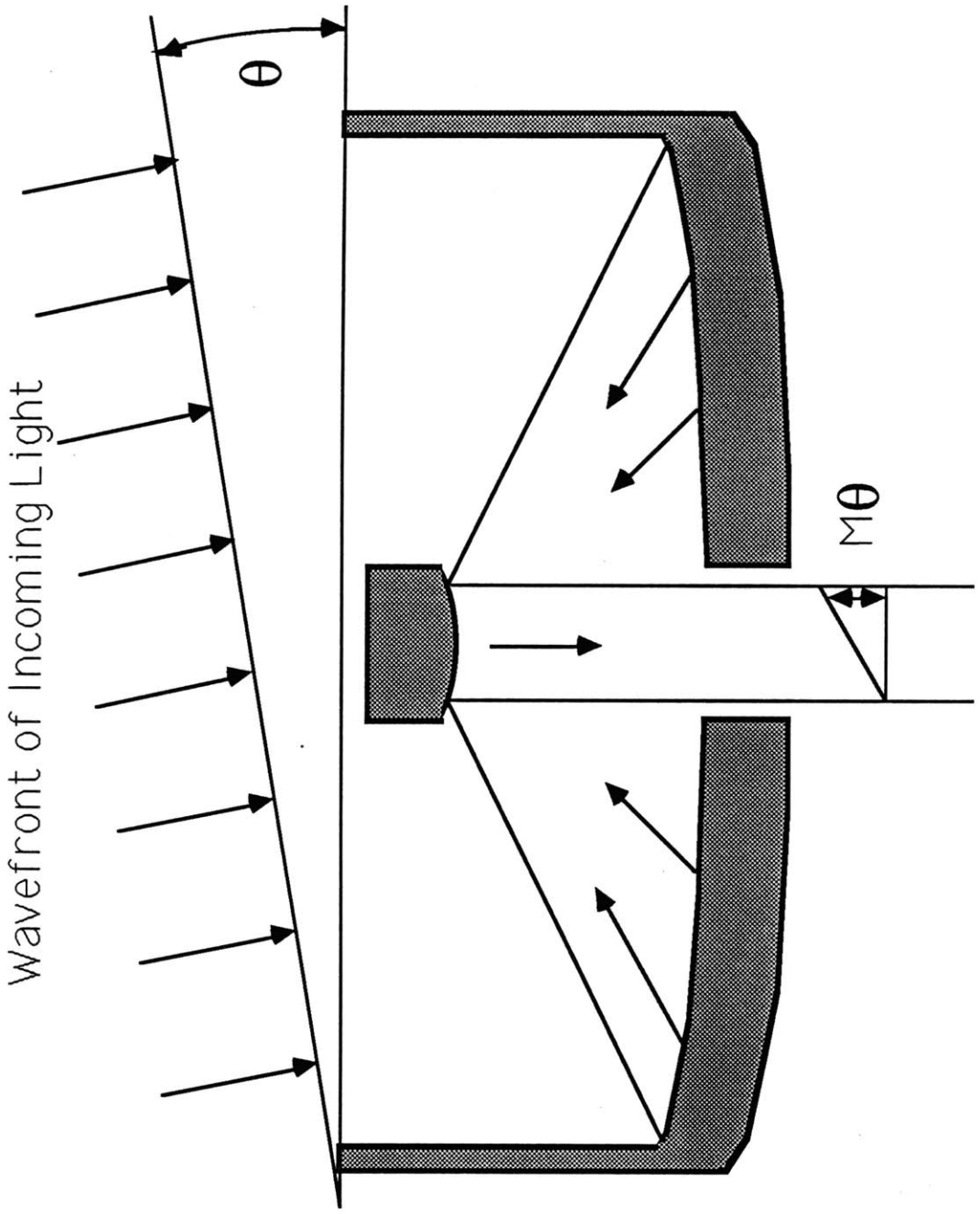

Figure 1.3.1-1 Beam Compressor Angle Magnification Property

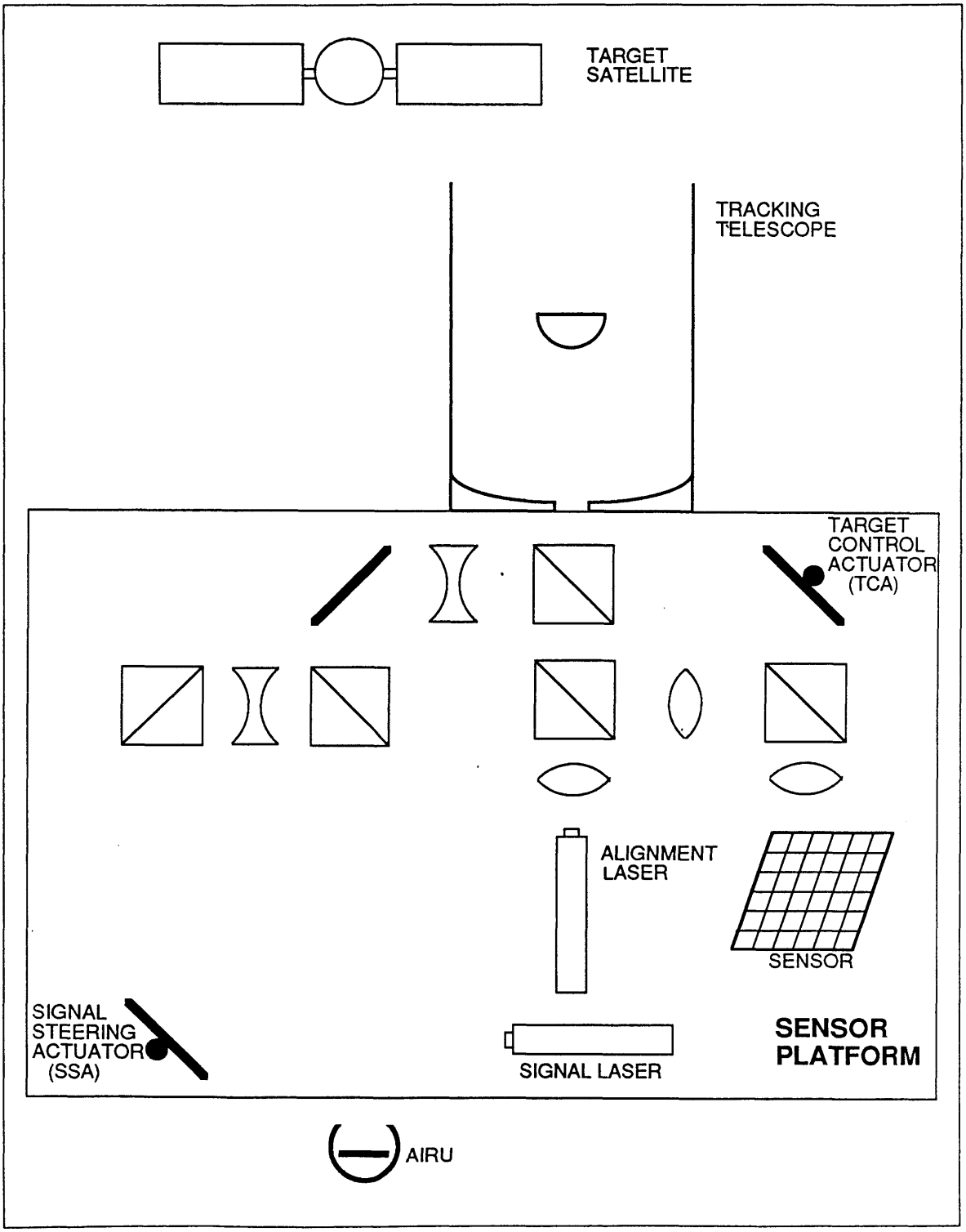

Figure 1.3.1-2 Direct Projection Method Sensor Platform Optics

vibration noise which appears on the sensor platform. This steering mirror is labelled in the figure as the target control actuator (TCA) because it is used to control the position of the target spot on the sensor. In order to measure the position of the TCA very accurately and at a high sampling rate, a reference spot RS is reflected from the TCA, and its position is measured with the sensor.

The AIRU, which has a mirror on its stable platform, can be seen below the sensor platform in Figure 1.3.1-2. Because the pseudo star will only allow the vibrations of the sensor platform to be measured, some means must be found to measure any other vibrations in the path of the target spot. The assumption has been made that all of the components on the sensor platform can be made very rigid, and will not vibrate with respect to the primary mirror of the tracking telescope. This assumption will be valid if all the components on the sensor platform are small and rigid. The only other component in the path of the target spot which can cause vibration disturbances is the secondary mirror of the tracking telescope. Another alignment spot must be included in order to measure the motion of the secondary mirror. This spot will be called the secondary spot (SS).

The last spot which will have to be included in the sensor platform optics is the beacon spot (BS). This spot is used to keep track of where the signal laser is pointing. In order to keep the signal laser pointing at the target, the signal steering actuator (SSA) is included in the path of the beacon.

There are also some constraints which affect the sensor platform optics. All of the alignment spots which will fall on the sensor must be of roughly the same intensity so that they are all bright enough to be measured accurately, but not so bright that the sensor is saturated. Consequently, the total attenuation factor of the optical paths for all of the reference spots must be nearly the same, because all of the alignment spots will originate from the alignment laser. The reflectivities of the beam splitters are used to match the attenuation factors of the paths, and neutral density filters are used where beam splitter reflectivities fail

to make the match.

The large number of beam splitters used in this configuration adds another problem. There are extra optical paths which allow unwanted spots to reach the sensor. It would be nice to eliminate these extra spots, because they add to the noise level on the sensor, and may confuse the tracking algorithms. The side effects of these parasitic spots are reduced by causing the extra spots to be very out of focus when they reach the sensor. To see how each of the objectives were met, the optical paths of each spot will be discussed individually.

The method chosen for measuring the secondary mirror vibrations strongly influences the entire set of optical paths. The secondary mirror will be a curved surface, and will be nearly, but not exactly, spherical. For now it is assumed that the secondary mirror is indeed spherical. Figure 1.3.1-3 shows a spherical surface being illuminated by a collimated beam, where the illuminated area is within the area marked as the secondary mirror. If the center of curvature of the spherical surface is translated by a distance x as shown in Figure 1.3.1-4, the illuminated area can be seen to remain a subset of the secondary mirror. Suppose that a new secondary mirror is cut from the spherical surface at the boundary of the illuminated part of the surface. This new secondary mirror does not appear to have any horizontal translation as measured at the vertex of this new secondary mirror, but has acquired a tilt θ, where

$$\theta = \sin^{-1} \frac{x}{R} \qquad (1.3.1\text{-}3)$$

or

$$\theta \approx \frac{x}{R} \quad \text{for} \quad x \ll r \qquad (1.3.1\text{-}4)$$

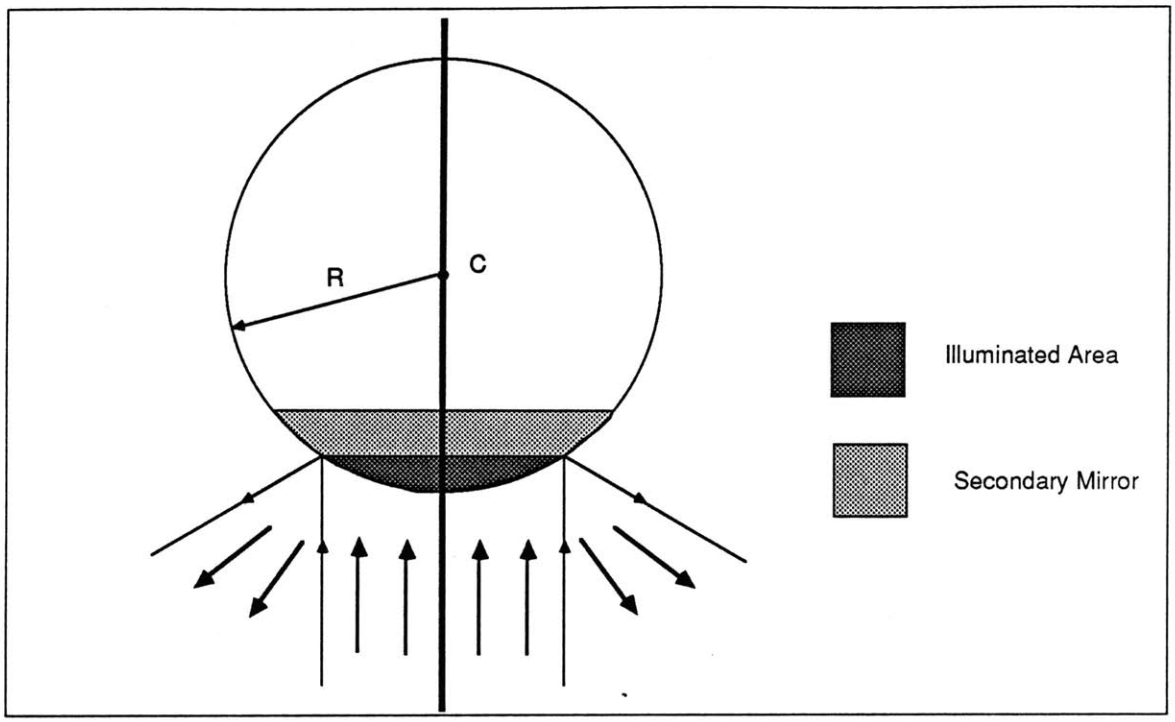

Figure 1.3.1-3 Collimated Beam Reflects from Secondary Mirror

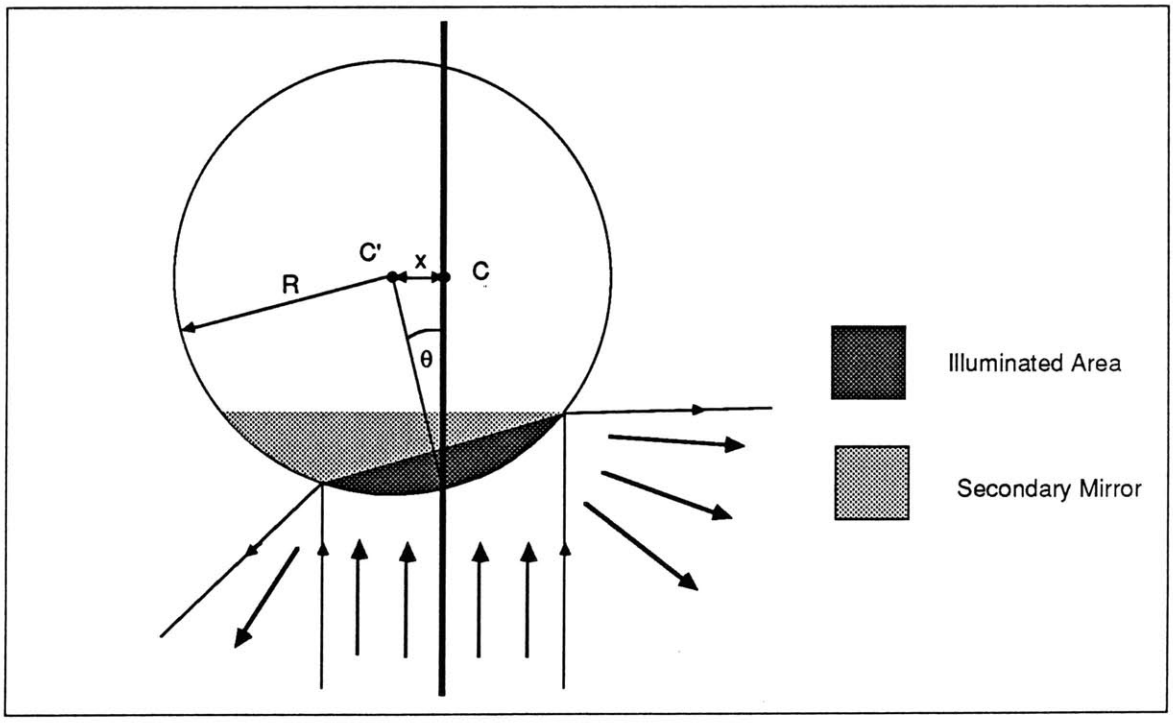

Figure 1.3.1-4 Collimated Beam Reflects from Decentered Secondary Mirror

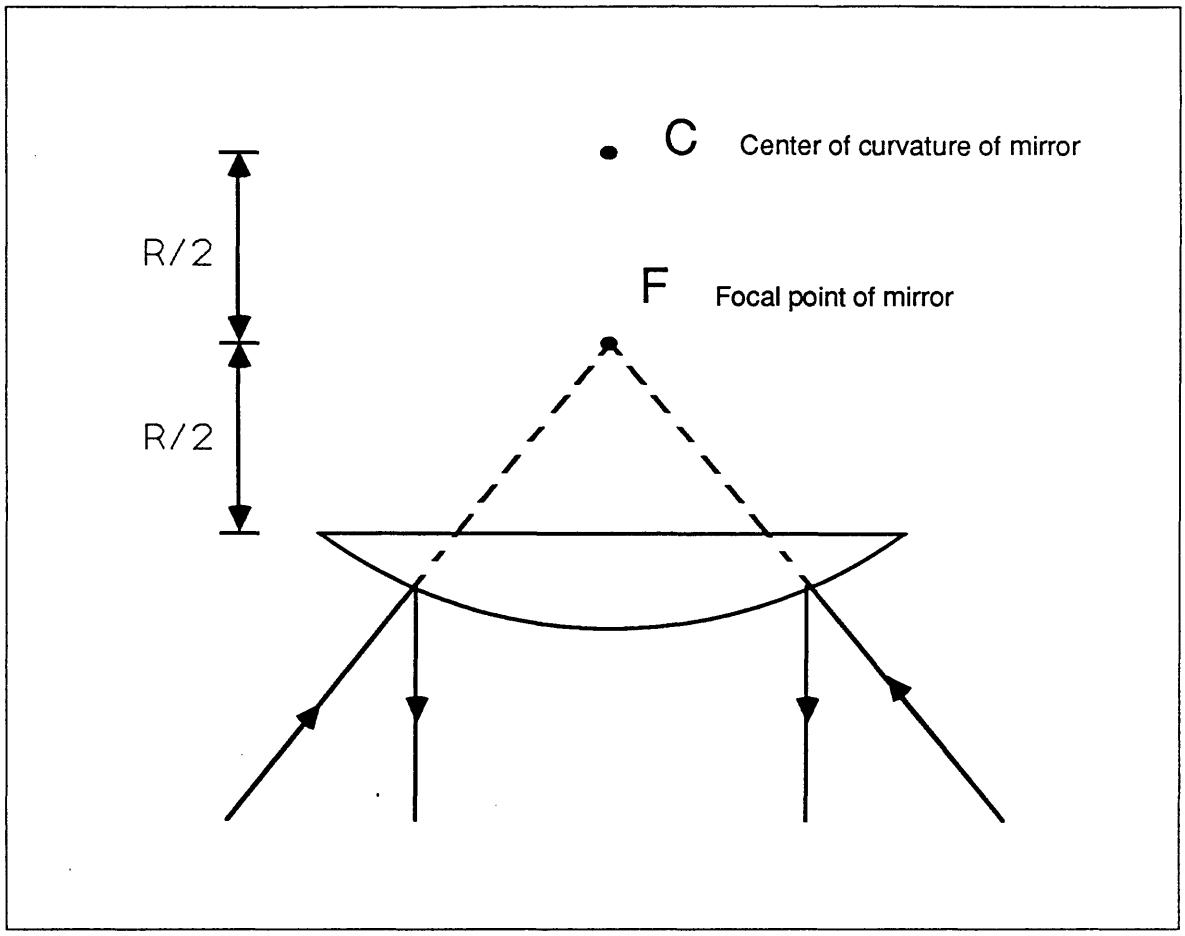

Figure 1.3.1-5 Alignment Beam Focussed On Focal Point of Secondary Mirror

It can be seen then, that for small displacements of the secondary mirror the error can be compensated by applying a tilt which is proportional to the translation of the center of curvature of the secondary mirror. Because of the direct relationship of tilt to translation, both translation and tilt errors can be considered as a single error source. Therefore, the only error source which will appear in the model of the secondary mirror will be tilt, and the control which will be used to eliminate the tilt error will be an actuator which can tilt the secondary mirror. It can be shown that although the secondary mirror is parabolic rather than spherical, for small disturbances its optical behavior is approximately the same as for a spherical mirror [3].

The curved surface of the secondary mirror causes problems with the focus of the secondary spot. If a collimated beam from the alignment laser were reflected from the secondary mirror, assuming that there are no disturbances on the secondary mirror, the reflected beam would be highly divergent. In fact, much of the energy of the beam would be reflected from the primary mirror out the front aperture of the telescope. Instead of reflecting a collimated beam from the secondary mirror, a means must be found to pre-distort the alignment beam so that all of the beam returns to the sensor platform. This can be done in two ways. Either the beam can be completely precompensated so that the return from the secondary mirror is collimated, or it can be partially precompensated so that the return beam must also be compensated.

If the alignment beam were focussed on the focal point of the secondary mirror as Figure 1.3.1-5 shows, the beam returning from the secondary mirror will be collimated. The advantage of totally precompensating the alignment beam is that only one compensating lens is needed to collimate the alignment beam. If only one compensating lens is needed for the secondary spot, the whole set of optical paths for all of the alignment spots becomes much more flexible, and can be designed so that very few unwanted spots reach the sensor. There is only one major problem with this design. Figure 1.3.1-6 shows how the alignment beam is focussed on the focal point of the secondary mirror. Because the diameter of the collimated return beam will be the same as the diameter of the illuminated area of the secondary mirror, the similar triangles in the figure can be used to find the diameter of the return beam. If the alignment beam starts 5 cm (d1) in diameter, the secondary mirror is 10 meters (x2) from the primary mirror, the compensating lens is 50 cm (x1) from the primary mirror, and the focal length of the secondary mirror is 0.1 meter (x3), then

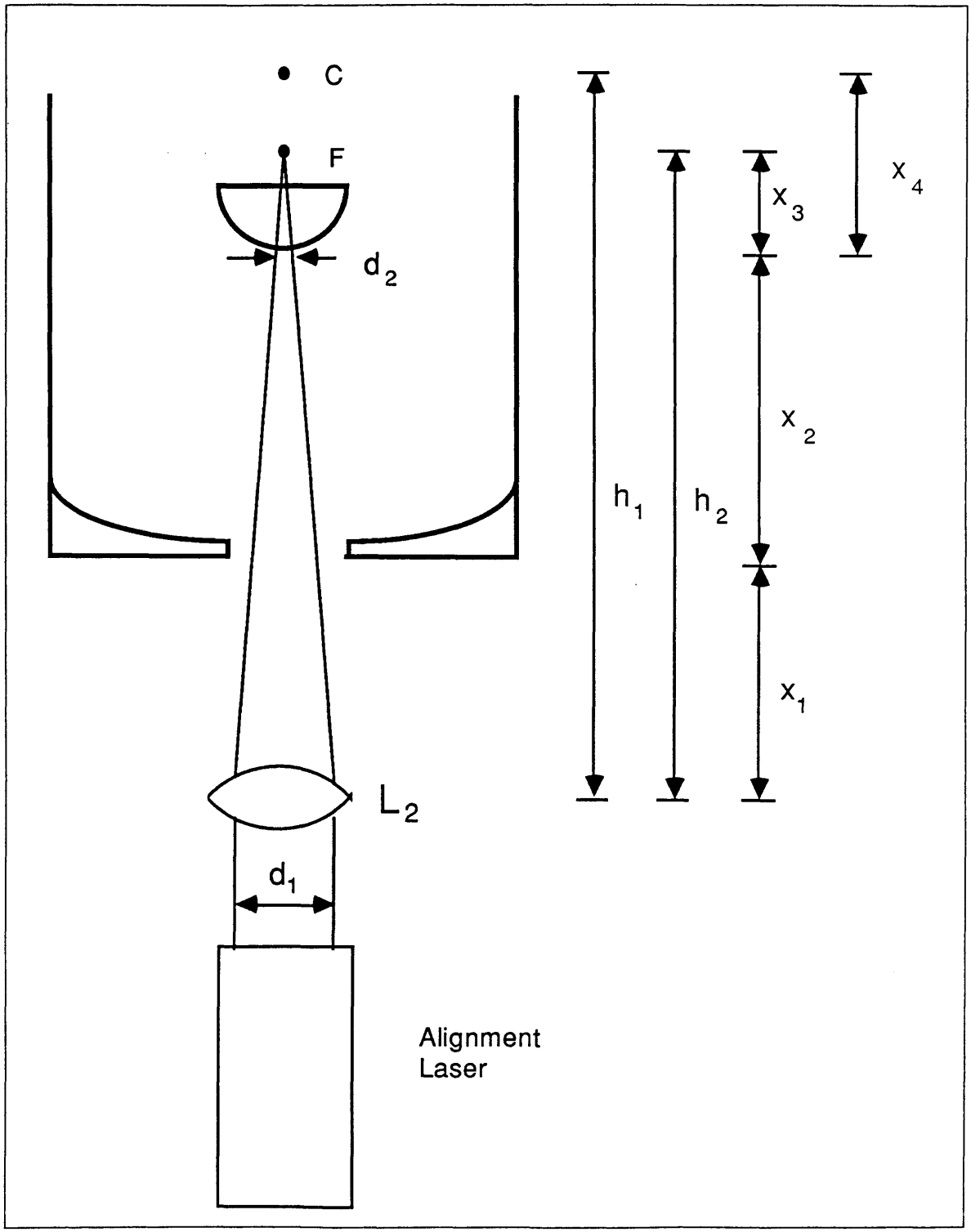

Figure 1.3.1-6 Dimensions of Secondary Spot Optical Paths

$$x1 = 0.5 \text{ m}$$
$$x2 = 10.0 \text{ m}$$
$$x3 = 0.1 \text{ m}$$
$$x4 = 0.2 \text{ m}$$
$$d1 = 0.05 \text{ m}$$
$$h1 = x1 + x2 + x4 = 10.7 \text{ m}$$
$$h2 = x1 + x2 + x3 = 10.6 \text{ m} \qquad (1.3.1\text{-}5)$$

so that

$$d2 = d1 * x3 / h2 = 0.047 \text{ cm} \qquad (1.3.1\text{-}6)$$

Since all other spots will have diameters of 5 cm, there will be a severe mismatch in spot sizes when the spots reach the array. In fact, this spot size mismatch is worse than the mismatch created by the indirect pseudo star projection method discussed in Section 1.2.

The second way the compensation lenses could be placed is to compensate partially for the curvature of the secondary mirror before the alignment spot reaches the secondary mirror, and partially after the beam reflects from the secondary mirror. To do this, the first lens is used to focus the alignment beam on the center of curvature of the secondary mirror, which is twice the focal length from its surface. Since each ray of the alignment beam would be perpendicular to the surface of the mirror where the ray struck the mirror, it would be reflected back along the exact same path which it took to the mirror. When the beam again goes through the compensating lens, it comes out collimated and exactly the same diameter as it started out. Because the two lens compensation technique does not suffer the fatal flaw of spot size differences, the two lens technique will be used in the remainder of the description.

Figure 1.3.1-7 shows the paths which the secondary mirror alignment spot will follow. The beam originates at the alignment laser, passes through lens L2, through the alignment laser beam splitter BS2, to the telescope exit beam splitter BS3. It then transmits through BS3,

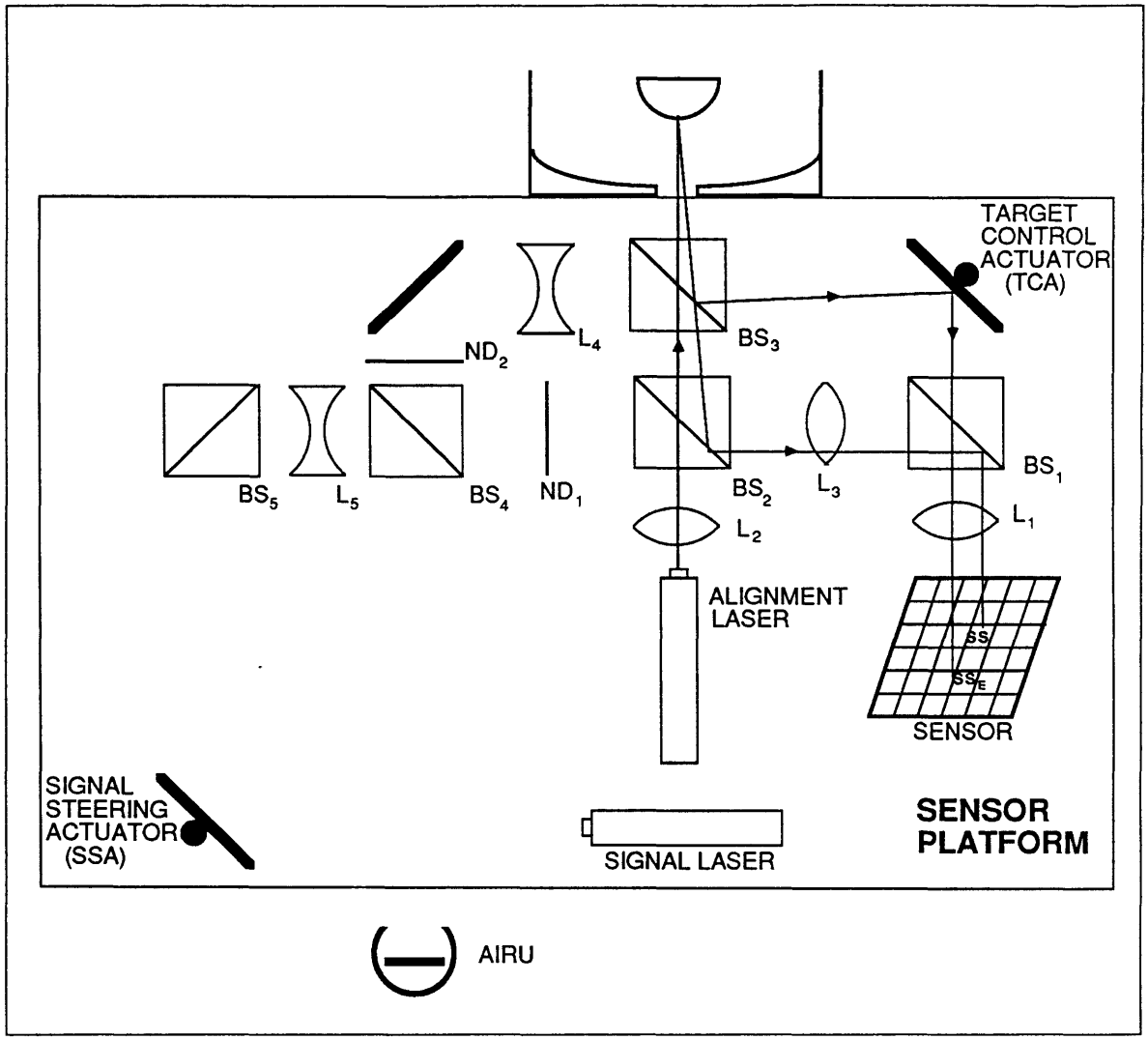

Figure 1.3.1-7 Direct Projection Method Secondary Spot Optical Paths

reflects from the secondary mirror, transmits back through BS3, and reflects from BS2. From there it transmits through compensation lens L3, reflects from the sensor beam splitter BS1, transmits through imaging lens L1, and onto the sensor. The figure also shows a parasitic spot (SS_E) which appears when the secondary spot is split at BS3. This unwanted spot is reflected from BS3, reflected from the TCA, and then transmitted through BS1. From there it transmits through the imaging lens L1 and onto the sensor.

Beam Splitter Reflectivities

Beam Splitter	Reflectivity
BS_1	0.1
BS_2	0.5
BS_3	0.9
BS_4	0.5
BS_5	0.1

Neutral Density Filters

Filter	Transmission Coefficient
ND_1	0.043
ND_2	0.23

Lens Focal Lengths

Lens	Focal Length
L_1	1.0 m
L_2	10.7 m
L_3	10.7 m
$*L_4$	-10.7 m
$*L_5$	-10.7 m

* These focal lengths assume that the sensor platform optics are infinitely close together. Actual focal lengths will depend upon actual path lengths.

Table 1.3.1-1 Parameters of Direct Projection Method Sensor Platform Optical Components

At this point a factor called the energy multiplier of a path can be defined. The energy multiplier will be the percentage of the source energy which reaches the sensor by following that path. For example, if half of the energy of the alignment laser were to reach the sensor along the secondary path, the energy multiplier for this path would be 0.5.

The reflectivity of each of the beam splitters is listed in Table 1.3.1-1. If a beam is reflected from a beam splitter with a reflectivity r, the corresponding energy multiplier m is m = r. If the beam is

transmitted through the beam splitter, the energy multiplier is m = (1-r). All mirrors are assumed to have a reflectivity of 1, and all lenses are assumed to have a reflectivity of 0.

The energy multipliers for the paths travelled by the secondary spot and the parasitic spot associated with it are

$$m_{SS} = 0.5 \times 0.1 \times 0.1 \times 0.5 \times 0.1 = 2.5\text{x}10^{-4} \qquad (1.3.1\text{-}7)$$

$$m_{SSE} = 0.5 \times 0.1 \times 0.9 \times 0.9 = 4.05\text{x}10^{-2} \qquad (1.3.1\text{-}8)$$

From the energy multipliers it appears that the parasitic spot will be much brighter than the secondary spot. However, the parasitic spot will not be collimated when it reaches the focussing lens, so it will be out of focus when it reaches the sensor.

To see how the intensities of the secondary spot and the parasitic spot compare, the two spot sizes must be found. Using the thin lens approximation, the diameter of the secondary spot at the sensor can be found using

$$\sin \theta = \frac{\lambda}{d} \qquad (1.3.1\text{-}9)$$

where λ is the wavelength of light, d is the diameter of the aperture, θ is the angle between the center of the spot and the first diffraction minimum. Alternatively,

$$\sin \theta = \frac{d_{SS}}{2\ f_{L1}} \qquad (1.3.1\text{-}10)$$

where d_{SS} is the diameter of the secondary spot, and f_{L1} is the focal length of lens L1. Thus

$$d_{SS} = \frac{2\ f_{L1}\ \lambda}{d} \qquad (1.3.1\text{-}11)$$

$\lambda = 6.33 \times 10^{-7}$ meters

$f_{L1} = 1.0$ meters

$d = 5.0$ cm

so that

$$d_{SS} = 2.5 \times 10^{-5}\ m \qquad (1.3.1\text{-}12)$$

The total area of the secondary spot then will be

$$A_{SS} = \frac{(d_{SS})^2}{4} \times \pi = 3.8 \times 10^{-10}\ m^2 \qquad (1.3.1\text{-}13)$$

The area of the extra secondary spot can be found by using ray optics; see Figure 1.3.1-8. Because the alignment beam was focussed on the center of curvature of the secondary mirror by lens L2, the virtual source for the extra spot will be a point source located at the center of curvature of the secondary mirror. The distance from the virtual source to the focussing lens L1 will be approximately

$h1 = x1 + x2 + x4 = 10.7$ m

$f_{L1} = 1.0$ m

$$\frac{1}{h1} + \frac{1}{i} = \frac{1}{f_{L1}} \qquad (1.3.1\text{-}14)$$

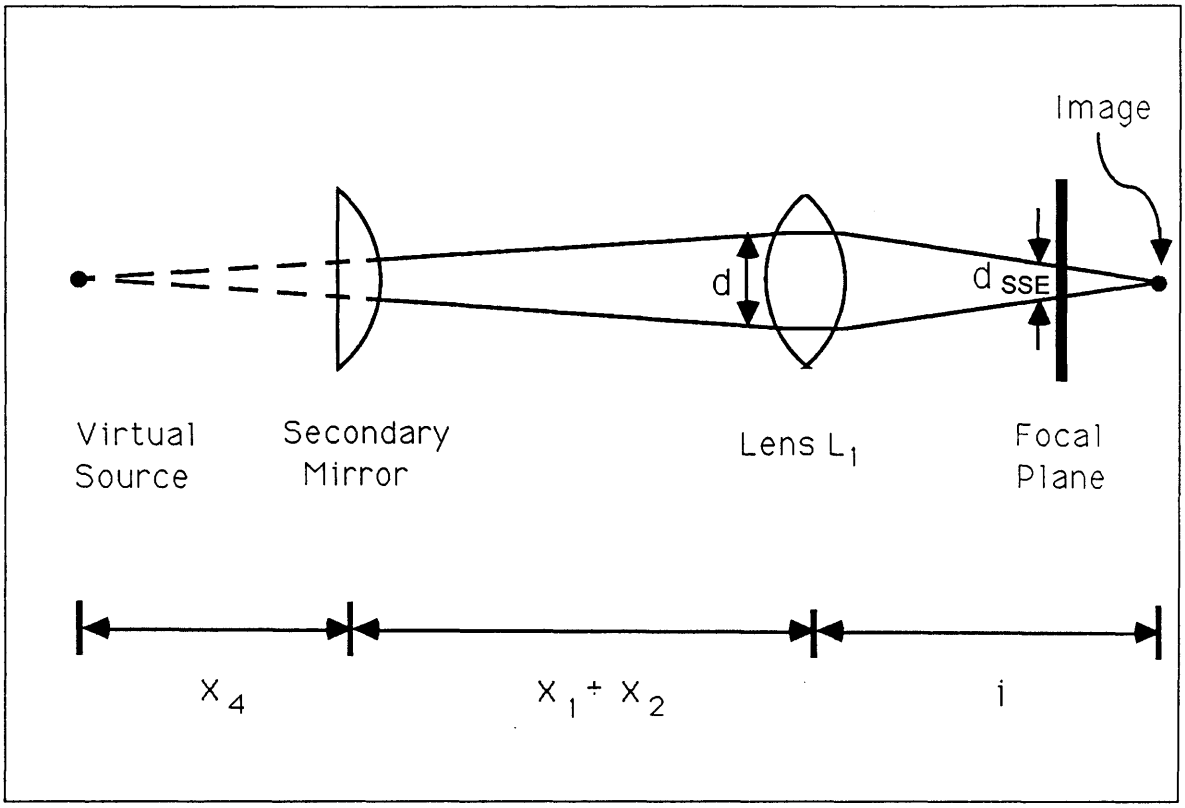

Figure 1.3.1-8 Focal Point of Extra Secondary Spot

Thus,

$$i = \frac{1}{\frac{1}{f_{L1}} - \frac{1}{h1}} = \frac{1}{1 - \frac{1}{10.7}}\ m = 1.103\ m \qquad (1.3.1\text{-}15)$$

Because the lens forms the base of a triangle and the focal plane forms the base of a similar triangle,

$$\frac{d_{SSE}}{d} = \frac{i - f_{L1}}{i} \qquad (1.3.1\text{-}16)$$

so that

$$d_{SSE} = \frac{(i - f_{L1})d}{i} = 4.67 \times 10^{-3} \text{ m} \qquad (1.3.1\text{-}17)$$

Thus, the area of the extra secondary spot is

$$A_{SSE} = \frac{(d_{SSE})^2}{4} \pi = 1.71 \times 10^{-5} \text{ m}^2 \qquad (1.3.1\text{-}18)$$

If the intensities of the two spots are now compared at the sensor,

$$I_{SS} = \frac{E_{LASER} \times m_{SS}}{A_{SS}} = E_{LASER} \times 5.0 \times 10^5 \text{ m}^{-2} \qquad (1.3.1\text{-}19)$$

$$I_{SSE} = \frac{E_{LASER} \times m_{SSE}}{A_{SSE}} = E_{LASER} \times 2.37 \times 10^3 \text{ m}^{-2} \qquad (1.3.1\text{-}20)$$

and the ratio of the spot intensities is

$$\frac{I_{SS}}{I_{SSE}} = 211.0 \qquad (1.3.1\text{-}21)$$

This means that the secondary spot will be much brighter than the extra spot.

Another important issue is that for accurate centroid calculations the diameter of the secondary spot on the sensor must cover approximately three pixel widths [4]. Therefore, the pixel spacing on the sensor must be approximately 7.5×10^{-6} m between pixel centers. This means that the extra spot diameter will cover approximately 7000 pixels. Because the sensor will be much smaller than this, the intensity of the extra spot will be nearly constant over the sensor. The extra spot will add approximately uniform background noise to the entire sensor which will effectively add to the dark current noise inherent in the sensor.

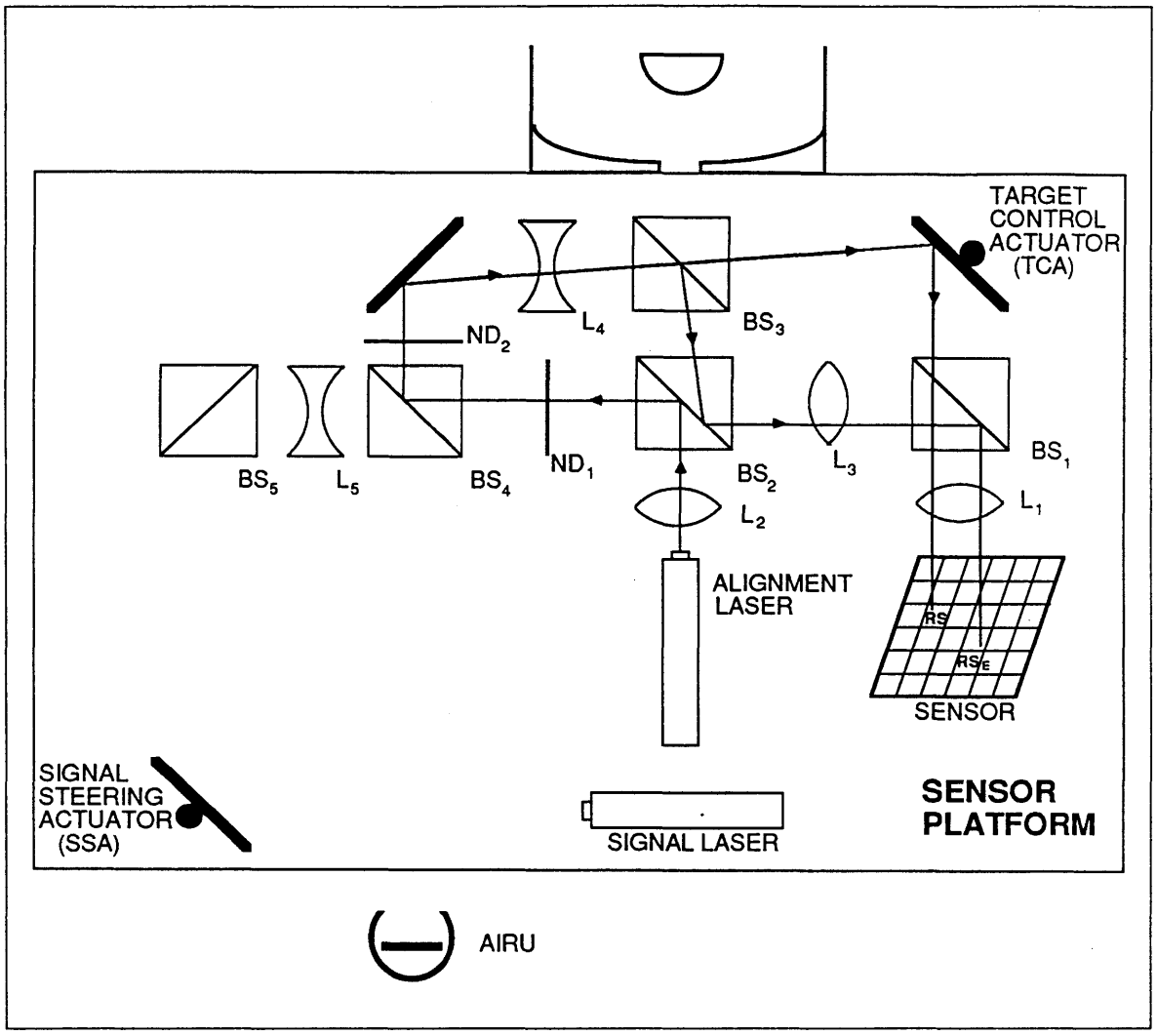

Figure 1.3.1-9 Direct Projection Method Reference Spot Optical Paths

The paths traced by the TCA reference spot (RS) and its extra (RS_E) are shown in Figure 1.3.1-9. Both paths transmit through lens L2, reflect from BS2, transmit through neutral density filter ND1, and reflect from BS4. They then transmit through neutral density filter ND2, reflect from the flat mirror, and transmit through compensation lens L4. When they reach BS3 the two paths split. The reference spot transmits through BS3 and is then reflected from the TCA. It then transmits through BS1, through the focussing lens L1, and onto the sensor. The extra spot reflects from BS3, then reflects from BS2. It then transmits through

compensation lens L3, reflects from BS1, transmits through L1, and then reaches the sensor.

The energy multipliers can now be found for these two spots to be

$$m_{RS} = 0.5 \times 0.043 \times 0.5 \times 0.23 \times 0.1 \times 0.9$$
$$= 2.25 \times 10^{-4} \qquad (1.3.1\text{-}22)$$

$$m_{RSE} = 0.5 \times 0.043 \times 0.5 \times 0.23 \times 0.9 \times 0.5 \times 0.1$$
$$= 1.125 \times 10^{-4} \qquad (1.3.1\text{-}23)$$

The extra spot will contain almost as much energy as the reference spot. Once again, though, the energy of the extra spot will be diffused because it will be out of focus. L4 will collimate the beam which passed through L2, so the extra spot will be collimated when it reaches L3. L3 will focus the spot at a point O which is approximately 10.7 meters behind the focussing lens (Figure 1.3.1-10). The thin lens approximation indicates that the focussing lens will cause the extra spot to focus at the point i, where

$$i = \frac{1}{\frac{1}{f_{L1}} + \frac{1}{h1}} = \frac{1}{1 + \frac{1}{10.7}} m = 0.914 \text{ m} \qquad (1.3.1\text{-}24)$$

where it is assumed that the distance between lenses L3 and L1 is negligibly small. Because of the similar triangles, the diameter of the resulting spot is

$$d_{RSE} = \frac{(f_{L1} - i)d}{i} = 4.72 \times 10^{-3} \text{ m} \qquad (1.3.1\text{-}25)$$

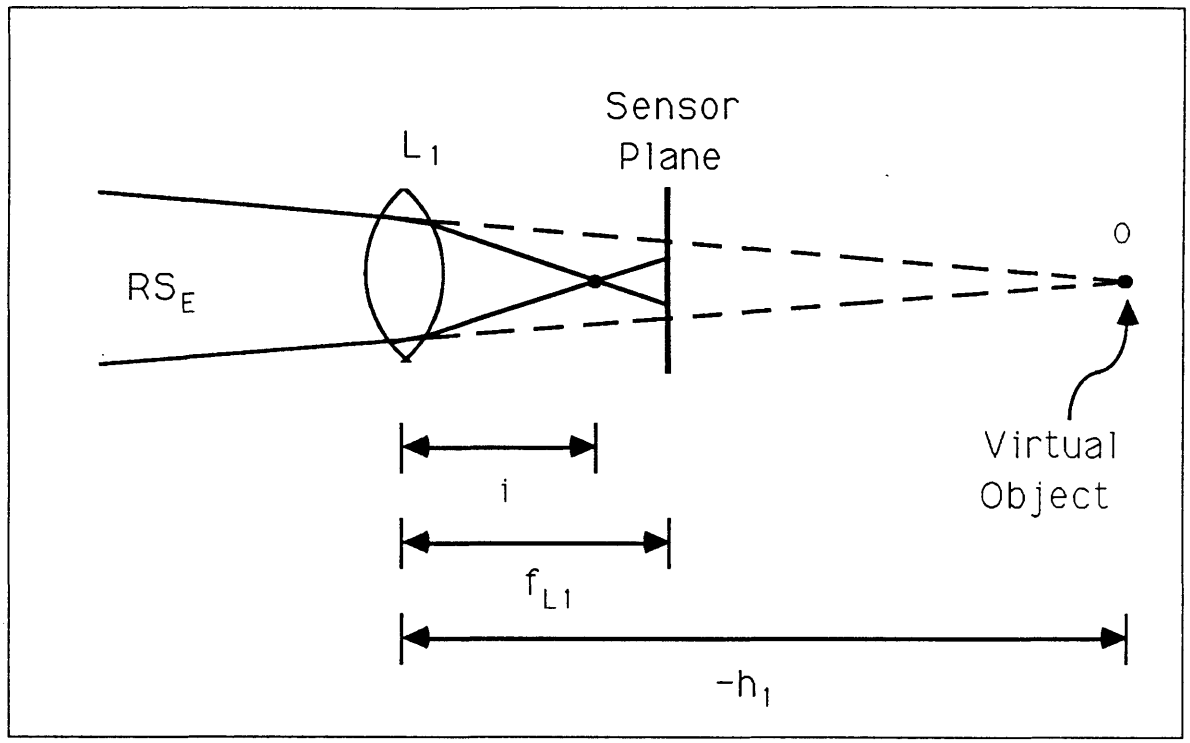

Figure 1.3.1-10 Focal Point of Extra Reference Spot

$$A_{RSE} = \frac{(d_{RSE})^2}{4}\pi = 1.75 \times 10^{-5}\ m^2 \qquad (1.3.1\text{-}26)$$

The size of the reference spot on the sensor will be the same as the secondary spot, which means that the ratio of the intensity of the reference spot to the intensity of the extra spot will be

$$\frac{I_{RS}}{I_{RSE}} = 7.0 \times 10^4 \qquad (1.3.1\text{-}27)$$

So the reference spot will be about five orders of magnitude brighter than

the extra spot. The extra spot will have a diameter of approximately 5800 pixels, so its energy will be very evenly distributed across the sensor, again adding to the background noise level.

Figure 1.3.1-11 shows the paths followed by the pseudo star and two extra spots. The pseudo star originates at the alignment laser, transmits through L2 and BS2, and reflects from BS3. It transmits through compensation lens L4, reflects from the flat mirror, transmits through ND2, and transmits through BS4. It then reflects from the mirror on the stable member of the AIRU, back through BS4 and ND2, reflects from the flat mirror, transmits through L4, back to BS3. It reflects from BS3, reflects from BS2, and transmits through lens L3. From there it reflects from BS1, and is focussed on the sensor by lens L1. Because the spot reaches the focussing lens L1 as a collimated beam with a diameter of approximately five centimeters, its size on the sensor will be approximately the same as the size of the secondary spot SS.

The first extra spot PS_{E1} splits from the pseudo star the first time the pseudo star reaches BS4. It reflects from BS4, transmits through ND1, BS2, and lens L3, then reflects from BS1 and transmits through L1 to reach the sensor. The second extra spot PS_{E2} does not split from the pseudo star beam until it returns to BS3 from the AIRU. It then transmits through BS3, is reflected by the TCA, transmits through BS1 and L1, and then hits the sensor.

The energy multipliers can be calculated for the three spots to be

$$m_{PS} = (0.5 \times 0.9 \times 0.23 \times 0.5) \times (0.5 \times 0.23 \times 0.9) \times 0.5 \times 0.1$$
$$= 2.68 \times 10^{-4} \qquad (1.3.1\text{-}28)$$

$$m_{PSE1} = (0.5 \times 0.9 \times 0.23 \times 0.5) \times (0.043 \times 0.5) \times 0.1$$
$$= 1.11 \times 10^{-4} \qquad (1.3.1\text{-}29)$$

$$m_{PSE2} = (0.5 \times 0.9 \times 0.23 \times 0.5) \times (0.5 \times 0.23 \times 0.1) \times 0.9$$
$$= 5.36 \times 10^{-4} \qquad (1.3.1\text{-}30)$$

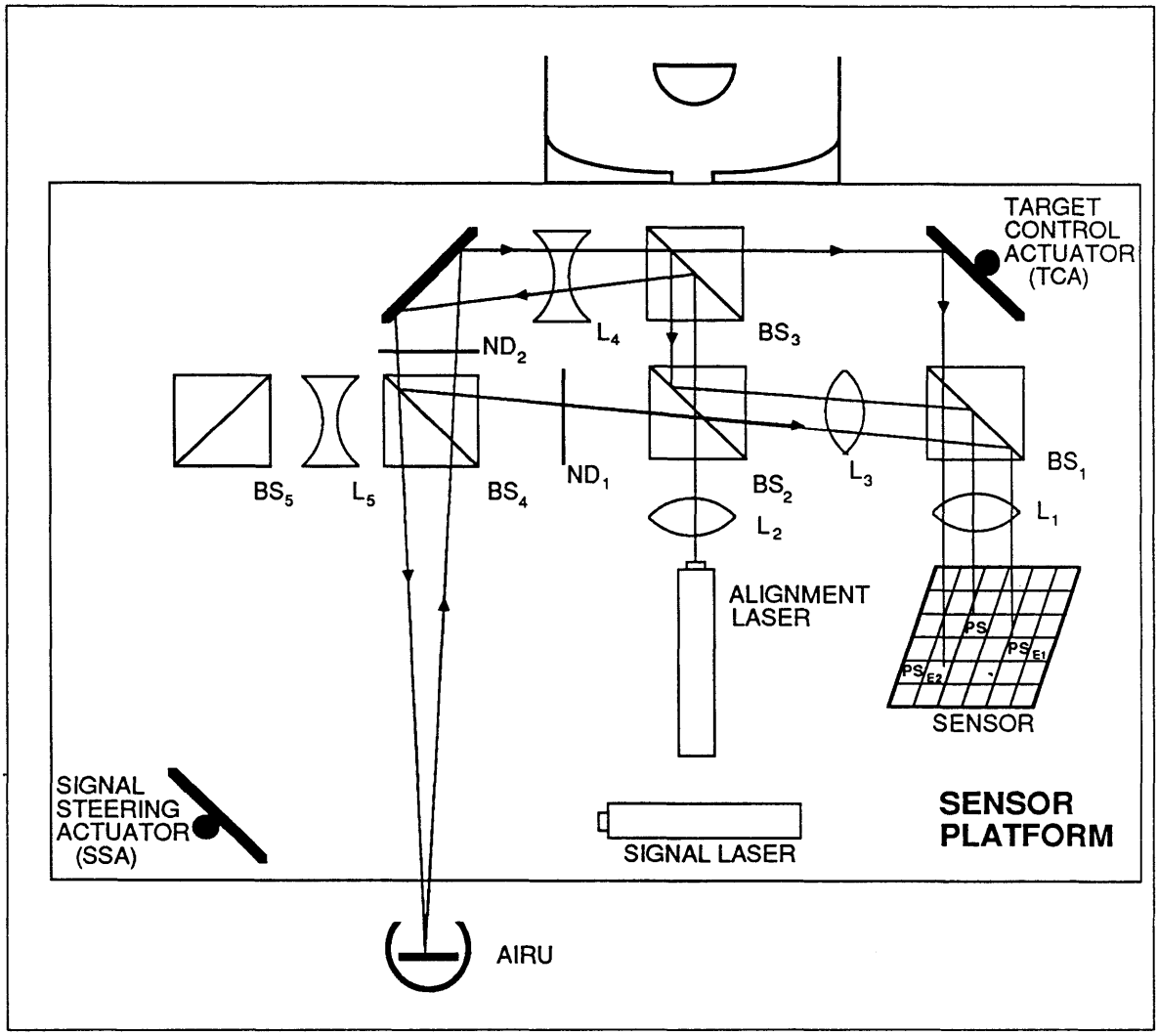

Figure 1.3.1-11 Direct Projection Method Pseudo Star Spot Optical Paths

It can be seen from the figure that the two extra spots will be defocussed by the compensation lenses. The resulting diameters of these spots can be calculated in a manner similar to the manner used to calculate the diameters of the extra secondary spot and extra reference spot.

PS_{E1} will reach lens L3 as a collimated beam with diameter approximately five centimeters. Since the extra reference spot RS_E also reaches L3 collimated and with a diameter of five centimeters, the resulting spot sizes will be the same. Thus,

$$d_{PSE1} = 4.72 \times 10^{-3} \text{ m} \quad (1.3.1\text{-}31)$$

$$A_{PSE1} = 1.75 \times 10^{-5} \text{ m}^2 \quad (1.3.1\text{-}32)$$

This means that the intensity ratio for the first extra pseudo star spot will be

$$\frac{I_{PS}}{I_{PSE1}} = 8.45 \times 10^{4} \quad (1.3.1\text{-}33)$$

Because the extra spot is so large its low intensity will be uniform over the area of the sensor, and will contribute uniform noise to the dark current level in the sensor.

The second extra pseudo star spot reaches lens L4 as a collimated beam heading toward the sensor. Lens L4 will cause the beam to diverge, as though the beam originated at a point source h_1 meters in front of the lens, with the lens removed. If the beam splitters and compensation lenses are small and close together, the beam will be focussed on the sensor in the same way that the extra secondary spot was (see Figure 1.3.1-11). So the size of the second extra pseudo star spot on the sensor will be the same as the size of the extra secondary spot. That is

$$d_{PSE2} = 5.15 \times 10^{-3} \text{ m} \quad (1.3.1\text{-}34)$$

$$A_{PSE2} = 2.09 \times 10^{-5} \text{ m}^2 \quad (1.3.1\text{-}35)$$

Again the diameter of the extra spot will be much larger than the sensor,

so its energy will be distributed quite evenly across the sensor. The ration of its intensity to the intensity of the desired pseudo star spot will be

$$\frac{I_{PS}}{I_{PSE2}} = 2.09 \times 10^{4} \qquad (1.3.1\text{-}36)$$

so the extra spot should just add to the background noise and dark current.

The next set of paths which will be described are the target spot paths. They were designed to allow light from the target to reach the sensor with as little attenuation as possible, while allowing the spot to be steered by the TCA. The target spot reaches the sensor platform after reflecting from the primary and secondary mirrors of the tracking telescope. As Figure 1.3.1-12 shows, the spot then reflects from the telescope exit beam splitter BS3, and then reflects from the TCA. It transmits through BS1, reaches lens L1 as a collimated beam, and is focussed on the sensor. Its size on the sensor will be the same as the size of the alignment spots since its aperture is the same and its wavelength is the same as the alignment spots. An extra target spot TS_E will also reach the sensor. This extra spot splits from the target spot at BS3, where it transmits through, and is reflected by BS2, and decollimated by lens L3. It then reflects from BS1 and reaches the sensor after transmitting through lens L1.

The energy multipliers of the two target spots are

$$m_{TS} = 0.9 \times 0.9 = 0.81 \qquad (1.3.1\text{-}37)$$

$$m_{TSE} = 0.1 \times 0.5 \times 0.1 = 5.0 \times 10^{-3} \qquad (1.3.1\text{-}38)$$

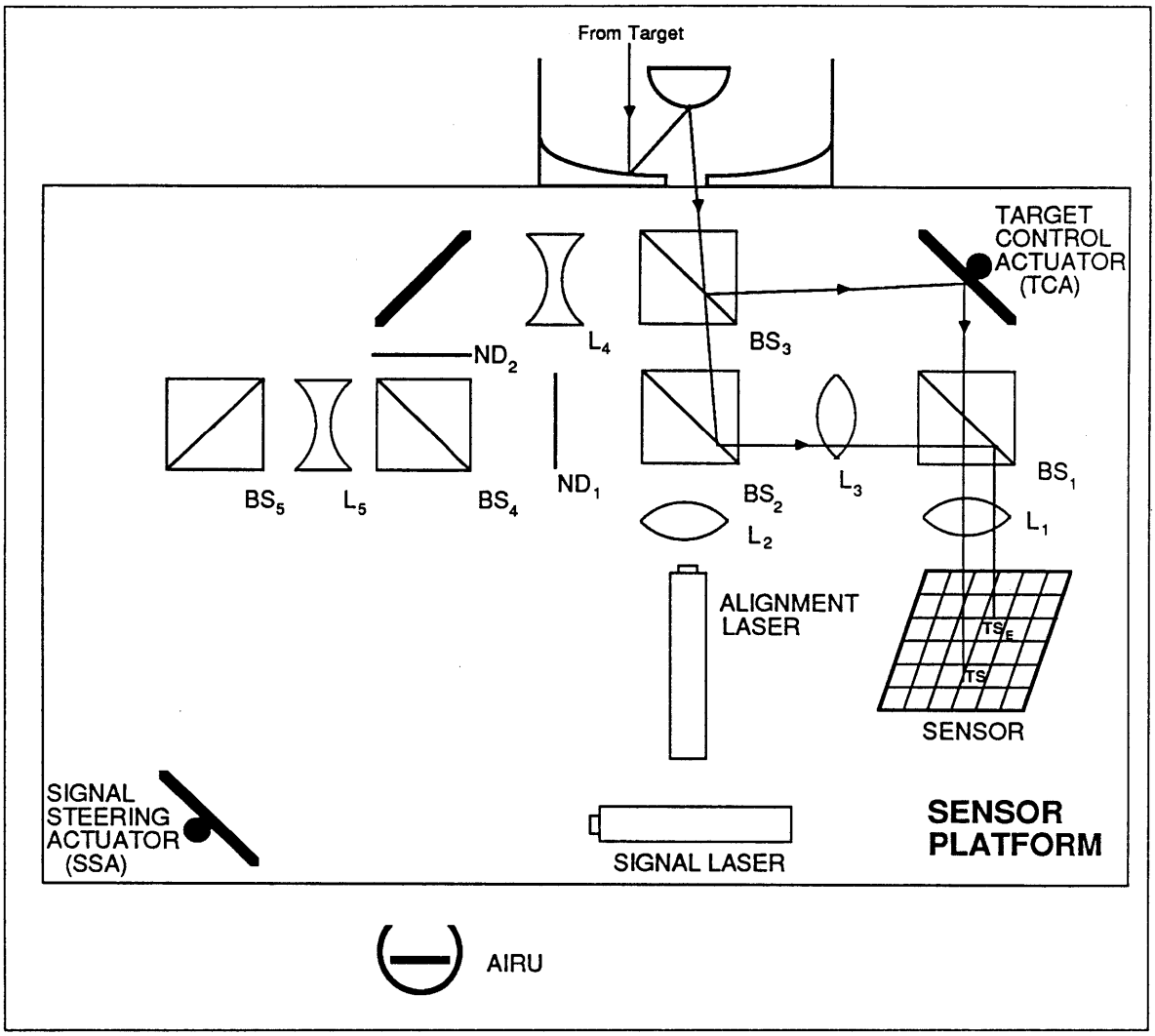

Figure 1.3.1-12 Direct Projection Method Target Spot Optical Paths

Notice that because these spots originate at a different source than the alignment spots do, these energy multipliers cannot be used to compare these target spots with the alignment spots. However it can be seen that the extra spot contains much less energy than the target spot, and the extra spot is also out of focus. The extra spot reaches lens L3 as a collimated beam, so its diameter and area on the sensor will be the same as the diameter and area of the extra reference spot R_{SE}.

$$d_{TSE} = 4.717 \times 10^{-3} \text{ m} \qquad (1.3.1\text{-}39)$$

$$A_{TSE} = 1.75 \times 10^{-5} \text{ m}^2 \qquad (1.3.1\text{-}40)$$

So the ratio of the intensity of the target spot to the extra spot will be

$$\frac{I_{TS}}{I_{TSE}} = 5.67 \times 10^{6} \qquad (1.3.1\text{-}41)$$

Because this ratio is so large, and the target energy which enters the telescope will be low, the extra spot will be an insignificant addition to the background noise level.

The last set of paths are for the beacon spot, and are shown in Figure 1.3.1-13. The beacon spot will allow the system to measure the direction of the signal laser beam so that it can be directed to the target satellite. The beacon spot originates at the signal laser, reflects from the signal steering actuator (SSA), and then reflects from BS5. The beam is made divergent then by lens L5, and then transmits through BS4, ND1, and BS2. The beam is recollimated by lens L3, and then it reflects from BS1, and is focussed on the sensor by L1. The two extra beacon spots split from the beacon spot beam just after that beam is made divergent. BS4 causes these two spots to be reflected to the AIRU, where they follow the paths of the pseudo star spots PS and PS_{E2}.

The energy multipliers for the beacon spots are

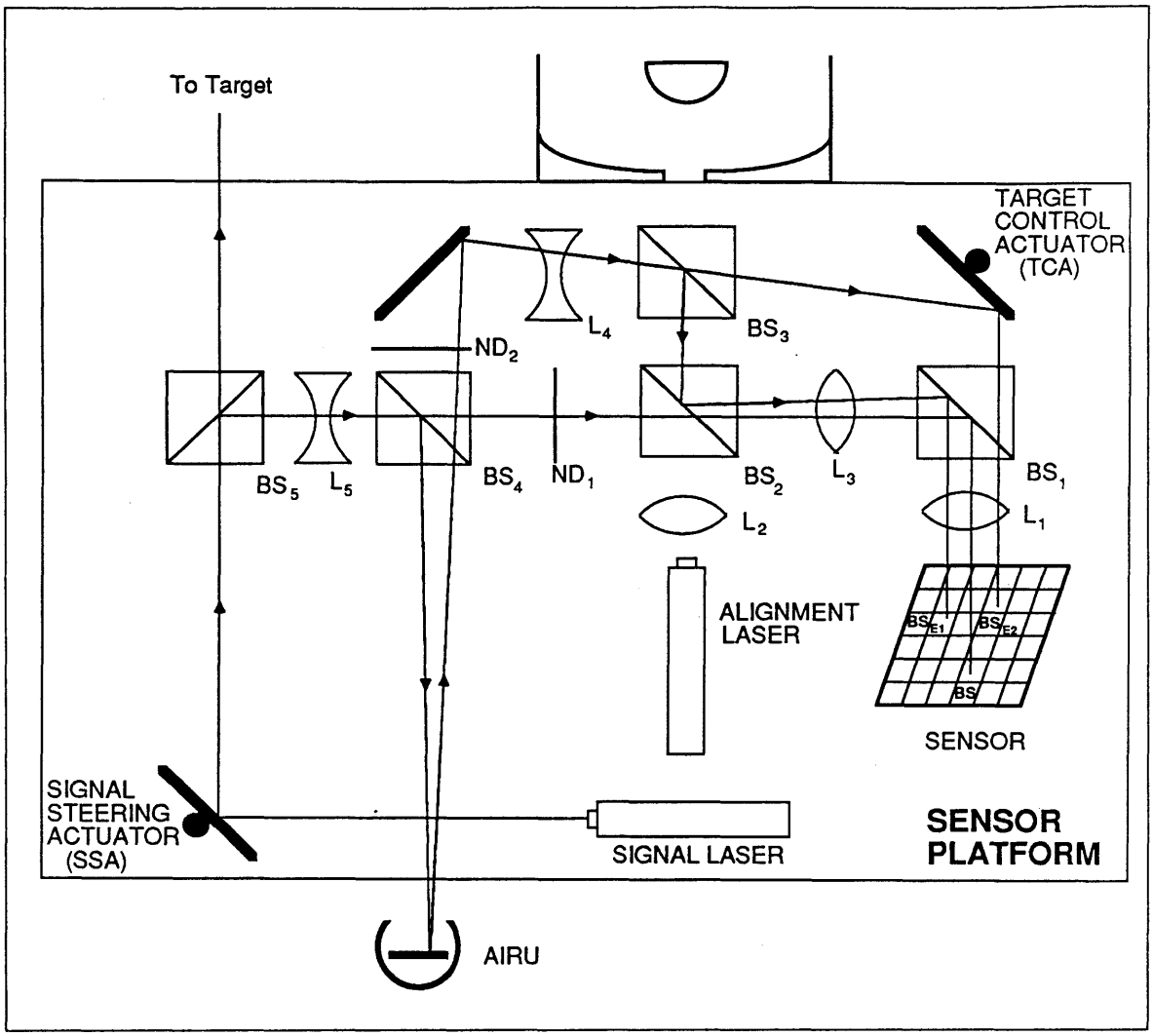

Figure 1.3.1-13 Direct Projection Method Beacon Spot Optical Paths

$$m_{BS} = 0.1 \times 0.5 \times 0.043 \times 0.5 \times 0.1$$
$$= 1.1 \times 10^{-4} \qquad (1.3.1\text{-}42)$$

$$m_{BSE1} = 0.1 \times 0.5 \times 0.5 \times 0.23 \times 0.9 \times 0.5 \times 0.1$$
$$= 2.6 \times 10^{-4} \qquad (1.3.1\text{-}43)$$

$$m_{BSE2} = 0.1 \times 0.5 \times 0.5 \times 0.23 \times 0.1 \times 0.9$$
$$= 5.2 \times 10^{-4} \qquad (1.3.1\text{-}44)$$

The beacon spot BS will reach the focussing lens as a collimated beam five centimeters wide, and will be focussed on the sensor as a spot the same diameter as the target spot and the other alignment spots. Both of the extra spots will be defocussed.

The first extra spot, BS_{E1}, will see lenses L3, L4, and L5 in its path. Since all three lenses will be very close together compared with their focal lengths, and since the absolute value of their focal lengths are all the same, the effects of L3 and L4 on the focus of this extra spot will approximately cancel. This means that the spot will be divergent at the focussing lens only due to lens L5. L5 causes the virtual point source to be located at the focal point of the secondary mirror as was the case with the extra pseudo star spot PS_{E2}. So, the diameter and area of BS_{E1} will be the same as for PS_{E2}. Thus,

$$d_{BSE1} = 5.15 \times 10^{-3} \text{ m} \qquad (1.3.1\text{-}45)$$

$$A_{BSE1} = 2.09 \times 10^{-5} \text{ m}^2 \qquad (1.3.1\text{-}46)$$

$$\frac{I_{BS}}{I_{BSE1}} = 1.77 \times 10^{4} \qquad (1.3.1\text{-}47)$$

As was the case for the other defocussed extra spots, light from the extra spot will be evenly distributed over the entire sensor and will add to the dark current.

The second extra spot BS_{E2} will see lenses L4 and L5 before reaching the focussing lens, and each of these lenses will cause the beam to diverge. To estimate the size of the spot on the array, it will be assumed that lenses L1, L4, and L5 have no space between them. Lens L5 will cause the beam to diverge as though it came from a point source a distance h_1 from the other lenses; see Figure 1.3.1-14. From the thin lens approximation for L4,

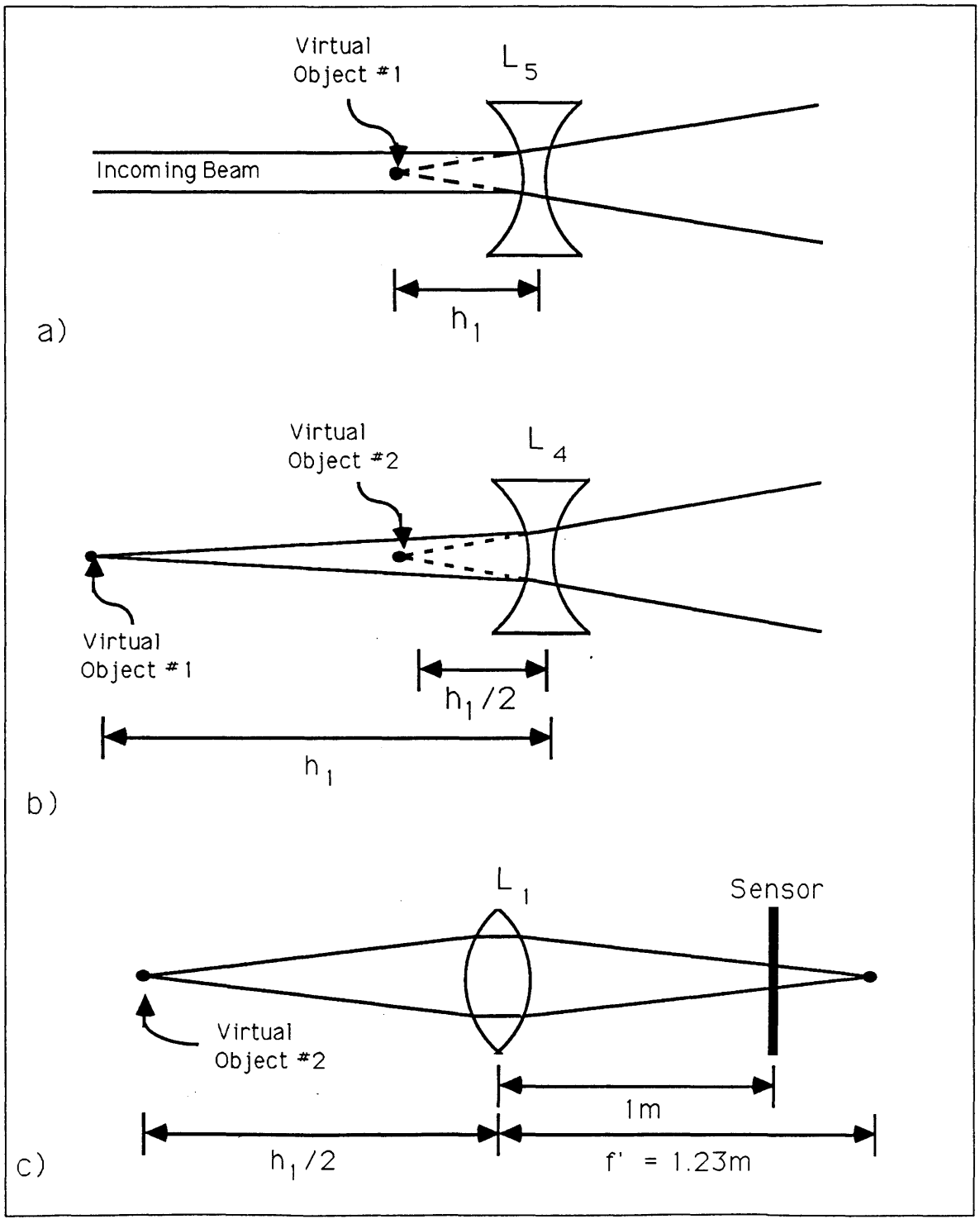

Figure 1.3.1-14 Focal Point of Second Extra Beacon Spot

$$\frac{1}{h1} + \frac{1}{i} = \frac{-1}{f} \qquad (1.3.1\text{-}48)$$

where i is the image distance and f is the focal length of L4. Thus,

$$i = \frac{-1}{\frac{1}{f} + \frac{1}{h1}} = \frac{-1}{\frac{2}{h1}} = \frac{-h1}{2} \qquad (1.3.1\text{-}49)$$

This means that the light which reaches L1 appears to have originated at a point source half the distance as the original virtual source. The focal point of the spot on the sensor side of L1 will be

$$\frac{1}{o} + \frac{1}{i} = \frac{1}{f} \qquad (1.3.1\text{-}50)$$

where f = 1 meter, and o = h1 / 2, so that i = 1.23 m. Using similar triangles, the diameter and area of BS_{E2} can then be found to be

$$d_{BSE2} = 1.15 \times 10^{-2} \text{ m} \qquad (1.3.1\text{-}51)$$

$$A_{BSE2} = 1.04 \times 10^{-4} \text{ m}^2 \qquad (1.3.1\text{-}52)$$

The resulting intensity ratio is

$$\frac{I_{BS}}{I_{BSE2}} = 4.0 \times 10^4 \qquad (1.3.1\text{-}53)$$

The intensity of this extra spot will be distributed evenly over the entire array because of the large size of the spot.

1.3.2 Control System Considerations

The goal of the control system is to place the communication laser beam exactly on the target satellite. Some of the sub-tasks which the system must also accomplish are to track the target with the tracking telescope, track the target with the AIRU, dampen the vibrational motion of the secondary mirror, and subtract vibration motion from the dim target spot. To achieve these five goals, there are five actuators which will affect the five spots whose paths were described in the last section. The Signal Steering Actuator (SSA) will be used to steer the signal laser beam to the target. The telescope actuator will move the telescope, but the bandwidth of this actuator will be too low to compensate for telescope vibrations, and will actually contribute to telescope vibration disturbances. The AIRU actuator will be used to cause the AIRU to track the target so that accurate LOS measurements can be made. The secondary mirror actuator will be used to compensate for vibrations of the secondary mirror. The Target Control Actuator (TCA) will be used to subtract vibration noise from the target image.

Before the control system can be designed, the physical system outputs must be characterized. That is, each of the spots which reach the sensor will be affected by different actuator angles, and the equations which describe how these spots are affected must be found. It must be noted that these equations describe the angles of the spots before they reach the focussing lens and the sensor. These equations are

$$\phi_{TS} = 2\theta_{TCA} + 2\theta_{SEC} + M(\theta_{TARG} - \theta_{TEL})$$

$$\phi_{PS} = 2\theta_{AIRU} - 2\theta_{TEL}$$

$$\phi_{RS} = 2\theta_{TCA}$$

$$\phi_{SS} = 2\theta_{SEC}$$

$$\phi_{BS} = 2\theta_{SSA}$$

(1.3.2-1)

The angle ϕ_{XX} designates the angle of an alignment spot before it reaches the focussing lens on the sensor platform. The angles θ_{TCA}, θ_{SEC}, and θ_{SSA} are the angles of the TCA, secondary mirror, and SSA respectively, and are measured with respect to their rest positions in the coordinate frame of the sensor platform. The angles θ_{AIRU} and θ_{TARG} are the pointing angle of the AIRU and angular position of the target, respectively, and are measured as absolute angles with respect to an inertial coordinate system. Finally, θ_{TEL} is the actual pointing angle of the telescope, and consists of two summed components, namely θ'_{TEL}, which is the pointing angle of the telescope actuator, and is measured in inertial coordinates, and θ_{DIST}, which is a disturbance angle of the telescope. M is the beam compression ratio of the telescope.

In matrix form, Equations (1.3.2-1) become

$$\begin{bmatrix} \phi_{TS} \\ \phi_{PS} \\ \phi_{RS} \\ \phi_{SS} \\ \phi_{BS} \end{bmatrix} = \begin{bmatrix} -M & 0 & 2 & 2 & 0 \\ -2 & 2 & 0 & 0 & 0 \\ 0 & 0 & 2 & 0 & 0 \\ 0 & 0 & 0 & 2 & 0 \\ 0 & 0 & 0 & 0 & 2 \end{bmatrix} \begin{bmatrix} \theta'_{TEL} \\ \theta_{AIRU} \\ \theta_{TCA} \\ \theta_{SEC} \\ \theta_{SSA} \end{bmatrix} + \begin{bmatrix} -M & M \\ -2 & 0 \\ 0 & 0 \\ 0 & 0 \\ 0 & 0 \end{bmatrix} \begin{bmatrix} \theta_{DIST} \\ \theta_{TARG} \end{bmatrix}$$

or

$$\underline{\phi} = C_1\underline{\theta}_A + L_1\underline{\theta}_D \qquad (1.3.2\text{-}2)$$

where $\underline{\theta}_A$ is the actuator angle vector and $\underline{\theta}_D$ is the disturbance angle vector. The angles of the spots at the focussing lens will not be available to the control algorithm. First they must be measured by the sensor, which has a gain and additive noise associated with it. The output of the sensor, including the noise, will be called the physical output vector, and will be designated $\underline{y}_p$.

$$\underline{y}_P = g_s\underline{\phi} + \underline{N}_s \qquad (1.3.2\text{-}3)$$

where g_s is the sensor gain, and

$$\underline{N}_s = \begin{bmatrix} n_1 \\ n_2 \\ n_3 \\ n_4 \\ n_5 \end{bmatrix}$$

is the noise on each spot measurement. A block diagram of the system from actuator inputs to physical outputs is shown in Figure 1.3.2-1.

The outputs which are most useful to the compensator are not the same as the physical outputs. For example, to keep the telescope pointing at the target the pointing error must be measured and regulated to zero. This means that a desired output might be $\theta_{TARG} - \theta_{TEL}$, but none of the physical outputs realizes this.

For a desired set of outputs to be realizable in the absence of noise, they must satisfy the equation

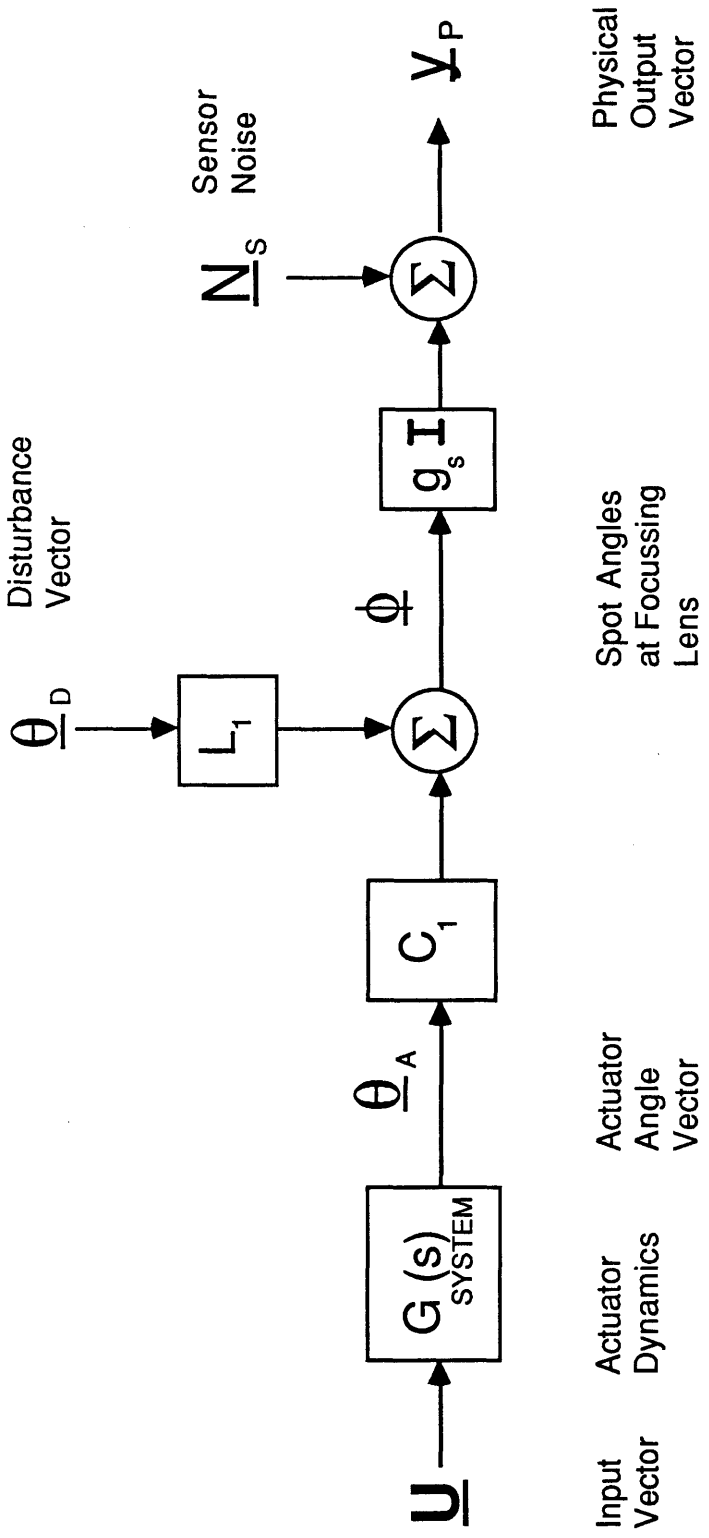

Figure 1.3.2-1 Block Diagram of Direct Projection Method Dynamic System.

$$\underline{y}_D = D\underline{y}_P \Big|_{\underline{N}_s = \underline{0}} = Dg_s\underline{\phi} \qquad (1.3.2\text{-}4)$$

because the desired outputs must be derived from the physical outputs. This also means that in the presence of sensor noise, the vector which the compensator will see will be the desired output with measurement noise. Thus,

$$\underline{y}_{DM} = Dg_s\underline{\phi} + D\underline{N}_s \qquad (1.3.2\text{-}5)$$

The desired outputs can now be chosen, and the appropriate D must be found. To do so, five errors are defined as

Telescope Tracking Error: $\epsilon_1 = M(\theta_{TARG} - \theta_{TEL})$
AIRU Tracking Error: $\epsilon_2 = M(\theta_{TARG} - \theta_{AIRU})$
TCA Tracking Error: $\epsilon_3 = M(\theta_{AIRU} - \theta_{TEL}) + 2\theta_{TCA} + 2\theta_{SEC}$
Secondary Tilt Error: $\epsilon_4 = 2\theta_{SEC}$
Signal Pointing Error: $\epsilon_5 = 2\theta_{SSA} + \theta_{TEL} - \theta_{AIRU}$

(1.3.2-6)

The telescope tracking error is the difference between the absolute angle of the target and the angle at which the telescope is pointing. Similarly, the AIRU tracking error is the difference between the angular position of the target and the angle at which the AIRU is pointing. The TCA tracking error is more complicated. The TCA is supposed to subtract the disturbance angle from the target spot. So, some means must be found to measure the high frequency disturbance on the telescope. If the AIRU is made to track the target very precisely at low frequencies, then θ_{AIRU} can be used to measure the telescope pointing error at high sampling

rates. The TCA is then used to compensate for the telescope pointing error at high frequencies. The secondary tilt error is a direct measurement of the tilt of the secondary mirror of the telescope. The signal pointing error is supposed to measure the telescope pointing error at high sampling rates and compensate for the error with θ_{SSA}, so that the signal beam is placed on the target. Finally, Equations (1.3.2-6) can be expressed in matrix form as

$$\underline{y}_D = \begin{bmatrix} \epsilon_1 \\ \epsilon_2 \\ \epsilon_3 \\ \epsilon_4 \\ \epsilon_5 \end{bmatrix} = \begin{bmatrix} -M & 0 & 0 & 0 & 0 \\ 0 & -M & 0 & 0 & 0 \\ -M & M & 2 & 2 & 0 \\ 0 & 0 & 0 & 2 & 0 \\ 1 & -1 & 0 & 0 & 2 \end{bmatrix} \begin{bmatrix} \theta'_{TEL} \\ \theta_{AIRU} \\ \theta_{TCA} \\ \theta_{SEC} \\ \theta_{SSA} \end{bmatrix} + \begin{bmatrix} -M & M \\ 0 & M \\ -M & 0 \\ 0 & 0 \\ 1 & 0 \end{bmatrix} \begin{bmatrix} \theta_{DIST} \\ \theta_{TARG} \end{bmatrix}$$

or

$$\underline{y}_D = C_2\underline{\theta}_A + L_2\underline{\theta}_D \qquad (1.3.2\text{-}7)$$

Equation (1.3.2-2) allows $\underline{\theta}_A$ to be found as a function of $\underline{\phi}$ according to

$$\underline{\theta}_A = C_1^{-1}(\underline{\phi} - \underline{L}_1\underline{\theta}_D) \qquad (1.3.2\text{-}8)$$

If this is substituted into Equation (1.3.2-7) and the result is solved for y_D, the result is

$$\underline{y}_D = C_2C_1^{-1}\underline{\phi} + (L_2 - C_2C_1^{-1}L_1)\underline{\theta}_D \qquad (1.3.2\text{-}9)$$

The desired outputs must be obtained directly from the physical outputs, without the disturbance vector $\underline{\theta}_D$ explicitly being measuring. According to Equation (1.3.2-9), this can only happen when

$$L_2 = C_2 C_1^{-1} L_1 \qquad (1.3.2\text{-}10)$$

In Appendix B it is shown that, for $M \neq 0$, this equation will always be satisfied. So Equation (1.3.2-9) can be simplified to

$$\underline{y}_D = C_2 C_1^{-1} \underline{\phi} \qquad (1.3.2\text{-}11)$$

By comparing Equation (1.3.2-11) to Equation (1.3.2-4) the matrix D can be found as

$$D = \frac{1}{g_s} C_2 C_1^{-1} \qquad (1.3.2\text{-}12)$$

Therefore, Equation (1.3.2-5) can be rewritten to express the desired output with measurement noise.

$$\underline{y}_{DM} = C_2 C_1^{-1} \underline{\phi} + \frac{1}{g_s} C_2 C_1^{-1} \underline{N}_s \qquad (1.3.2\text{-}13)$$

or

$$\underline{y}_{DM} = \frac{1}{g_s} C_2 C_1^{-1} \underline{y}_P \qquad (1.3.2\text{-}14)$$

Finally, Equation (1.3.2-2) can be used to substitute for $\underline{\phi}$ in Equation (1.3.2-13) above to yield

$$\underline{y}_{DM} = C_2\underline{\theta}_A + C_2C_1^{-1}L_1\underline{\theta}_D + \frac{1}{g_s} C_2C_1^{-1}\underline{N}_s \qquad (1.3.2\text{-}15)$$

Figure 1.3.2-2 shows a block diagram from actuator inputs to $\underline{y}_{DM}$. Figure 1.3.2-3 shows the same system, with the disturbance entering the system at the system outputs.

In order to control the system with output feedback, the system must be both controllable and observable. The observability criterion can be checked in parts, starting with the desired outputs. To be observable, it must be possible to reconstruct the states of the system at time t0, given the system inputs and outputs from time t_0 to a finite time t_1 [5, pg 66]. Because both the noise and disturbance vectors originate outside the system, they can be treated as system inputs which are known quantities for $t > t_0$ when assessing the observability criterion. This means that the actuator angles $\underline{\theta}_A$ can be found for all $t > t_0$ from Equation (1.3.2-14) as long as C_2 is invertible. Thus,

$$\underline{\theta}_A = C_2^{-1}(\underline{y}_{DM} - C_2C_1^{-1}L_1\underline{\theta}_D + \frac{1}{g_s} C_2C_1^{-1}\underline{N}_s) \qquad (1.3.2\text{-}16)$$

In this equation $\underline{y}_{DM}$ are the known outputs, and $\underline{\theta}_D$ and $\underline{N}_s$ are the disturbances and noise inputs respectively, both of which are known. Thus the system is observable if and only if it is observable from the actuator angles.

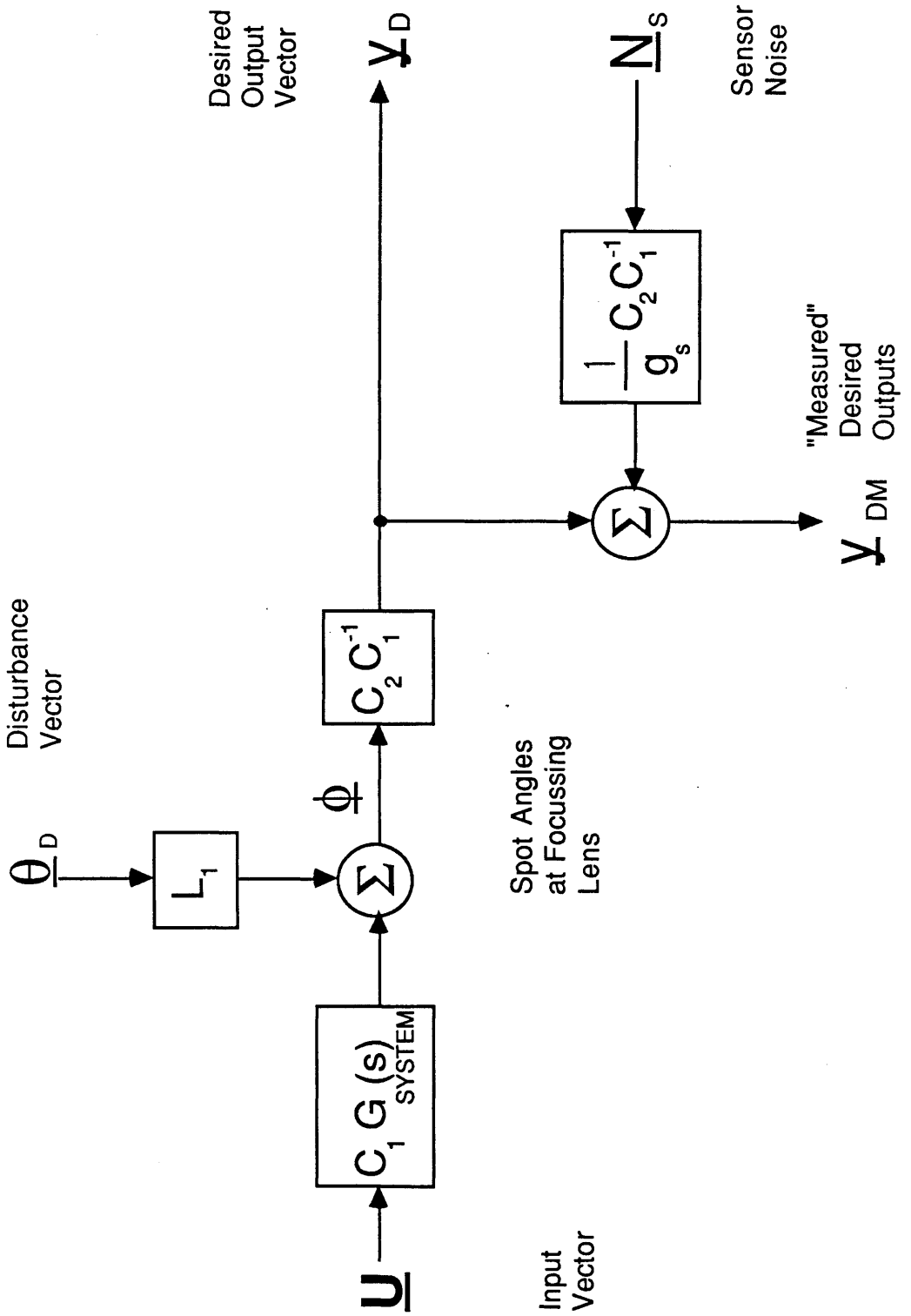

Figure 1.3.2-2 Block Diagram of System From Actuator Inputs to Desired Outputs.

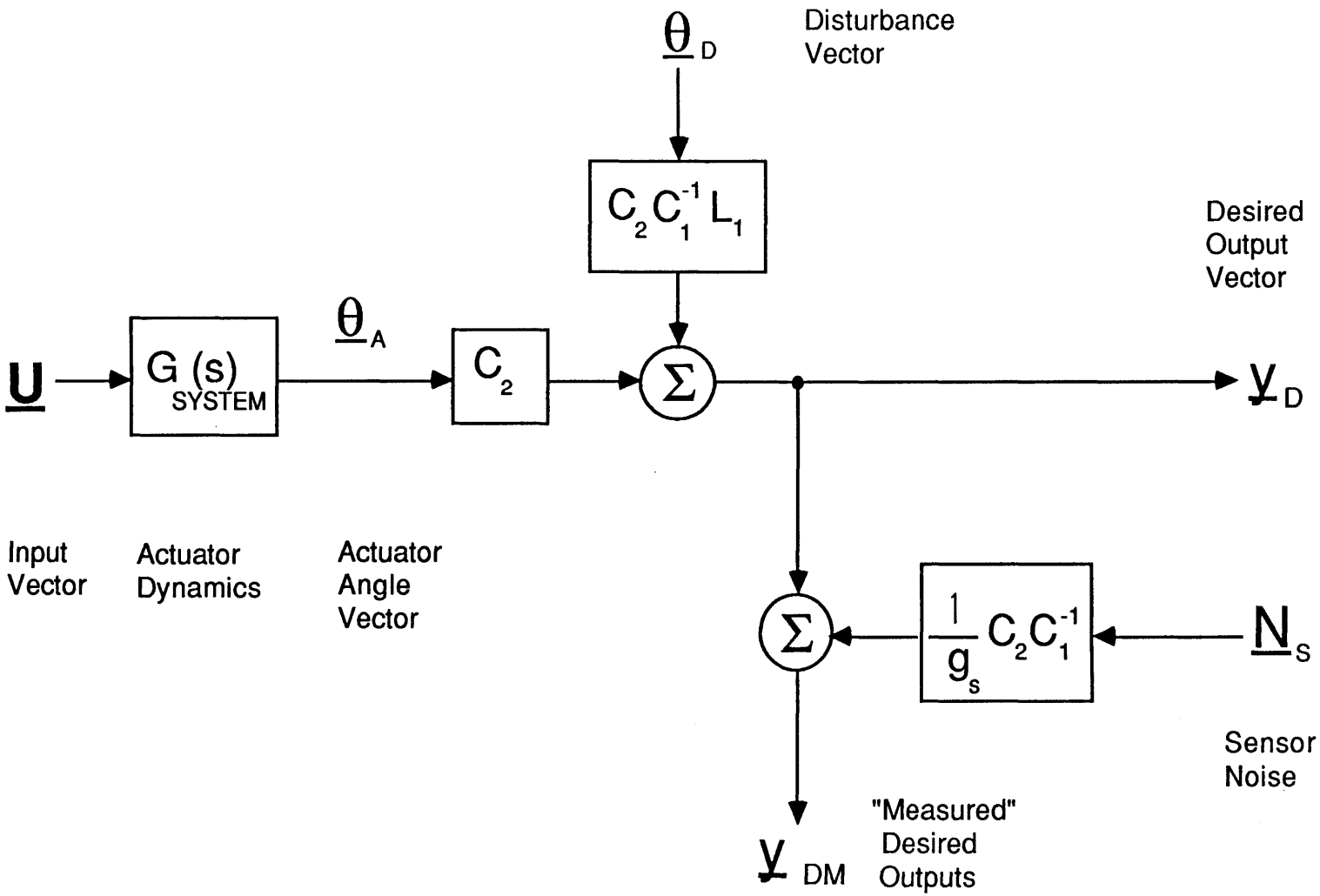

Figure 1.3.2-3 Block Diagram of System Showing Observability Through C_2.

1.3.3 Implementation Problems

The last topic to be discussed concerning the direct projection method is the problems which must be overcome when the method is implemented. First the problems which are inherent to this method are discussed. Problems which must be overcome by technological advances are discussed second.

One of the major problems with the direct projection method is that many useless extra spots reach the sensor. It was shown in Section 1.3.1 that these spots are very defocussed, resulting in low intensity and fairly uniform illumination of the entire sensor. Although this illumination is low intensity, it may add significantly to the background noise of a "quiet" sensor. It is impossible to say how much this affects the accuracy of the spot centroid calculations without knowing the actual specifications of the sensor to be used.

It was also noted in Section 1.3.1 that the energy multipliers could be used to compare only the spots which originated at the alignment laser. The only thing that is known about the target spot intensity is that it is much lower than the alignment spot intensities, which requires that the target position be sampled at a much lower rate than the positions of the alignment spots. So, even though the intensities of the extra spots are much lower than the alignment spot intensities, they may be significant when compared with the target spot intensity.

Another problem which is inherent in this design is that the disturbances are subtracted from the target image, rather than nulled. The disturbance is measured, and then subtracted from the target image by the TCA. Unfortunately, if there is an error in the measurement of the disturbance, then this error will show up in the target image, smearing the image on the sensor. Because this error does not appear in a feedback loop, it will not be attenuated, so the disturbance measurement err will

add directly to the system error budget.

In addition to the two problems inherent with the direct projection method, several technological advances are necessary to make it work well. First, a high speed, low noise mosaic array sensor must be developed. The disturbances which are expected will occur at frequencies as high as 100 Hz. This means that to get an attenuation factor of 10 or more at this frequency the feedback loop must cross over unity gain at 1000 Hz or more. Thus, the sensor must be able to track spots with a sampling rate as high as 10000 to 20000 samples per second. Also, the pixels in the array must have $\approx 10\mu m$ spacing center to center to accommodate the size of the spots which will appear on the sensor. Further, to manage the sensor, a computer using a parallel architecture will probably be needed to transfer sensor data, centroid each spot, and implement the fast control algorithm.

An AIRU must be developed which is well modelled and very accurate, as well as highly isolated from vibrational disturbances on its outside case. As was noted before, The Charles Stark Draper Laboratory is currently developing an AIRU which may be useful in this application. Additionally, the assumption was made that the sensor platform was rigidly attached to the back of the primary mirror of the tracking telescope. This assumption can only be made if the primary mirror itself is rigid. Since this mirror is a circular structure five meters in diameter, this will probably be the technological limitation of the pointing and tracking system. However, because the ability to track a dim target is a specification of the system, any tracker design will require a large telescope, and the rigidity of the primary mirror will be a limitation for any tracking system.

1.4 Comparison of the Direct and Indirect Projection Methods

In the preceding two sections, trackers using two methods of projecting the pseudo star onto the sensor platform were designed. The second stage of this thesis requires that one of these methods be chosen so that a scaled tracker can be designed and tested in the laboratory. To decide which method to use in the scaled system, the two methods will be compared on the basis of the implementation problems foreseen for a full scale system.

As the previous section showed, there are two problems with the direct projection method which might cause implementation to be difficult. First, the extra spots which reach the sensor can interfere with the accuracy to which the desired spots can be centroided. It is not clear, however, that these spots will interfere, or that other filtering methods such as using polarized filters will not be able to solve the problem. The second problem is that the disturbances are subtracted from the target image rather than nulled. This means that sensor non-linearities will cause a major degradation to the disturbance rejection capabilities of the tracker. However, non-linear sensors can be linearized by using lookup tables to translate between measured and actual spot positions.

The implementation problems for the indirect projection method can be summarized as follows. First, the indirect projection method requires a large extended corner cube to be mounted on the tracking telescope. This corner cube will add weight and complexity to the tracker, but is not a major drawback. Second, the pseudo star used in this method requires that a laser be mounted on the AIRU. The size and weight that this would add to the AIRU stable member makes this an undesirable proposition. More importantly, the temperature gradients which the laser would cause in the AIRU may make the thermal design of the AIRU unsolvable. The last problem with the indirect projection method is that the pseudo star spot will be two orders of magnitude larger than the other three spots when the spots reach the sensor. The requirement that the system have only one sensor

means that either the pseudo star spot will cover many pixels on the sensor, or the other spots will be much smaller than a pixel. But in order to get an accurate centroid measurement, a spot diameter must be about three pixels wide. This size mismatch would be very difficult to overcome.

Because the problems inherent with the direct projection method appear to be solvable, and two of the problems with the indirect projection method appear to be very difficult to solve, the direct projection method is explored further in this thesis. In the next chapter, the system designed in Section 1.3 is scaled and a control system is designed, and in Chapter 3 the scaled system is tested in the laboratory.

CHAPTER 2
SCALED TRACKER DESIGN

2.0 INTRODUCTION

There are several advantages of the direct projection method over the indirect method, as was described in Chapter 1. In this chapter, a scaled tracker employing the direct projection method is designed using available hardware. Of interest here are any major drawbacks to the design which have not yet been considered. The object of the scaled tracker is not to examine every possible implementation problem or every error source in the full scale system, but to test its underlying concept. That is, the scaled system is to demonstrate that a dim target can be tracked in the presence of sensor platform vibrations using the direct pseudo star projection method. With this objective in mind, the full scale system developed in the last chapter is scaled and simplified to allow a small laboratory system to be built. Then, a dynamic model is developed and the control system will be designed and tested. Test results are presented in the next chapter.

2.1 SCALED OPTICAL PATHS

2.1.0 Introduction

To test the direct pseudo star projection method, its optical paths are scaled to dimensions which are convenient for a laboratory

experiment, and simplified to make evaluation of the concept easier. The most important size limitation in the laboratory is the size of the tracking telescope. This telescope will have a front aperture diameter of approximately six inches, and a beam compression ratio of three. After the scaled optical paths are designed, the spot position equations are calculated for the scaled tracker. These equations are used in the two subsequent sections of this chapter to model the system and design a controller for the system.

2.1.1 Optical Path Description

The principal problem which this thesis addresses is the problem of tracking a dim target in the presence of sensor platform disturbances. The problem of pointing the signal laser at the target is not the main thrust of this thesis. Once the alignment of the target is known with respect to the telescope, it is a relatively simple matter to transfer that alignment to the signal beam. Thus, the beacon can be removed from the optical paths of the scaled system. Likewise, the secondary spot may be removed from the optical paths. This can be done without seriously changing the system because the laboratory model is quite small, and the secondary mirror can be mounted very rigidly to reduce its disturbance amplitude. Also, the accuracy of the sensor will not be as great as the sensor required for the full scale system, which means that the secondary mirror motion will not be large enough to be measured. In addition, the construction of the laboratory telescope prohibits the installation of an actuator which could control the secondary mirror.

By removing the beacon spot and the secondary spot, the size of the system is reduced from five inputs and five outputs to three inputs and three outputs. The three remaining spots which the sensor will see are the target, reference, and pseudo star spots. The actuators to be

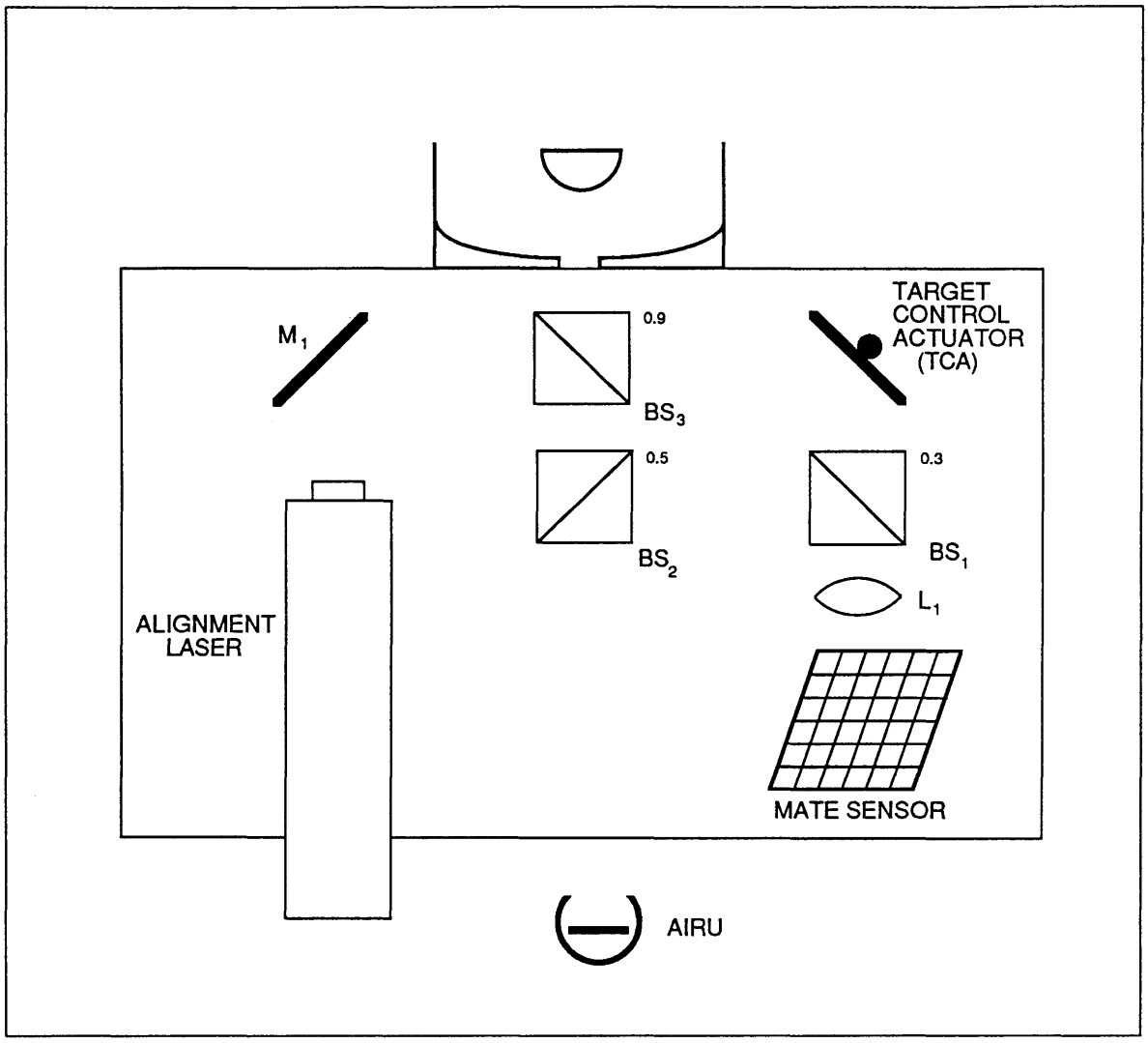

Figure 2.1.1-1 Scaled Alignment Transfer System Sensor Platform

controlled are the AIRU, TCA, and telescope actuator.

In the full scale system, the alignment laser is located directly behind the exit aperture of the telescope. This is done to allow energy from the alignment laser to reflect from the secondary mirror and reach the sensor as the secondary spot. In the scaled paths, the secondary spot will be eliminated, so the alignment laser will be offset from the telescope exit aperture, as shown in Figure 2.1.1-1.

Because there is no need to compensate for the beam divergence

which was caused by the secondary mirror in the full scale design, there is no need to place compensation lenses on the sensor platform. The only lens that is needed is at the sensor to focus the collimated beams on the sensor. The beam splitters in the scaled system have slightly different reflectivities than in the full scale system. These differences are used to eliminate the need for neutral density filters to match the alignment spot intensities. To explain the details of the optical paths more clearly, each path will be described individually.

The target spot follows exactly the same path in the scaled system as it does in the full scale system. It reaches the sensor platform after reflecting from both the primary and secondary mirrors of the telescope, as shown in Figure 2.1.1-2. It then reflects from the telescope exit beam splitter, and reflects from the TCA. Finally, the target spot transmits through BS1, and then is focussed on the sensor by lens L1. As in the full size system, there will be an extra spot associated with the target spot. This spot splits from the target spot at BS3. It transmits through BS3, and transmits through BS2 to the AIRU. It reflects from the mirror on the stable member of the AIRU, and then reflects from BS2. Finally, it reflects from BS1 and is focussed on the sensor by L1.

Before calculating the energy multipliers of the two spots, the reflectivity factors of the three beam splitters must be chosen. Rather than attempting to optimize the reflectivity factors of the beam splitters, these values are chosen to simulate the actual full scale system as closely as possible. For this reason, the reflectivity of BS3 is chosen to be 0.9, and the reflectivity of BS2 is chosen to be 0.5. In order to match the energy multipliers of the two alignment beams without using neutral density filters, the reflectivity of BS1 is chosen to be 0.3 rather than the value of 0.1 used in the full scale design.

The energy multipliers of the target spot and the extra spot associated with it are

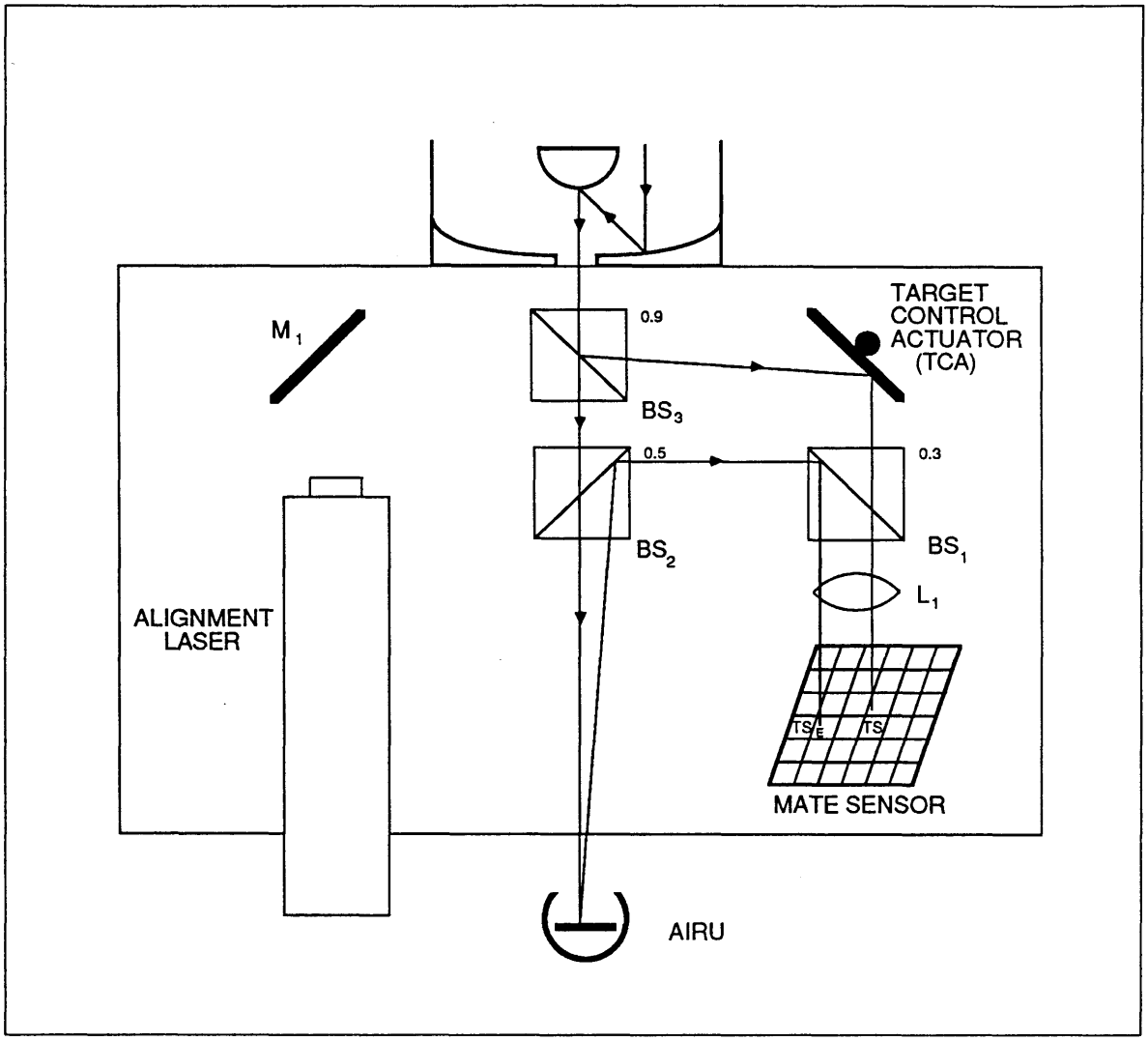

Figure 2.1.1-2 SATE Target Spot Optical Paths

$$m_{TS} = 0.9 \times 0.7 = 0.63 \qquad (2.1.1\text{-}1)$$

$$m_{TSE} = 0.1 \times 0.5 \times 0.5 \times 0.3 = 7.5 \times 10^{-3} \qquad (2.1.1\text{-}2)$$

Because there are no compensation lenses in the optical paths and both beams are collimated when they reach lens L1, the intensity ratio is

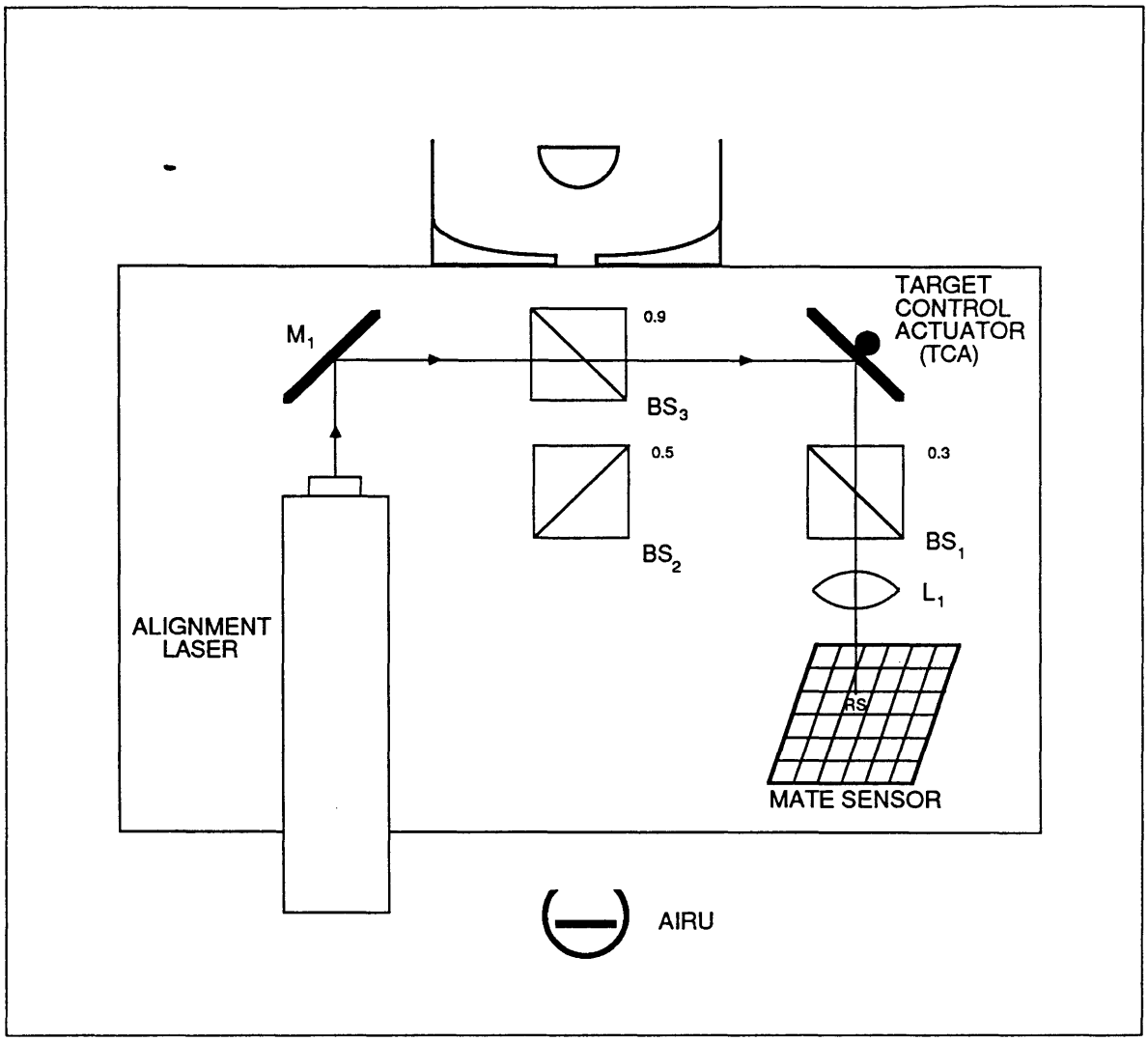

Figure 2.1.1-3 SATE Reference Spot Optical Paths

$$\frac{I_{TS}}{I_{TSE}} = \frac{m_{TS}}{m_{TSE}} = \frac{0.63}{7.5 \times 10^{-3}} = 84 \qquad (2.1.1\text{-}3)$$

This ratio is not very large, especially when compared with the ratio of 7.45×10^{6} for the full scale system. It can be expected that this large decrease in the signal to noise ratio will degrade the performance of the scaled system if the extra spot hits the sensor in the same window in

which the target falls, and if the intensity of the extra spot is significant compared with the dark current noise of the sensor.

As shown in Figure 2.1.1-3, the reference spot originates at the alignment laser, reflects from flat mirror M1, and transmits through BS3 to reach the TCA. It reflects from the TCA and transmits through BS1, and then reaches the sensor after being focussed by L1. Notice that no extra spots are generated by this path. The energy multiplier for this spot is

$$m_{RS} = 0.1 \times 0.7 = 0.07 \qquad (2.1.1\text{-}4)$$

The path of the pseudo star spot also generates no unwanted spots, as shown in Figure 2.1.1-4. It originates at the alignment laser, reflects from M1 and then BS3, to BS2. It transmits through BS2, reflects from the AIRU mirror, and then reflects from BS2. It travels to BS1, where it is reflected to L1 and is focussed on the sensor. The energy multiplier for the pseudo star spot is

$$m_{PS} = 0.9 \times 0.5 \times 0.5 \times 0.5 = 0.0675 \qquad (2.1.1\text{-}5)$$

The scaled optical paths are now designed. The scaling allows the sensor platform optics to be greatly simplified by eliminating the beacon spot and the secondary spot. The simpler optics lead to fewer unwanted spots reaching the sensor, thus reducing the possibility of confusing the spot tracking algorithm of the sensor. The energy multipliers of the two remaining alignment spots are matched to within 4% by adjusting the reflectivity of the beam splitter BS1. The area of greatest concern is that the intensity ratio of the target spot to extra target spot is only 84, which means that the extra spot will have to be spatially separated from the target spot on the sensor.

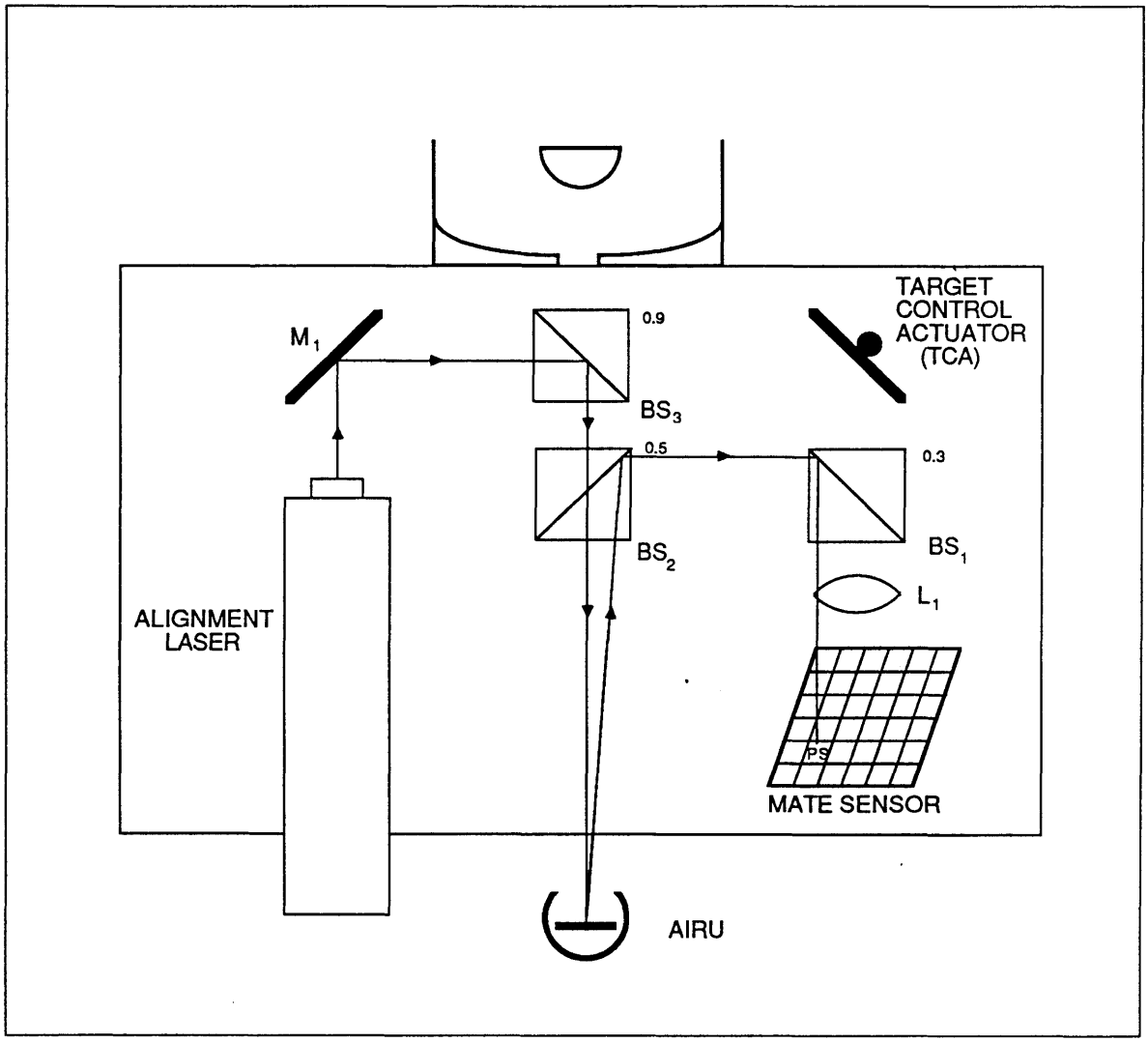

Figure 2.1.1-4 SATE Pseudo Star Optical Paths

Of primary concern in the original design was the ability for the system to track a dim target very accurately. Eliminating the secondary spot and the signal laser do not affect this aspect of the tracker. Despite the simplification, the laboratory system is interesting because it retains the dim target tracking capability of the original, though it will be less accurate.

2.1.2 Spot Position Equations

Now that the optical paths have been designed, a static model of the system can be formulated. That is, the relationship of the beam angles just before the beams reach the focussing lens can be related to the actuator angles at any particular instant, without yet describing the dynamics of the actuators. These relations can be put into the same form used in Section 1.3.2 according to

$$\phi_{TS} = 2\theta_{TCA} + M(\theta_{TARG} - \theta_{TEL})$$

$$\phi_{PS} = 2\theta_{AIRU} - 2\theta_{TEL}$$

$$\phi_{RS} = 2\theta_{TCA} \qquad (2.1.2\text{-}1)$$

As in Section 1.3.2, ϕ_{xx} designates the angle of each alignment spot just before it reaches the focussing lens L1. The angle θ_{TCA} is the angular deflection of the TCA relative to its equilibrium position, measured in the local coordinates of the sensor platform. The angle θ_{TARG}, θ_{TEL}, and θ_{AIRU} are the target, telescope, and AIRU angles measured in absolute inertial coordinates. It should be noted that these three equations are identical to the first three equations of (1.3.2-1) where secondary mirror motion is neglected.

Equation 2.1.2-1 can be placed in matrix form as

$$\begin{bmatrix} \phi_{TS} \\ \phi_{PS} \\ \phi_{RS} \end{bmatrix} = \begin{bmatrix} -M & 0 & 2 \\ -2 & 2 & 0 \\ 0 & 0 & 2 \end{bmatrix} \begin{bmatrix} \theta'_{TEL} \\ \theta_{AIRU} \\ \theta_{TCA} \end{bmatrix} + \begin{bmatrix} -M & M \\ -2 & 0 \\ 0 & 0 \end{bmatrix} \begin{bmatrix} \theta_{DIST} \\ \theta_{TARG} \end{bmatrix}$$

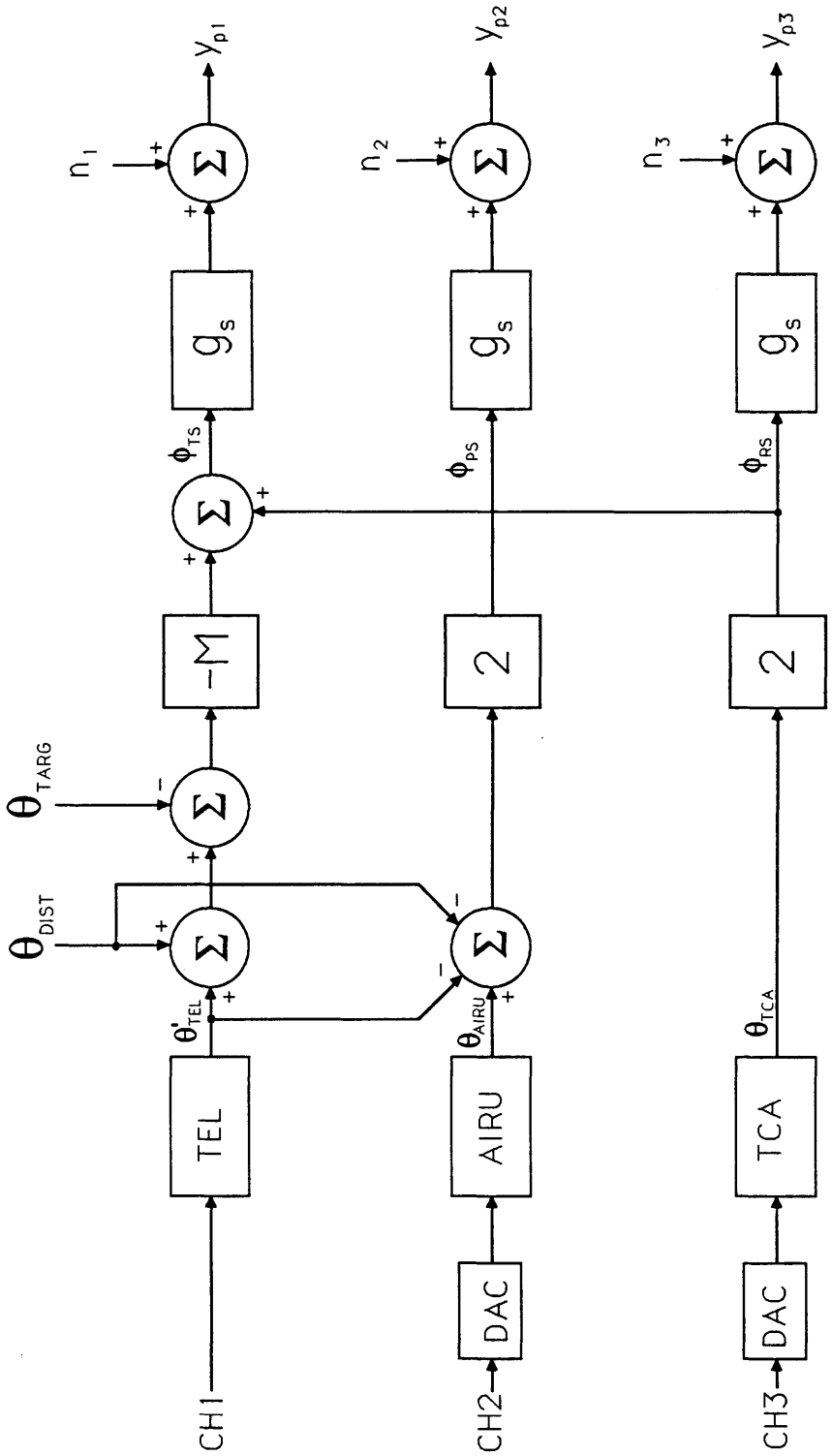

Figure 2.1.2-1 Block Diagram of SATE Physical Plant

$$\underline{y}_D = \begin{bmatrix} \epsilon_1 \\ \epsilon_2 \\ \epsilon_3 \end{bmatrix} = \begin{bmatrix} -M & 0 & 0 \\ 0 & -M & 0 \\ -M & M & 2 \end{bmatrix} \begin{bmatrix} \theta'_{TEL} \\ \theta_{AIRU} \\ \theta_{TCA} \end{bmatrix} + \begin{bmatrix} -M & M \\ 0 & M \\ -M & 0 \end{bmatrix} \begin{bmatrix} \theta_{DIST} \\ \theta_{TARG} \end{bmatrix}$$

or

$$\underline{y}_D = C_2\underline{\theta}_A + L_2\underline{\theta}_D \qquad (2.1.2\text{-}4)$$

Using exactly the same steps as in Section 1.3.2, the desired outputs can be found from

$$\underline{y}_{DM} = C_2C_1^{-1}\underline{\phi} + \frac{1}{g_s} C_2C_1^{-1}\underline{N}_s \qquad (2.1.2\text{-}5)$$

or

$$\underline{y}_{DM} = \frac{1}{g_s} C_2C_1^{-1}\underline{y}_P \qquad (2.1.2\text{-}6)$$

Now that the desired outputs have been determined, only the actuator dynamics, sensor gain, and telescope magnification factor must be determined before the controller can be designed. In the next section a model for the complete dynamic system is determined, and in the following section the controller is designed.

2.2 System Models

2.2.0 Introduction

In Section 2.1 the optical paths of the direct pseudo star projection method tracker were modified for the scaled system. This section discusses the modelling of the dynamics of the tracker. First, the sensor gain, which is known to be non-linear, is characterized, and the magnification factor of the telescope is measured. Then, the dynamics of each of the three actuators are measured and a model is fit to the measurements. Finally, the full dynamic system model is developed so that the control system can be designed in the Section 2.3.

2.2.1 Characterizing the Sensor

The sensor which will be used in the Scaled Alignment Transfer Experiment is known to be very non-linear. Fortunately, when a spot is kept near the center of a pixel, the sensor output is quite linear. It is therefore desirable to keep the physical outputs of the system as close to the center of a pixel as possible. Unfortunately, in a tracking system it is not always possible to control the range over which these outputs may vary. For example, when a target is acquired, the target spot may have to be moved across several pixels to place it in a position where it will not overlap with the alignment spots, or to move it away from the edge of the sensor. Because the physical outputs of the system may move across boundaries, it is necessary to characterize the sensor so that the loops will be stable even when the gain of the sensor changes.

The actual gain of the sensor cannot be measured because there are

no calibrated optical angular references available to the author. Instead, the relative gain difference between the largest gain which a loop would see and the gain of the sensor when spot motion is limited to within a single pixel will be found. If the three actuators are characterized by keeping a spot within a single pixel, then this ratio will be a minimum gain margin necessary for a loop to remain stable.

To measure the relative gain between different portions of the sensor, the telescope actuator is slewed so that the target spot moves across the sensor at a constant rate. Figure 2.2.1-1 shows the measured response of the target spot to the constant slew of the telescope. Because the output is difficult to see because of sensor noise, Figure 2.2.1-2 shows the same response after it has been filtered using a first order low pass filter with a cutoff frequency of 100 radians/sec.

The most obvious feature of these plots is the stairstep. This is caused by the spot reaching the edge of a pixel and the centroiding algorithm being non-linear at a pixel edge. This pixel-hopping is a well-documented phenomenon [6]. The stairstep is quite evident, but less obvious is that the gain is not quiet constant across a single pixel.

If the actuators are characterized while keeping the spot within a single pixel, then they will see the average gain within a single pixel. However, if the spot is driven across pixel boundaries, gain of the sensor will appear, on average, to be the gain of the sensor as measured between pixel centers. The gain of the sensor within a single pixel is proportional to the slope across a single pixel in Figure 2.2.1-2. That is, the local gain is proportional to the local slope

$$S_{LOCAL} = 74 \text{ LSB/sec} \qquad (2.2.1\text{-}1)$$

The global gain can also be estimated from the plot

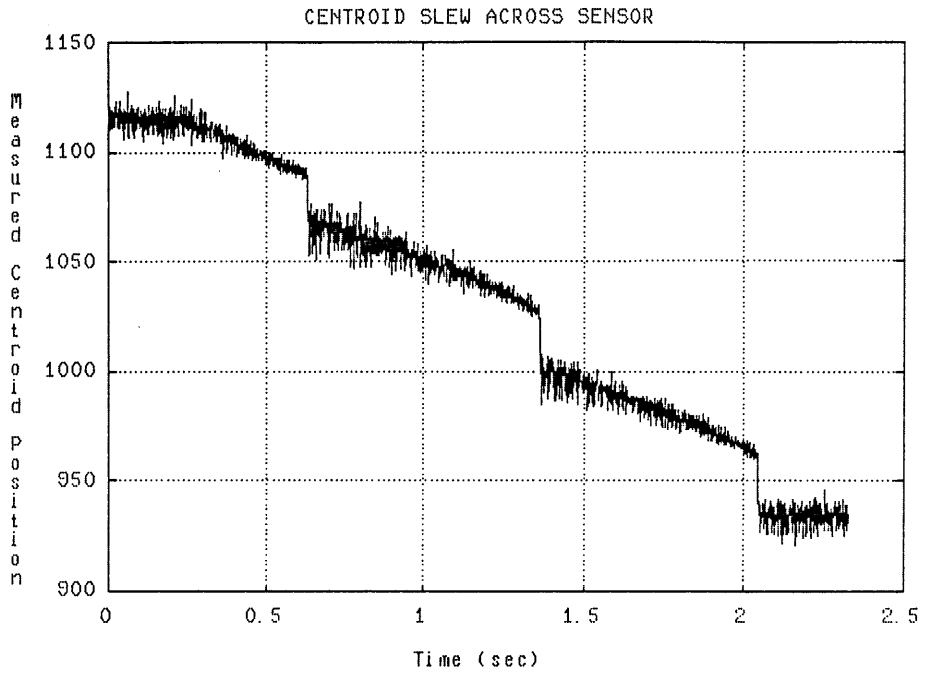

Figure 2.2.1-1 Sensor Output Driven By a Spot Moving At a Constant Rate

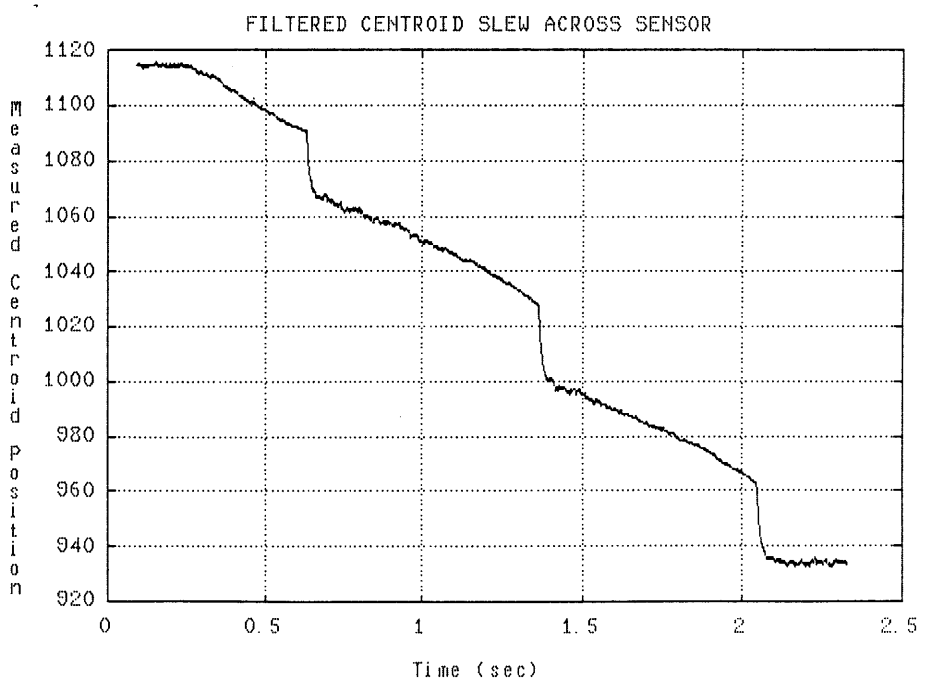

Figure 2.2.1-2 Filtered Sensor Output Driven By a Spot Moving At a Constant Rate

$$S_{GLOBAL} = 100 \text{ LSB/sec} \qquad (2.2.1\text{-}2)$$

The ratio of these slopes yield the deterioration of the gain margin of a loop due to sensor non-linearities

$$S_{GLOBAL} / S_{LOCAL} = 1.35 = 2.6 \text{ dB} \qquad (2.2.1\text{-}3)$$

This is only an estimated average value for loops with outputs which cross pixel boundaries. Notice that at a pixel boundary the slope is enormous. This means that if a spot is driven to a position near the pixel boundary, the gain of the sensor will be very large, and the loop will almost certainly be unstable.

2.2.2 Measuring the Telescope Magnification Factor

In order to calculate the desired outputs of the system from the physical outputs, it is necessary to know precisely the magnification factor of the telescope. Because an accurate value is needed, the telescope magnification factor will be measured. To make the measurement, a loop is closed around the telescope using the target spot for feedback, and the step response of the closed loop is measured. The motion on the pseudo star spot due to the motion of the telescope is compared with the step size of the target spot. The step size of the target spot on the sensor will be

$$\delta TS = M\ \delta TEL \qquad (2.2.2\text{-}1)$$

and the step size of the pseudo star spot on the sensor will be

$$\delta PS = 2\ \delta TEL \qquad (2.2.2\text{-}2)$$

where δTEL is the step size of the telescope. It is then clear that the ratio of the target spot step size to the pseudo star step size is

$$\frac{\delta TS}{\delta PS} = \frac{M}{2} \qquad (2.2.2\text{-}3)$$

The telescope magnification factor can be found from

$$M = 2\ \frac{\delta TS}{\delta PS} \qquad (2.2.2\text{-}4)$$

The step response was run four times, and the runs were then averaged to try to eliminate some of the noise on the measurements. The averaged data are shown in Figures 2.2.2-1 and 2.2.2-2. The step size of the target spot is 24 LSBs, and the step size of pseudo star spot is 12.5 LSBs. The resulting telescope magnification factor is

$$M = 2\ \frac{24.0}{12.5} = 3.84 \qquad (2.2.2\text{-}5)$$

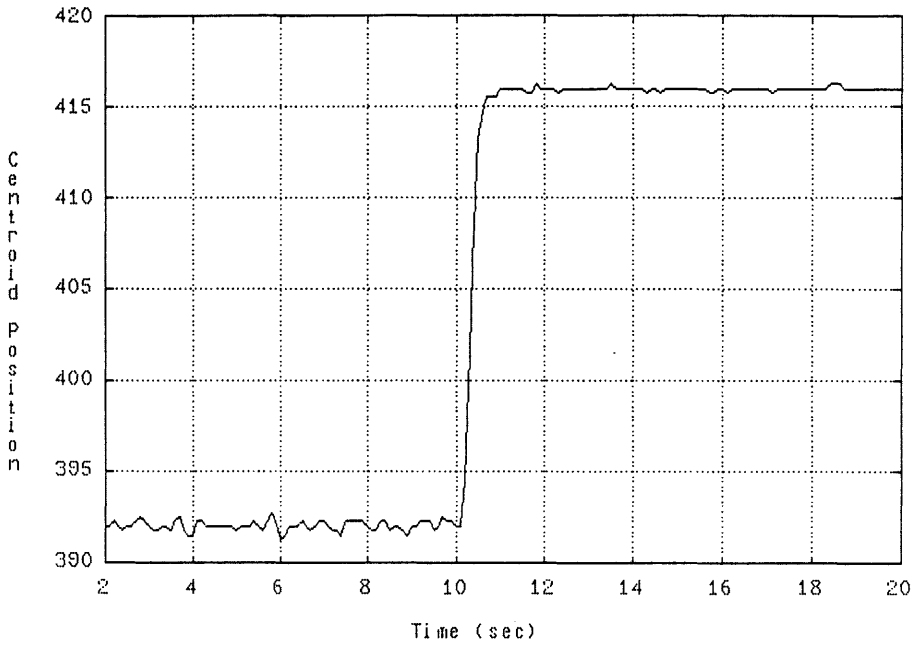

Figure 2.2.2-1 Averaged Target Spot Motion In Telescope Magnification Factor Test

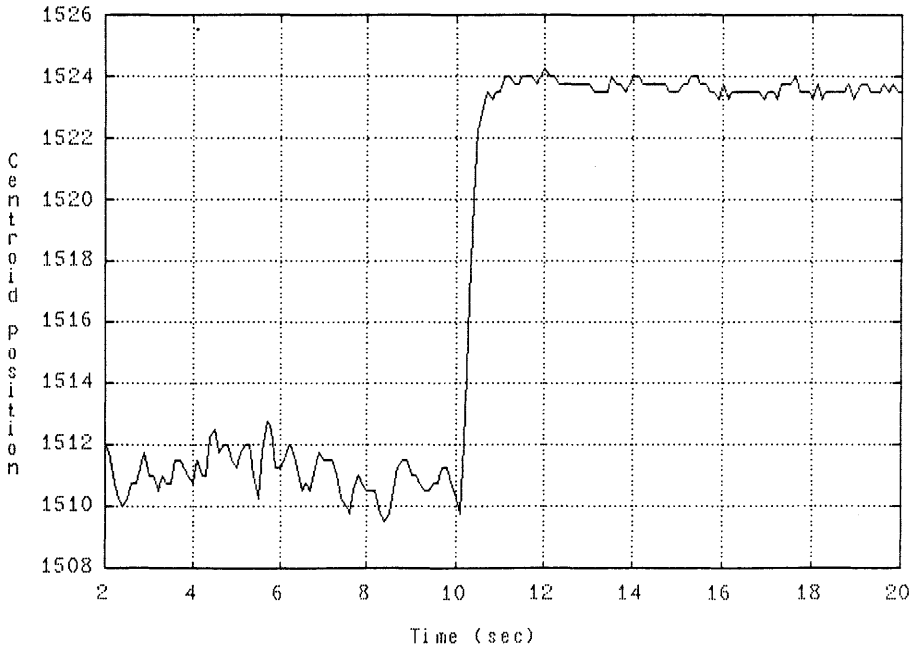

Figure 2.2.2-2 Averaged Pseudo Star Spot Motion In Telescope Magnification Factor Test

2.2.3 Modelling the Actuator Dynamics

There are three actuators in the scaled system, namely the TCA, the AIRU, and the telescope actuator. The TCA and AIRU are implemented using galvanometer scanners, and the telescope actuator is implemented using a stepper motor turning a motor-driven optical mount in which the telescope is mounted.

To measure the dynamics of the TCA and AIRU, a beam is reflected from the mirror mounted on each of the actuators and aimed at the sensor. The output of the sensor is sent to a digital-to-analog converter (DAC) and displayed on an oscilloscope. By comparing the voltage amplitude which drives the actuator with the output of the DAC, a gain can be associated with the measurement system. A block diagram of this measurement system appears in Figure 2.2.3-1. When the gain of this system is taken at different frequencies, a Bode magnitude plot of the measurement system can be made. If the gain of the measurement system is divided by two, the result is a Bode magnitude plot of the combination of actuator, sensor, and DAC, which is what should be measured in order to model the scaled system dynamics. This is shown in Figure 2.2.3-2, which is a block diagram of the scaled system, and is functionally identical to Figure 2.1.2-1.

The measurements are taken by driving the actuators with a sine wave such that the amplitude of the measured output angle is a specific value, approximately one pixel peak-to-peak. The signal driving the amplifier is then measured, and the ratio of output amplitude to input amplitude is calculated to produce the actuator gain. By driving the output to approximately the same amplitude for each measurement, the error which is introduced into the gain measurement by sensor non-linearities is kept to a minimum.

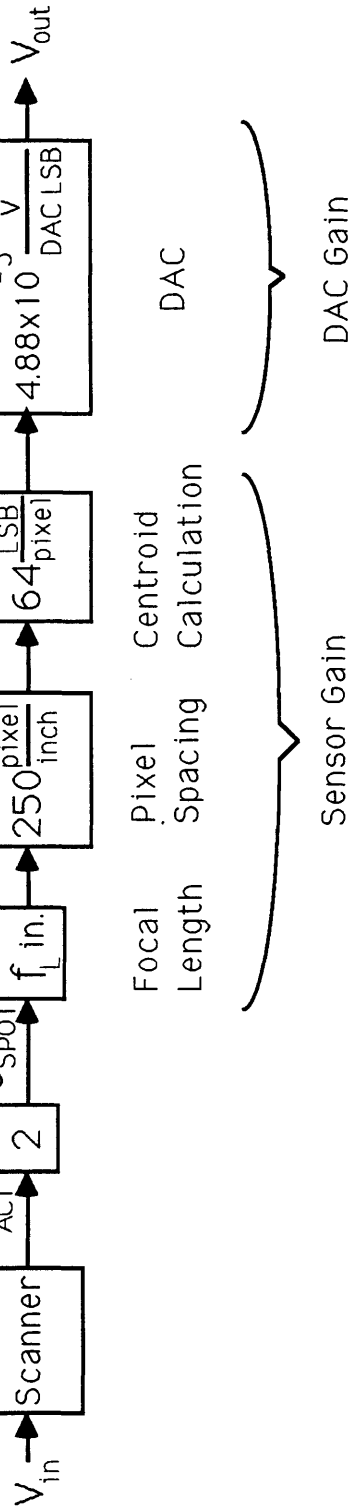

Figure 2.2.3-1 AIRU and TCA Actuator Characterization Block Diagram

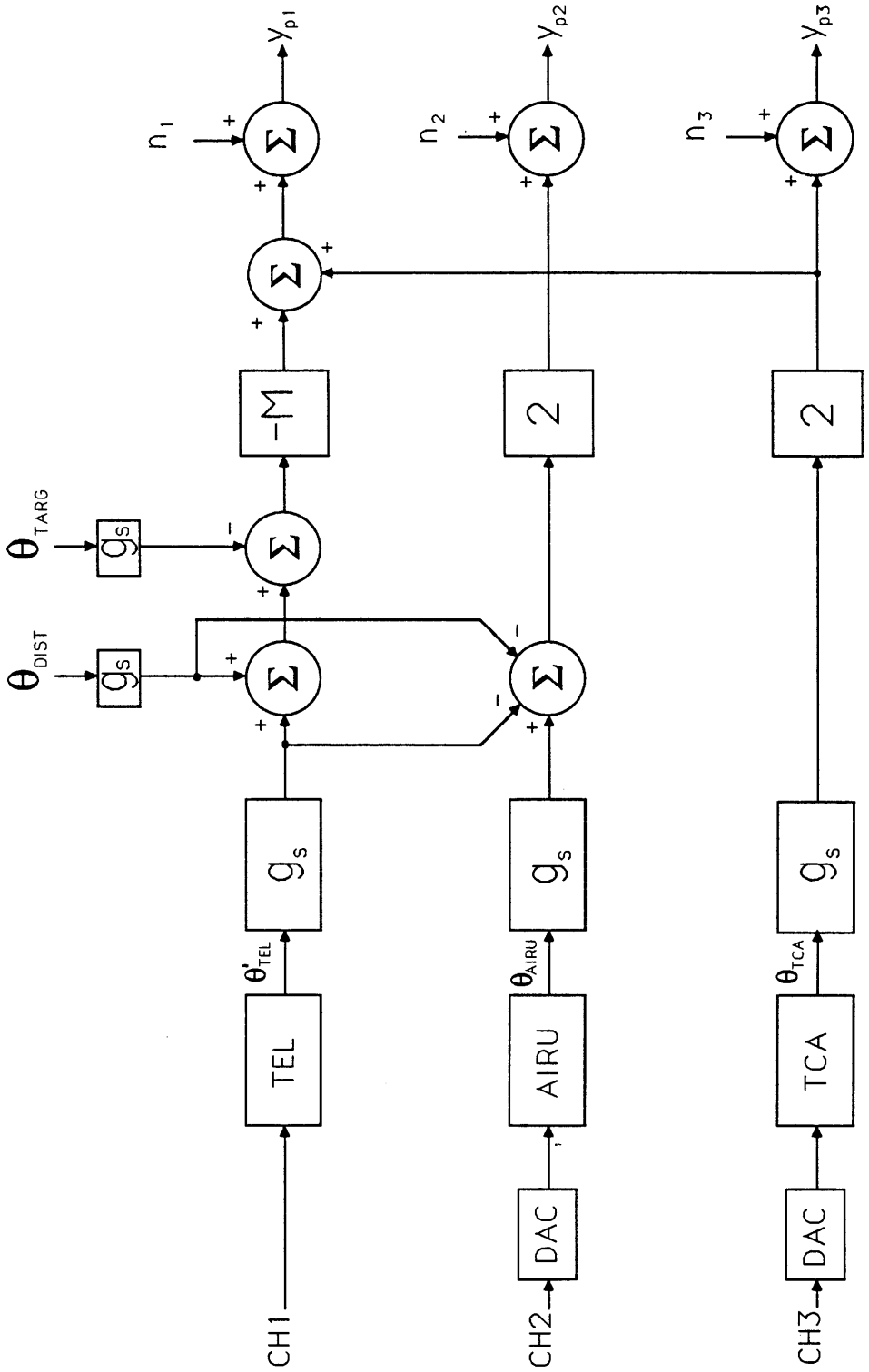

Figure 2.2.3-2 SATE System Block Diagram, Combining Sensor and Actuator Gains

A Bode plot of the TCA is made by taking gain measurements at twelve evenly spaced (log ω) frequencies from 25 rad/sec to 4000 rad/sec, as well as a measurement at the point of maximum gain. The apparent shape of this magnitude plot suggests that it is a second order system, with a low frequency gain of g_{LF} = -32.32 dB, and a resonant peak at ω_p = 1821 rad/sec with a magnitude of -20 dB.

To fit a second order magnitude curve to the data, only two parameters are needed. These are the frequency at which the peak magnitude occurs ω_p, and the ratio of the peak magnitude to the low frequency magnitude, M_p = 12.32 dB = 4.13. A second order system of the form

$$g(s) = \frac{g_{LF}}{(s^2/\omega_n^2) + 2\zeta s/\omega_n + 1} \quad (2.2.3\text{-}1)$$

can be fit to the data by using the relationships [7]

$$M_p = \frac{1}{2\zeta(1-\zeta^2)^{1/2}} \quad (2.2.3\text{-}2)$$

$$\omega_n = \omega_p(1-2\zeta^2)^{-1/2} \quad (2.2.3\text{-}3)$$

These relationships yield a natural frequency ω_n = 1848.7 rad/sec, and a damping ratio ζ = 0.1219.

To compare the model with the measured frequency response, a Bode magnitude plot is shown in Figure 2.2.3-3. In this plot, the model frequency response is drawn with a line, and the points marked with an X correspond with the measured response. The model can be seen to agree

very closely with the measured data. The multiplicative error between the measured data and the model serves as an indication of how well the model fits the data [8]. The multiplicative error is calculated from

$$|e_m| = \left| \frac{M_a(\omega)}{M_m(\omega)} - 1 \right| \qquad (2.2.3\text{-}4)$$

where e_m is the multiplicative error, M_a is the measured magnitude and M_m is the modelled magnitude. The maximum magnitude of the multiplicative error for the TCA is 0.2, which means that the maximum difference between the measured and modelled gains is 20%. A Bode Plot for the TCA actuator model, including its phase characteristics, is shown in Figure 2.2.3-4.

The model for the AIRU actuator is created in exactly the same way as the model for the TCA. The low frequency gain is g_{LF} = -22.9 dB, and the peak gain is M_p = 16.1 dB = 6.37 at a frequency ω_p = 860.8 rad/sec. From Equations 2.2.3-2 and 2.2.3-3, the second order model for the AIRU actuator will have a natural frequency ω_n = 866.2 rad/sec, and a damping ratio ζ = 0.0787. A Bode plot of the model and the data for the AIRU frequency response is shown in Figure 2.2.3-5.

The maximum magnitude of the multiplicative error is, from Equation 2.2.3-4,

$$|e_m|_{max} = 0.24 \qquad (2.2.3\text{-}5)$$

This means that the maximum difference between the measured and modelled gains is 24%. The Bode plot for the AIRU actuator model, including its phase characteristics, is shown in Figure 2.2.3-6.

To help improve the command following and disturbance rejection properties of the loops which will control the TCA and AIRU, each actuator

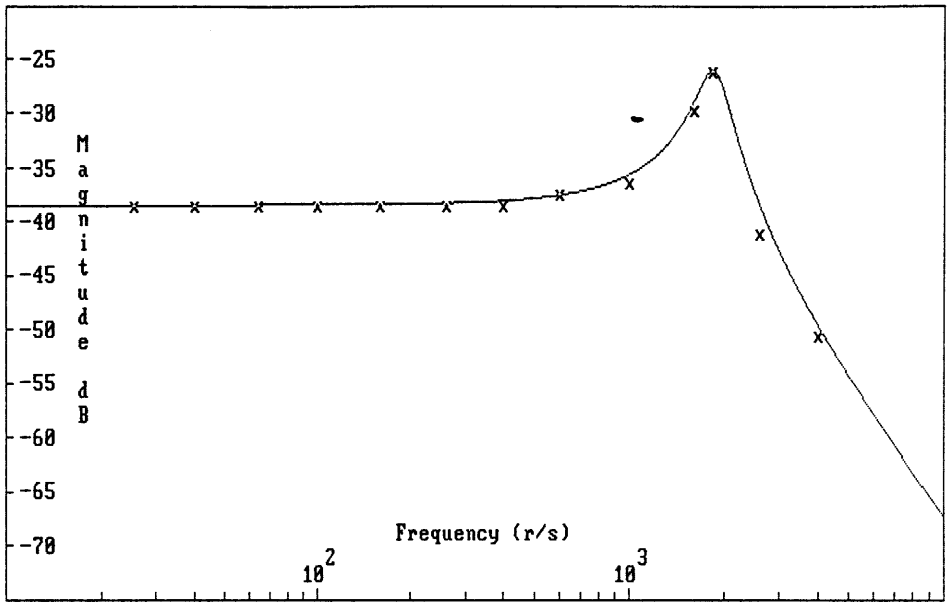

Figure 2.2.3-3 Comparison of the Measured and Modelled Frequency Response of the TCA Actuator

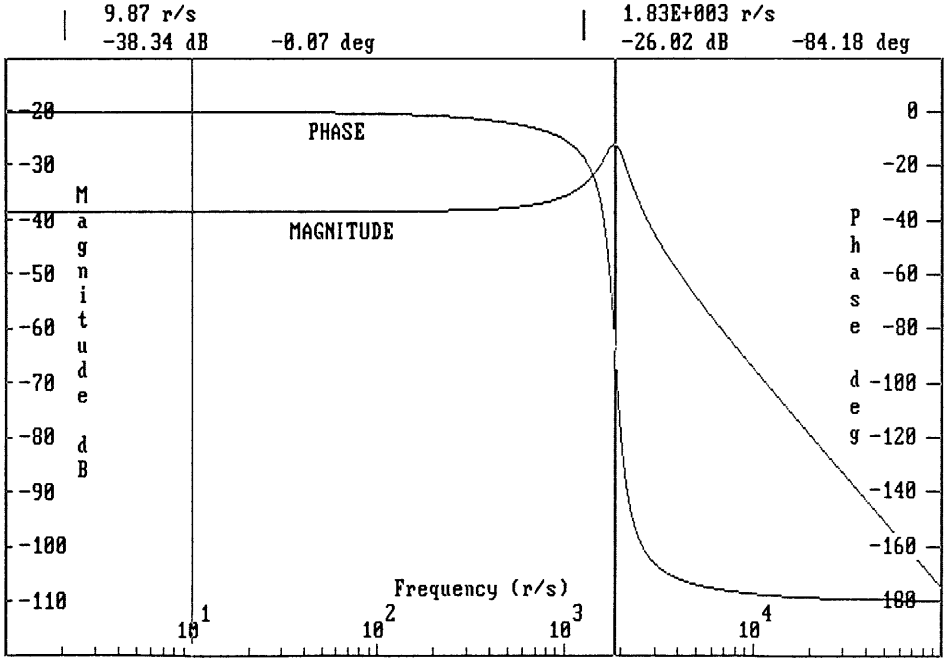

Figure 2.2.3-4 Bode Plot of the TCA Model

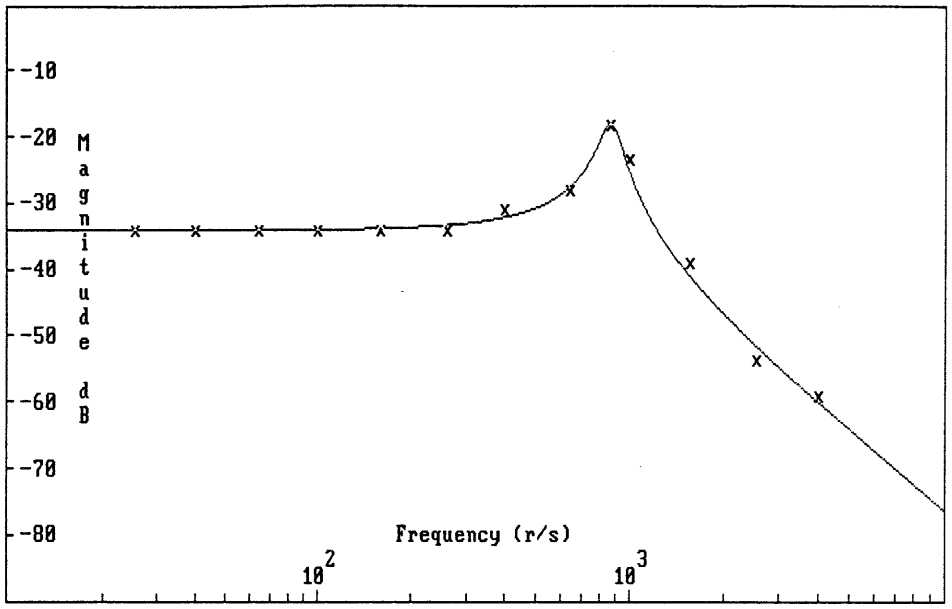

Figure 2.2.3-5 Comparison of the Measured and Modelled Frequency Response of the AIRU Actuator

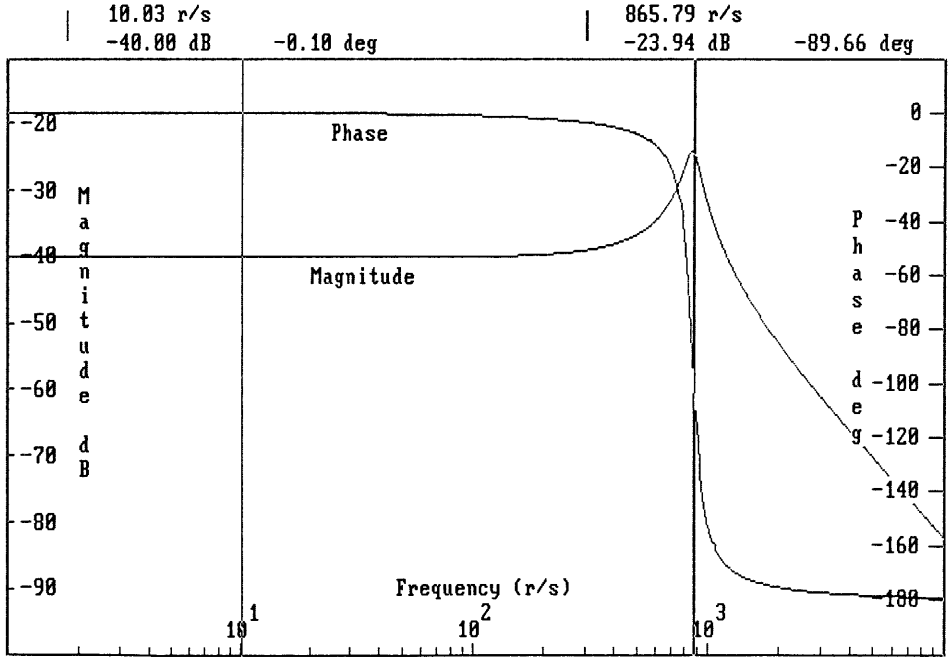

Figure 2.2.3-6 Bode Plot of the AIRU Model

is augmented by a unity gain integrator. This integrator acts as an anti aliasing filter on the output of the DAC.

Before the models which have been developed for the TCA and AIRU can be useful for designing the control system, they must be transformed into discrete time. First, the TCA model will be transformed into the z-plane, and then the AIRU model will be transformed following a similar procedure.

After including the integrator (1/s) and the dynamics of a zero order hold ($(1-e^{-sT})/s$), the dynamics of the TCA in the s plane are

$$g_{TCA}(s) = \frac{(1-e^{-sT})A_{TCA}}{s^2(s^2/\omega_n^2 + 2s\zeta/\omega_n + 1)} \qquad (2.2.3\text{-}6)$$

where A_{TCA} is 0.0121, T is the sampling period of the fast loop which is 0.91 ms, ω_n is 1848.7 r/s, and ζ is 0.1219.

The dynamics of the TCA can also be expressed as a sum of partial fractions according to

$$g_{TCA}(s) = A_{TCA}(1-e^{-sT})\left[\frac{-2s\zeta/\omega_n+1}{s^2} + \frac{2s\zeta/\omega_n^3+(2\zeta^2-1)/\omega_n^2}{s^2/\omega_n^2 + 2s\zeta/\omega_n + 1}\right]$$

$$= A_{TCA}(1-e^{-sT})\left[\frac{1}{s^2} - \frac{2\zeta/\omega_n}{s} + \frac{G(s/\Phi + 1)}{s^2/\omega_n^2 + 2s\zeta/\omega_n + 1}\right] \qquad (2.2.3\text{-}7)$$

where $\Phi = \omega_n(1-2\zeta^2)/2\zeta$ and $G = (1-2\zeta^2)/\omega_n^2$. This transfer function can be transformed into the z plane by using a standard look up table to transform it term by term. The result is

$$g_{TCA}(z) = A_{TCA}\,(1-z^{-1})\left[\frac{Tz}{(z-1)^2} - \frac{2z\zeta/\omega_n}{z-1} + \frac{G\omega_n^2}{\Phi}\,\frac{z(z+Z_1)}{z^2+A_1z+A_0}\right] \qquad (2.2.3\text{-}8)$$

where

$$A_0 = e^{-2aT}$$

$$A_1 = -2\cos(bT)e^{-aT}$$

$$Z_1 = \frac{\Phi-a}{b}\,e^{-aT}\sin(bT) - e^{-aT}\cos(bT)$$

$$a = \omega_n\zeta$$

$$b = \omega_n(1-\zeta^2)^{1/2}$$

$$G\omega_n^2/\Phi = 2\zeta/\omega_n$$

Finally, after reduction and substitution of values, the z plane model of the TCA is

$$g_{TCA}(z) = G_{TCA}\,\frac{z^2 + B_1z + B_0}{(z-1)(z^2 + A_1z + A_0)} \qquad (2.2.3\text{-}9)$$

where

$$G_{TCA} = 1.43 \times 10^{-5}$$

$$B_1 = -0.541$$

$$B_2 = 0.945$$

$$A_1 = 0.161$$

$$A_0 = 0.664$$

The dynamics of the AIRU actuator are similar to the dynamics of the TCA. The AIRU is also augmented by an integrator to improve high frequency sensor noise rejection and low frequency tracking properties.

When the integrator and sample and hold are included, the dynamics of the AIRU in the s plane become

$$g_{AIRU}(s) = \frac{(1-e^{-sT})A_{AIRU}}{s^2(s^2/\omega_n^2 + 2s\zeta/\omega_n + 1)} \qquad (2.2.3\text{-}10)$$

where A_{AIRU} is 0.01, T is the sampling period of the slow loop of 0.1 sec, ω_n is 866.2 r/s, and ζ is 0.0787. At this point, the form of the AIRU s-plane dynamics is exactly the same as the TCA s-plane dynamics. The only difference between the two actuators is the values of the gain, sampling rate, natural frequency, and damping ratio. So, the AIRU z-plane dynamics can be put into the form of Equation 2.2.3-9. This is

$$g_{AIRU}(z) = G_{AIRU} \frac{z^2 + D_1 z + D_0}{(z-1)(z^2 + C_1 z + C_0)} \qquad (2.2.3\text{-}11)$$

where

$$G_{AIRU} = 1.0 \times 10^{-3}$$
$$D_1 = 1.94 \times 10^{-3}$$
$$D_2 = -1.11 \times 10^{-5}$$
$$C_1 = 9.30 \times 10^{-5}$$
$$C_0 = 1.20 \times 10^{-6}$$

The telescope actuator is a stepper motor, and can be directly described in the z-plane. It must be noted that, even though the telescope actuator is modelled in discrete time at a sampling rate of 0.1 seconds, the telescope will have some relatively high frequency jitter from the stepper motor. This jitter will not be explicitly modelled in the system, but will be considered to add to the telescope vibration disturbance θ_{DIST}. Figure 2.2.3-7 is a block diagram showing the discrete time dynamics of the telescope actuator.

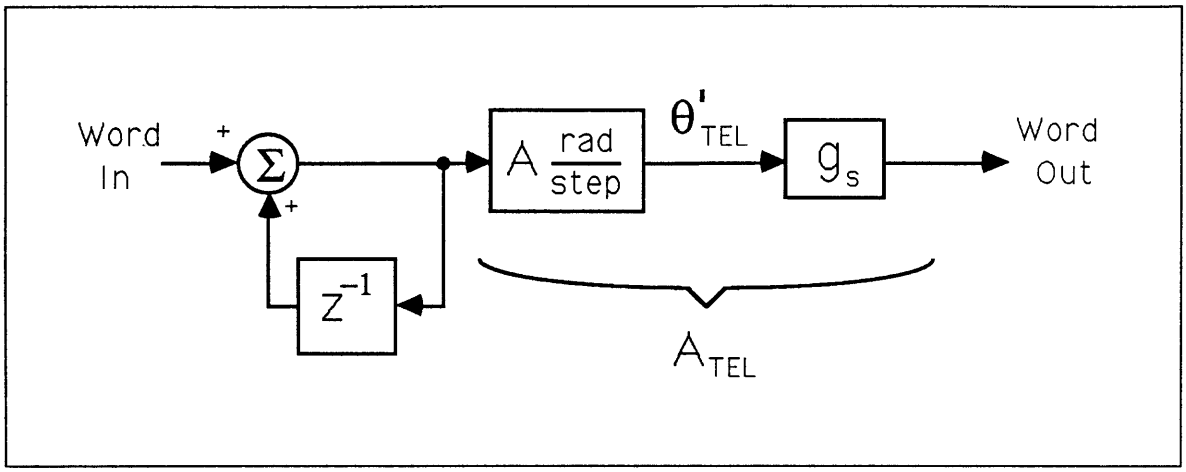

Figure 2.2.3-7 Block Diagram of Telescope Actuator Model

The gain A_{TEL} in the figure is a rate gain. That is, for a constant input, the output will be a constant rate. In Section 2.2.1, the sensor gain was characterized by slewing the telescope at a constant rate so that the target spot moved across the sensor. So, the data in Figure 2.2.1-2 can be used to find A_{TEL}.

The slew data in the figure shows a stairstep response. Unfortunately, this makes choosing the gain of the telescope actuator difficult because there are two gains to choose from, namely the local slope across an individual pixel gives one gain, and the global slope between pixel centers gives another gain.

In the application for which the telescope actuator is intended, the target will be very well behaved, so its motion will be low frequency and its maximum slew rate will be slow compared with the slew rate of the telescope. It is reasonable that if the control system keeps the target spot near the center of a pixel, the slope which will yield the correct gain will be the local slope. However, the global slope must be considered when the control system is designed to assure adequate stability robustness in the controller design, as discussed in Section 2.2.1.

The local slope is estimated in Section 2.2.1 to be 74 LSB/sec,

where the units are in least significant bits (LSB)calculated by the centroiding algorithm per second. The sampling interval for the telescope control loop is 0.1 seconds, so the rate of slew of the target spot is 7.4 LSB/sample. The commanded slew rate of the telescope was 80_{16} when Figure 2.2.1-2 was generated, and the slew rate also included a factor of 3.8 introduced by the magnification factor of the telescope. Thus, the gain of the telescope actuator A_{TEL}, including sensor gain, is $A_{TEL} = 2.4 \times 10^{-2}$ /command LSB, where a command LSB is the smallest non-zero command which can be sent to the actuator. Finally, the z-plane model of the telescope actuator can be found directly from Figure 2.2.3-7. It is

$$g_{TEL}(z) = \frac{z}{z-1} A_{TEL} \qquad (2.2.3\text{-}12)$$

To allow the use of continuous time classical control methods to design the control system, the models of the three actuators will be mapped to the w-plane via the Tustin transformation [9][10]. In the w-plane the ideas of gain margin, phase margin, and left half plane stability can be used to design the control loops. The Tustin or w transform is a bilinear transformation, where

$$z = \frac{1 + (T/2)w}{1 - (T/2)w} \qquad (2.2.3\text{-}13)$$

$$w = \frac{2}{T} \frac{z - 1}{z + 1} \qquad (2.2.3\text{-}14)$$

and T is the sampling interval.

Before the actuator models can be mapped into the w-plane, some details of the control system implementation must be explained. As was explained earlier, centroid measurements are calculated by the centroiding

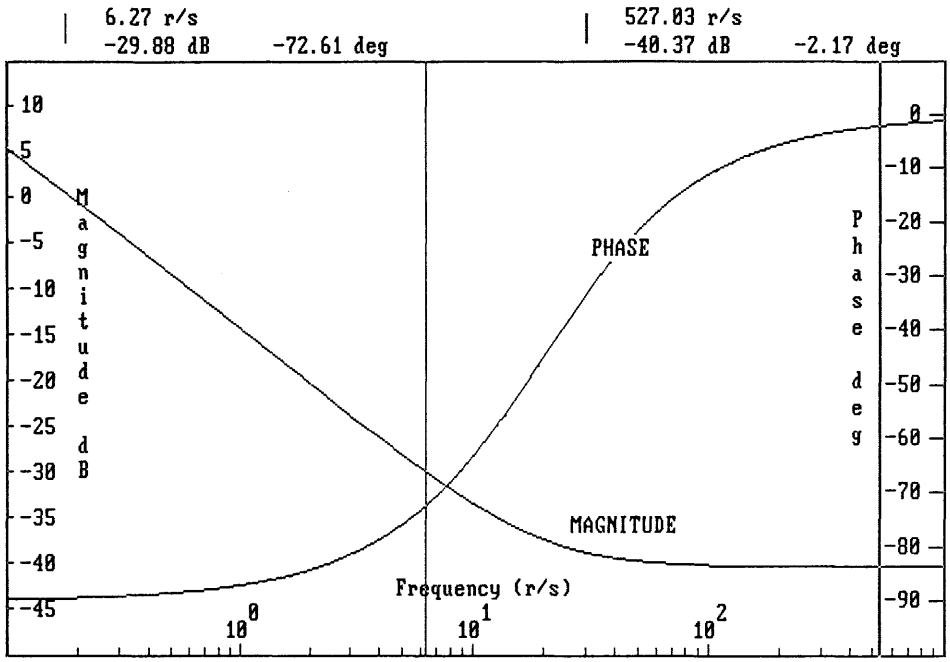

Figure 2:2.3-8 Bode Plot of the Telescope Actuator in the W-Plane

computer and are then passed to the control computer. The calculation of the centroid takes one period of the fast sampling interval, resulting in a delay of 0.9 ms. The control computer then calculates the resulting control signals one sampling interval later. The net result is that measurement and control algorithm calculations lead to a delay of two periods of the fast sampling interval, which must be accounted for in the the actuator models.

Because the telescope loop has a sampling rate which is much slower than the fast TCA loop, the total computation delay of 1.8 ms is insignificant compared with the sampling interval of 100 ms. Thus, the computation delay can safely be ignored for the telescope actuator model. In the w-plane, then, the model for the telescope actuator can be found by substituting Equation (2.2.3-13) into (2.2.3-12) to yield

$$g_{TEL}(w) = 0.24\,\frac{1 + 0.05w}{w} \qquad (2.2.3\text{-}15)$$

The Bode plot of this transfer function is shown in Figure 2.2.3-8.

Like the telescope actuator control loop, the AIRU control loop will have a low sampling rate, so the computation delay will have a negligible effect on the actuator dynamics. The AIRU actuator model is somewhat more complicated in the z-plane than the telescope actuator model, and so the w-plane model can be expected to be more complicated. It is derived by substituting Equation (2.2.3-13) into (2.2.3-11) to yield

$$g_{AIRU}(w) = G_{AIRU}\,\frac{A_3w^3 + A_2w^2 + A_1w + A_0}{(B_2w^2 + B_1w + B_0)w} \qquad (2.2.3\text{-}16)$$

where

$A_3 = -1.25 \times 10^{-4}$
$A_2 = -4.99 \times 10^{-3}$
$A_1 = 4.99 \times 10^{-2}$
$A_0 = 1.002$
$B_2 = 2.50 \times 10^{-4}$
$B_1 = 1.25 \times 10^{-2}$
$B_0 = 0.10$

The Bode plot for the AIRU actuator in the w-plane is shown in Figure 2.2.3-9.

The TCA control loop is a high bandwidth loop, with a sampling interval of 0.9 ms. Thus, the computation delay of two sampling intervals is a significant delay, and cannot be ignored. The computation delay is included in the model of the TCA by multiplying the z-plane model of Equation (2.2.3-9) by z^{-2}. When the TCA is mapped into the w-plane, this model becomes even higher order than the AIRU model, and is given by

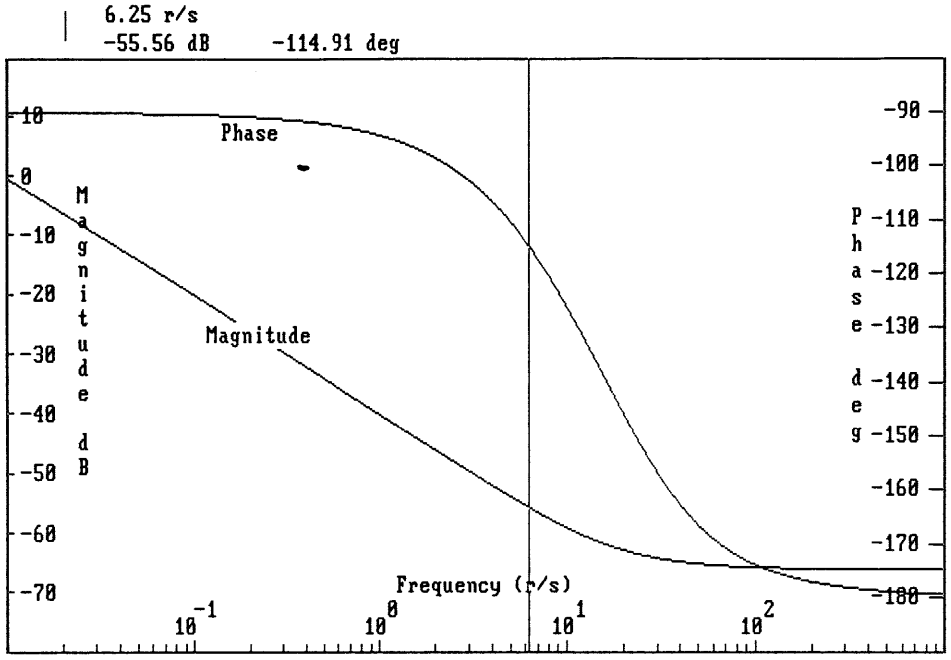

Figure 2.2.3-9 Bode Plot of the AIRU Actuator in the W-Plane

$$g_{TCA}(w) = G_{TCA} \frac{(C_3w^3 + C_2w^2 + C_1w + C_0)\ (1-(T/2)w)^2}{(D_2w^2 + D_1w + D_0)\ w\ (1+(T/2)w)^2} \qquad (2.2.3\text{-}17)$$

where

$C_3 = -2.34 \times 10^{-10}$

$C_2 = -5.14 \times 10^{-8}$

$C_1 = -5.88 \times 10^{-4}$

$C_0 = 1.403$

$D_2 = 2.83 \times 10^{-10}$

$D_1 = 1.03 \times 10^{-6}$

$D_0 = 1.66 \times 10^{-3}$

$T = 0.9$ ms

The Bode plot for the TCA in the w-plane is shown in Figure 2.2.3-10.

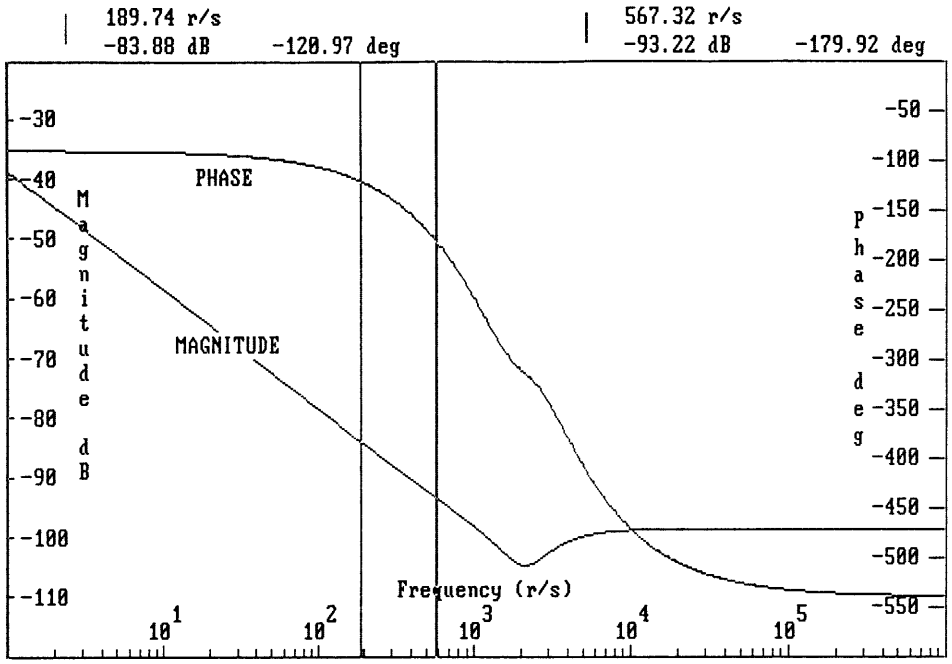

Figure 2.2.3-10 Bode Plot of the TCA Actuator in the W-Plane

The full linear dynamic model for the scaled system is now completed. A block diagram of the system dynamics in the w-plane as it appears when the compensation is added is shown in Figure 2.2.3-11. In the next section the controller is designed using the models developed in this section.

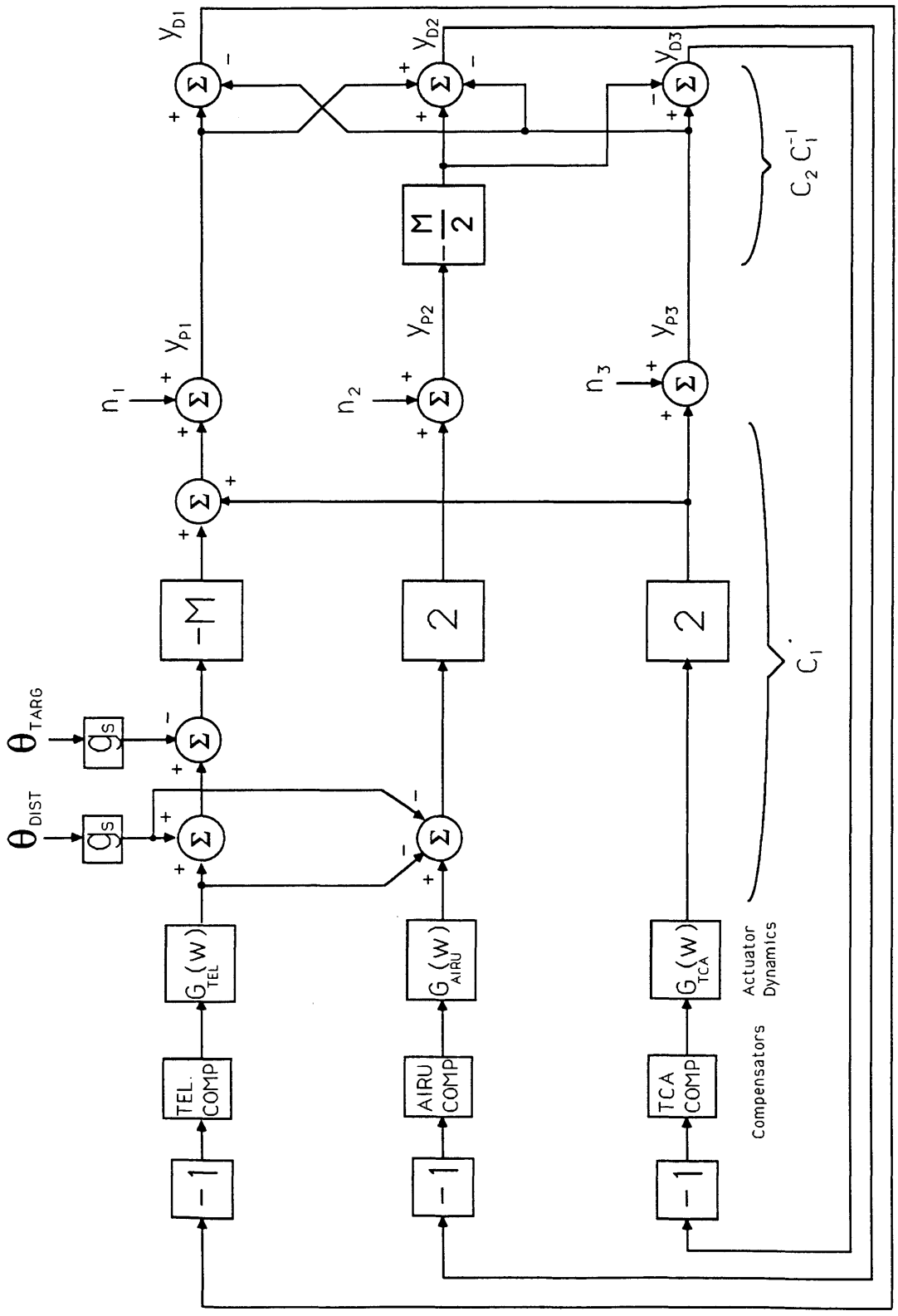

Figure 2.2.3-11 Block Diagram of Closed Loop SATE Regulator

2.3 Control System Design

2.3.0 Introduction

In this section the compensators for the telescope actuator, the AIRU actuator, and the TCA are designed then and modified to use integer arithmetic. It was shown in Section 2.1 that there will be no cross coupling between the control loops for each actuator if the system is well modelled. However, modelling errors and sensor non-linearities may cause the loops to cross couple. So, this section also investigates possible sources of loop coupling.

First, each loop is designed to have high open loop gain at low frequencies to ensure good low frequency tracking characteristics. An attempt is also made to make each loop robust to modelling errors. Then, sources of loop coupling are investigated. Finally, the controller is modified to be implemented using integer arithmetic.

2.3.1 Telescope Loop

When designing a control system, it is important to understand where the loop disturbances originate. Section 2.1 described the conversion between the physical outputs, which are the spots seen on the sensor, and the desired outputs, which are the actuator pointing errors. In that section, the desired outputs were found according to Equation

(2.1.2-6). In this section the details hidden by the matrix arithmetic in this equation are discussed, and then the controller for the telescope loop is designed.

The purpose of the telescope loop is to force the telescope to track the target, thereby keeping the target in the field of view of the telescope. The disturbances which affect the loop are the telescope disturbance θ_{DIST}, and the target angular position θ_{TARG}. A block diagram of the nominal system, which disregards sensor noise, appears in Figure 2.3.1-1. A third disturbance which enters the physical plant is labelled θ_{TCA} in the figure. This is the effort of the TCA loop to subtract the telescope disturbance from the target spot position on the sensor. If the TCA loop is working properly, the TCA should cancel the telescope disturbance, leaving only the target motion to be tracked by the loop. However, it would also be beneficial for the loop to track the low frequency telescope disturbances, such as telescope structure warping, with the telescope.

In order for the telescope to track the low frequency disturbances, the low frequency component of the disturbance must not be cancelled by the TCA. If the reference spot position, which measures the motion of the TCA, is low pass filtered, the low frequency components of θ_{TCA} can be subtracted from the target spot position on the sensor, allowing the low frequency components of θ_{DIST} to enter the loop unattenuated by the TCA. The low pass filter function is performed by an averager. The averaged reference spot position is labelled $\underline{REF}$ in the figure, where the under-bar denotes that it is an averaged position.

A more condensed form of the telescope loop with compensation is shown in Figure 2.3.1-2, where the dynamics are expressed in the w-plane, and C(w) is the compensation. Here the disturbances which enter the loop are the target position θ_{TARG} and the low frequency components of $\underline{\theta}_{DIST}$. The forward gain of the loop without the compensation, which will be the telescope loop plant, is

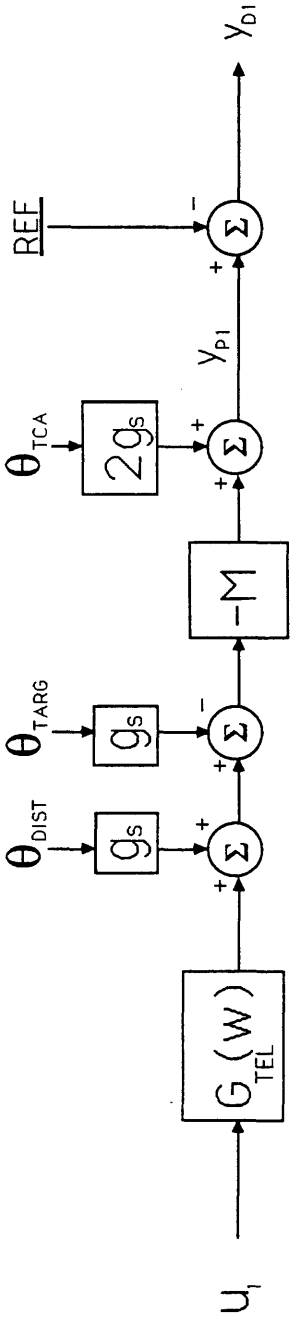

Figure 2.3.1-1 Block Diagram of Telescope Loop Plant

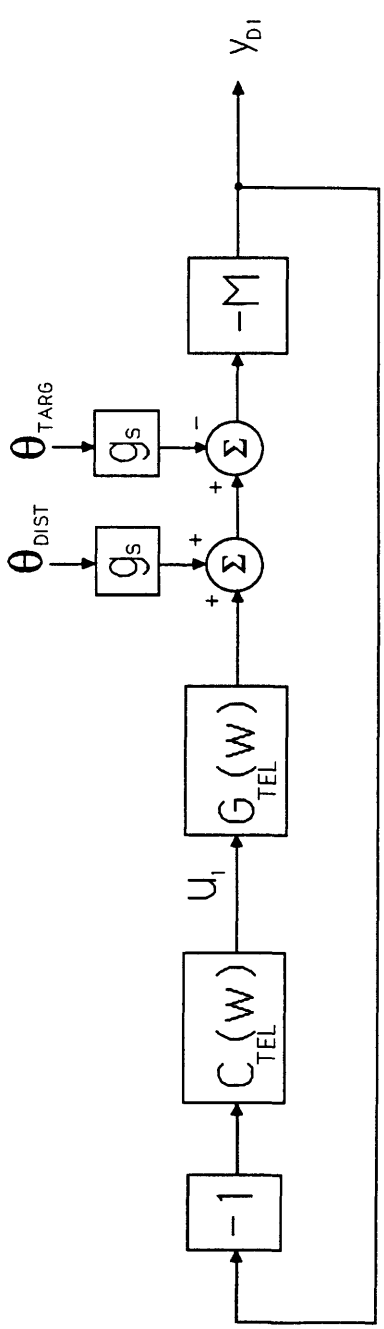

Figure 2.3.1-2 Block Diagram of Closed Telescope Loop

$$g_{TEL\_P}(w) = -Mg_{TEL}(w) \qquad (2.3.1\text{-}1)$$

where M = 3.8 is the magnification factor of the telescope and $g_{TEL}(w)$ is as given in Equation (2.2.3-15).

Figure 2.3.1-3 shows a Bode plot of $g_{TEL\_P}(w)$. The desired crossover frequency of the loop is 1 Hz, or 6.3 radians/sec. This crossover can be achieved by using a gain of -10 in the compensator. The forward gain of the loop then is shown in the Bode plot in Figure 2.3.1-4. The crossover frequency is then 6 radians/sec, or 0.95 Hz, with a phase margin of 106.8 degrees, and a gain margin of 10 dB. According to Section 2.2.1, a gain margin of at least 2.6 dB is needed to maintain stability if the target spot crosses pixel boundaries. Thus, unless the gain of the telescope actuator model at 1 Hz is too low by more than a factor of 2, the loop will be stable, unless some process introduces phase lag at 1 Hz. The telescope disturbance angle θ_{DIST} will be rejected by this loop by over 90% at frequencies less than 0.1 Hz.

2.3.2 AIRU Loop

The second loop to be closed is the loop around the AIRU. From the desired outputs derived in Section 2.1, it can be seen that the purpose of the AIRU loop is to force the AIRU to track the target. Because the target spot can only be measured at the slow sampling rate, the AIRU loop will also use the slow sampling rate. Figure 2.3.2-1 shows a block diagram of the AIRU plant from the AIRU input to the AIRU Tracking Error, or desired output 2. The disturbances which enter the loop are described by the equations in Section 2.1, so a more intuitive description is given here.

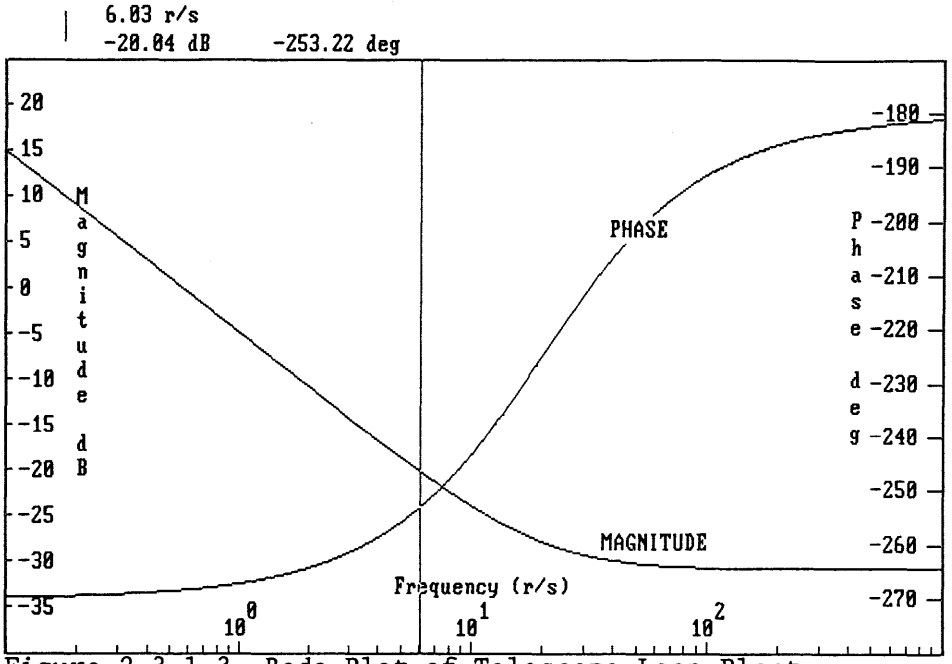

Figure 2.3.1-3 Bode Plot of Telescope Loop Plant

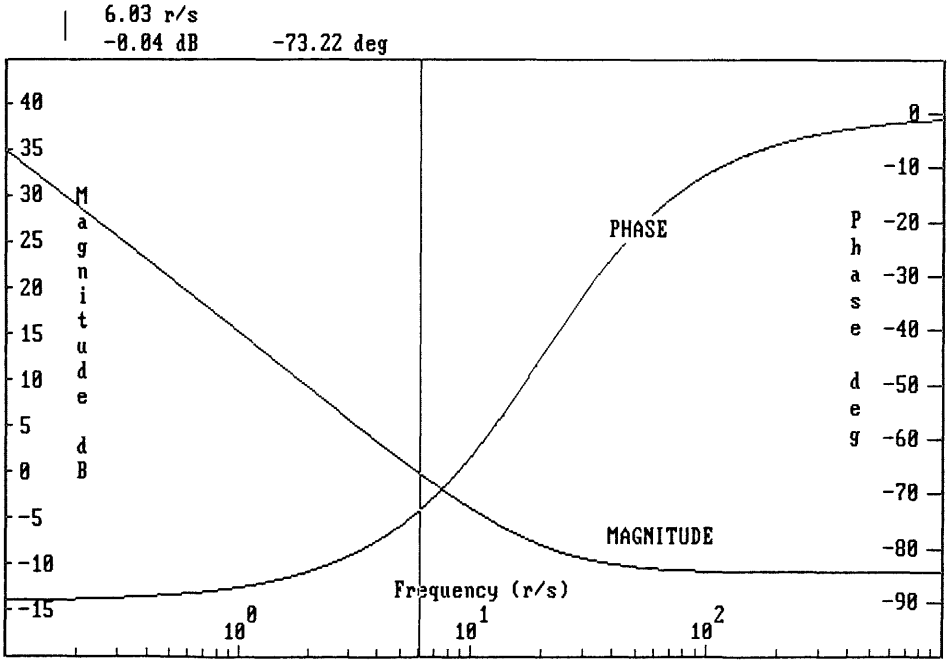

Figure 2.3.1-4 Bode Plot of Forward Gain of Compensated Telescope Loop

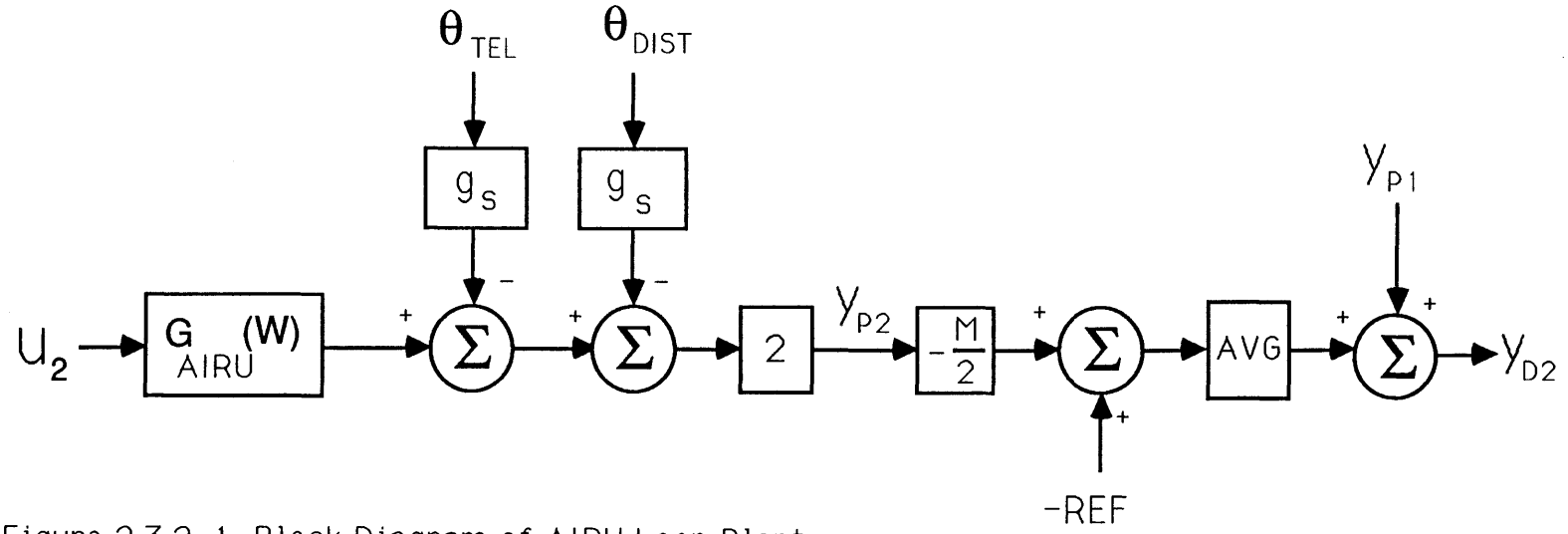

Figure 2.3.2-1 Block Diagram of AIRU Loop Plant

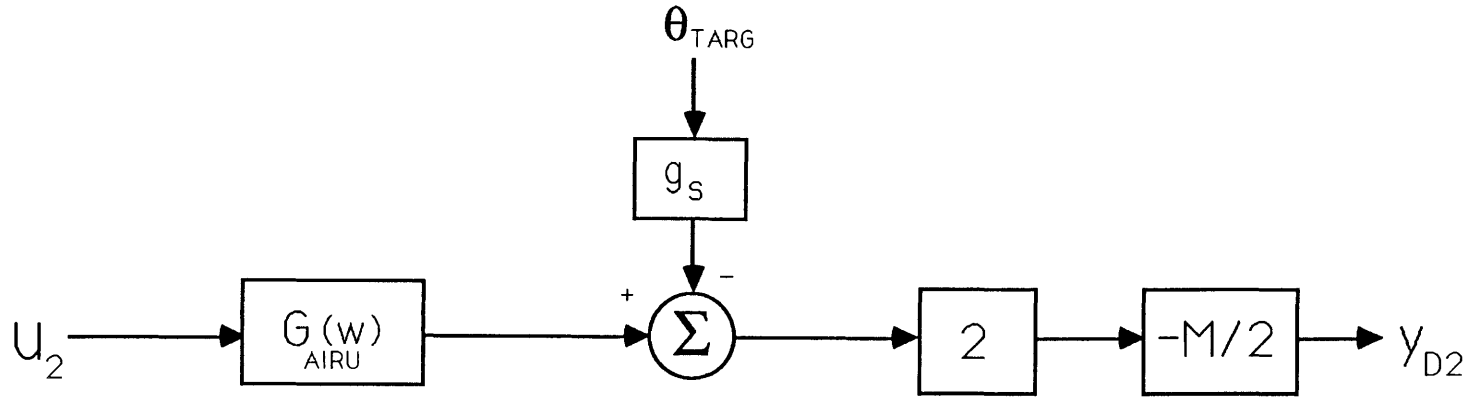

Figure 2.3.2-2 Simplified Block Diagram of AIRU Loop Plant

The physical plant can be seen to have two disturbances. The first is the commanded position of the telescope θ'_{TEL}, and the second is the telescope disturbance θ_{DIST}. The commanded position of the telescope is not a disturbance to the system as a whole, but it enters the AIRU loop as if it were a disturbance. So, the output of the physical plant is $\theta_{AIRU}-\theta'_{TEL}-\theta_{DIST}$ scaled by twice the sensor gain. To get the desired output from the physical output, the physical output is scaled by -M/2, and then added to -REF, where REF is the motion of the TCA reference spot. Notice that the motion of the TCA reference spot is not averaged before it is used in this loop, and therefore is not the same as REF used in the telescope loop. REF is used to subtract out θ_{DIST}, leaving only the telescope angle and the AIRU angle.

Until this point in the loop, the sampling rate has been at the fast rate because the loop must keep track of the high frequency disturbances. However, because the difference between the telescope angle and the AIRU angle will contain only low frequencies, the sampling rate of this angle can now be converted down to the slow sampling rate. This conversion will be of the form of an average of values of the difference between the telescope angle and the AIRU angle. This conversion method is chosen over a decimation method because the sensor measurements are very noisy, and the averaging acts as a low pass filter. The process of averaging the fast sampling rate centroids to convert them to the low sampling rate looks to the system like a pure time delay of approximately 1/2 of a slow sampling interval. Because the crossover frequency of the loop will be at 1 Hz, the unmodelled phase lag at crossover will be approximately 18 degrees.

At the point where the sampling rate conversion takes place, the output of the loop is the difference between θ_{TEL} and θ_{AIRU}. In order to obtain a signal which is proportional to the difference between the target angle and the AIRU angle, the telescope angle must be cancelled and the target angle must be added to the output. The measured position of the target spot, which was used as the measurement for the telescope loop, is proportional to $\theta_{TARG} - \theta_{TEL}$. By adding the target spot position to the

loop, the desired output which is proportional to $\theta_{TARG} - \theta_{AIRU}$ is achieved. This is true only if all of the spots are measured perfectly by the sensor.

The nominal plant can now be represented by the block diagram in Figure 2.3.2-2. The plant for the AIRU loop is

$$g_{AIRU\_P}(w) = -Mg_{AIRU}(w) \qquad (2.3.2\text{-}1)$$

where M = 3.8 is the telescope magnification factor, and $g_{AIRU}(w)$ is given by Equation (2.2.3-16). A Bode plot of g_{AIRU_P} is shown in Figure 2.3.2-3. The plot shows that the AIRU plant starts with 90 degrees of phase lead, even though the magnitude looks like an integrator. This is because the zero-frequency gain of the plant is negative, and the routine used to plot the phase represents the negative gain as having a phase of +180 degrees. So, to stabilize this plant, the compensation gain must be negative. The cross hair in the plot shows the magnitude and phase of the plant at the desired crossover frequency. It also shows that approximately 10 dB of gain margin and 65 degrees of phase margin results if a simple gain is used to compensate the loop. Figure 2.3.2-4 shows a Bode plot of the loop compensated with a gain of -200. The loop is robust, with a gain margin of 10 dB, and a phase margin of 65 degrees. The phase margin drops to 47 degrees when the sampling rate converter is considered. The 10 dB gain margin should be adequate, even considering the 2.6 dB of extra gain which the sensor would provide if the pseudo star spot were to cross a pixel boundary. The 47 degree phase margin will cause the step response of the closed loop to overshoot, and will cause the settling time to increase, but it also decreases the rise time for a system with a crossover frequency of 1 Hz.

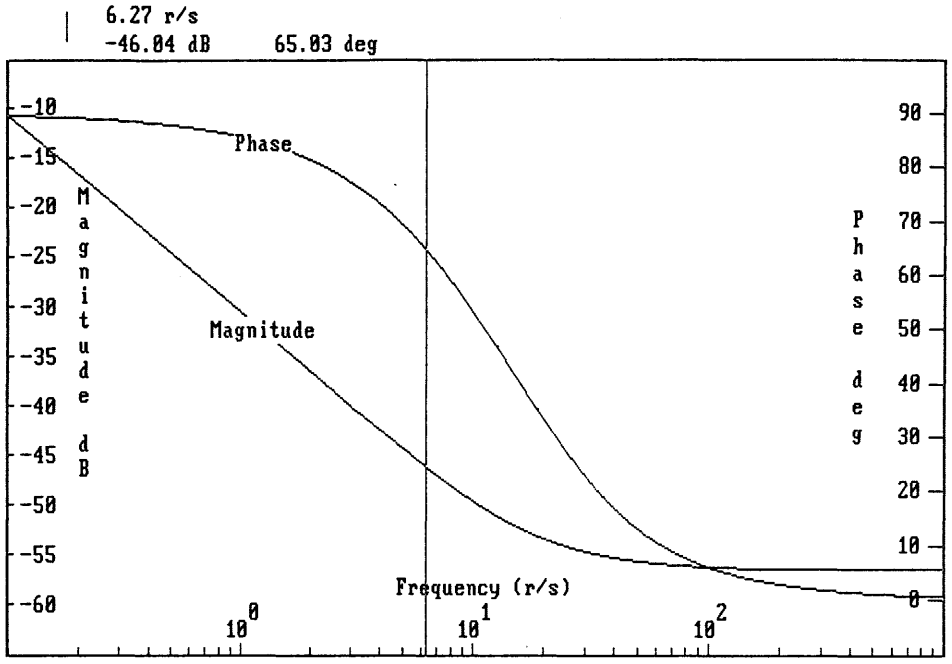

Figure 2.3.2-3 Bode Plot of AIRU Loop Plant

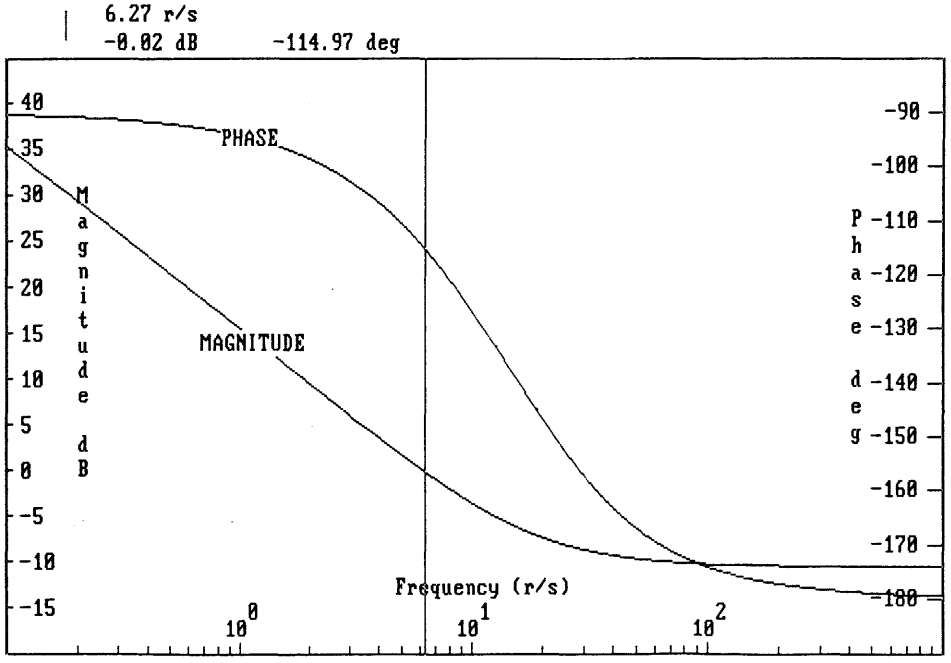

Figure 2.3.2-4 Bode Plot of Forward Gain of Compensated AIRU Plant

2.3.3 TCA Loop

The third and final loop to be closed is the TCA loop. The TCA loop is used to subtract the disturbances from the target spot. To do this, the disturbances are measured using the pseudo star spot, and the TCA is driven to counter the disturbances. A block diagram which shows this appears in Figure 2.3.3-1. When this is broken down farther, as Figure 2.3.3-2 shows, the pseudo star spot position is seen to be the difference between the AIRU angle and the telescope angle. Here it is presumed that the AIRU is on average pointing exactly at the target, and that the high frequency disturbances for which the TCA is compensating are the telescope pointing error.

A block diagram of the closed loop, including the compensation is shown in Figure 2.3.3-3. The plant to be compensated is then

$$g_{TCA\_P} = 2g_{TCA}(w) \qquad (2.3.3\text{-}1)$$

where $g_{TCA}(w)$ is given by Equation (2.2.3-17). A Bode plot of this plant is shown in Figure 2.3.3-4.

The Bode plot shows that if a simple gain is used to compensate the TCA loop, a gain margin of approximately 9 dB and a phase margin of 59 degrees is achieved if crossover is limited to 190 radians/sec. The phase falls very rapidly past this crossover frequency due to the second order all-pass network at 2200 radians/sec introduced by the computation delay. Using a higher order compensator may allow some additional bandwidth to be gained, but this would be accomplished at the expense of stability robustness. Therefore, the system will be compensated using a gain of

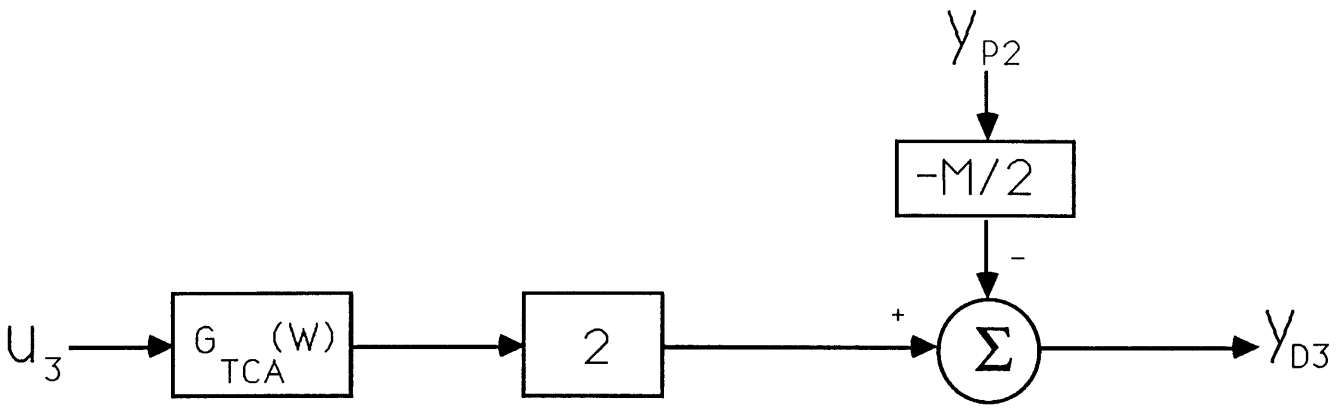

Figure 2.3.3-1 Block Diagram of TCA Loop Plant

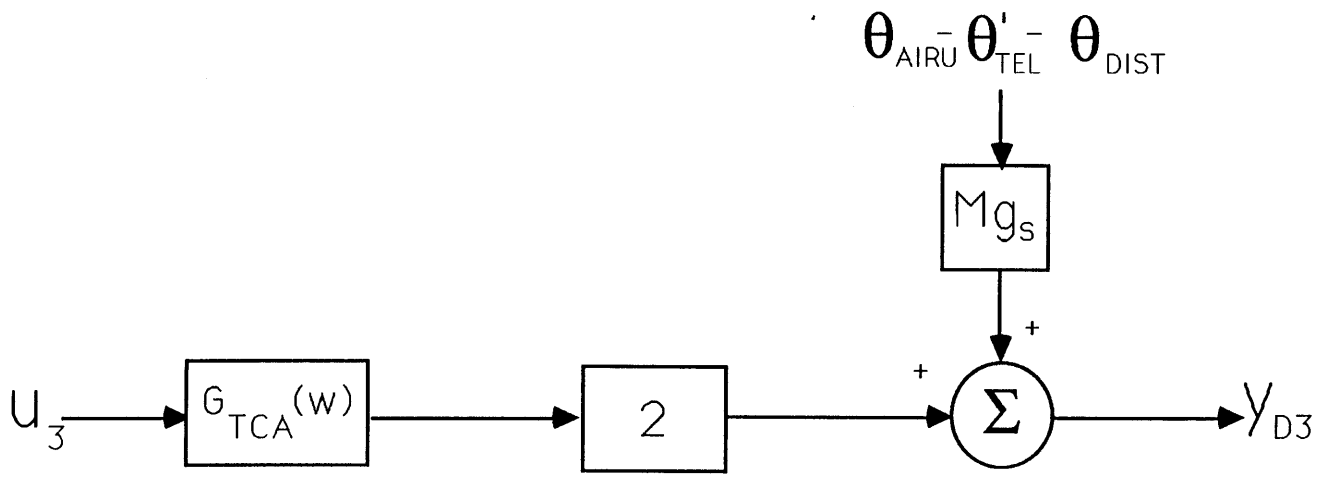

Figure 2.3.3-2 Simplified Block Diagram of TCA Loop Plant

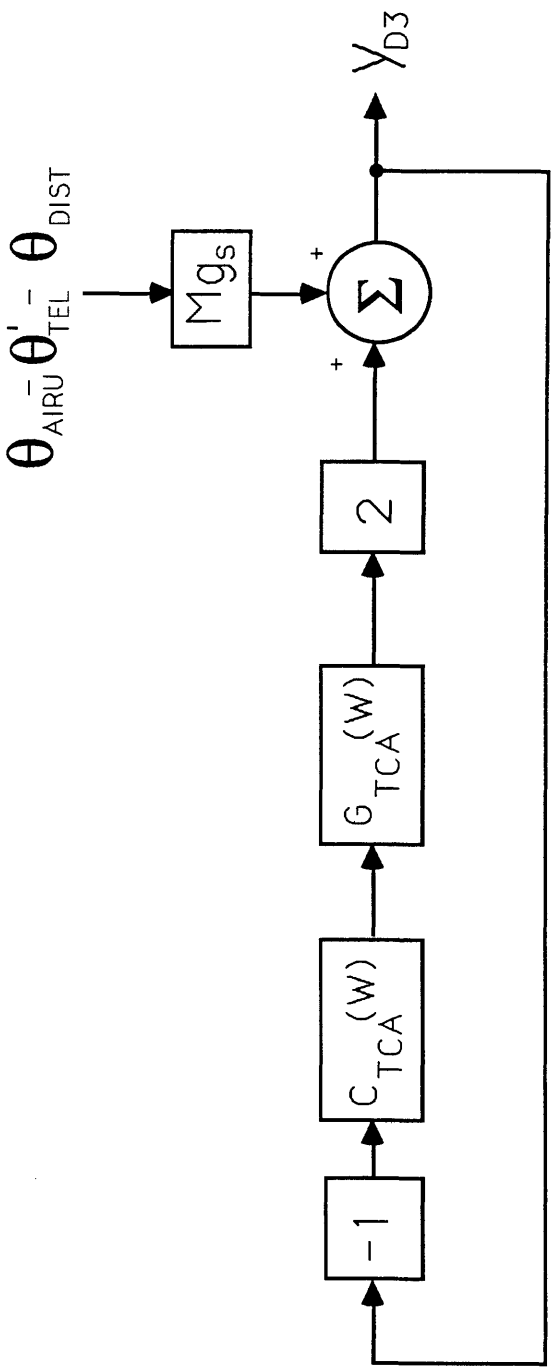

Figure 2.3.3-3 Block Diagram of Closed TCA Regulator Loop

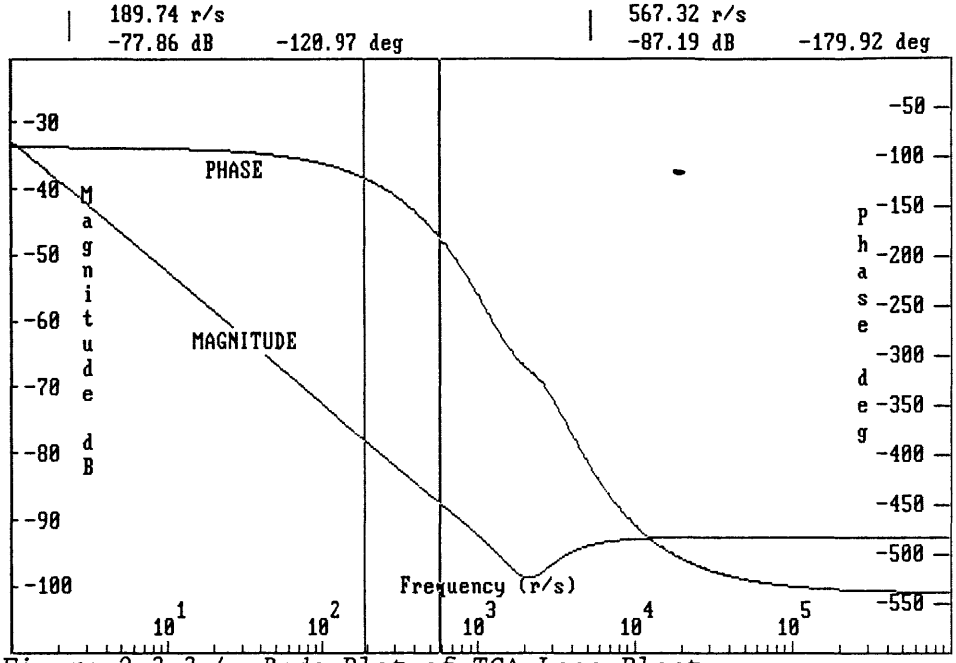

Figure 2.3.3-4 Bode Plot of TCA Loop Plant

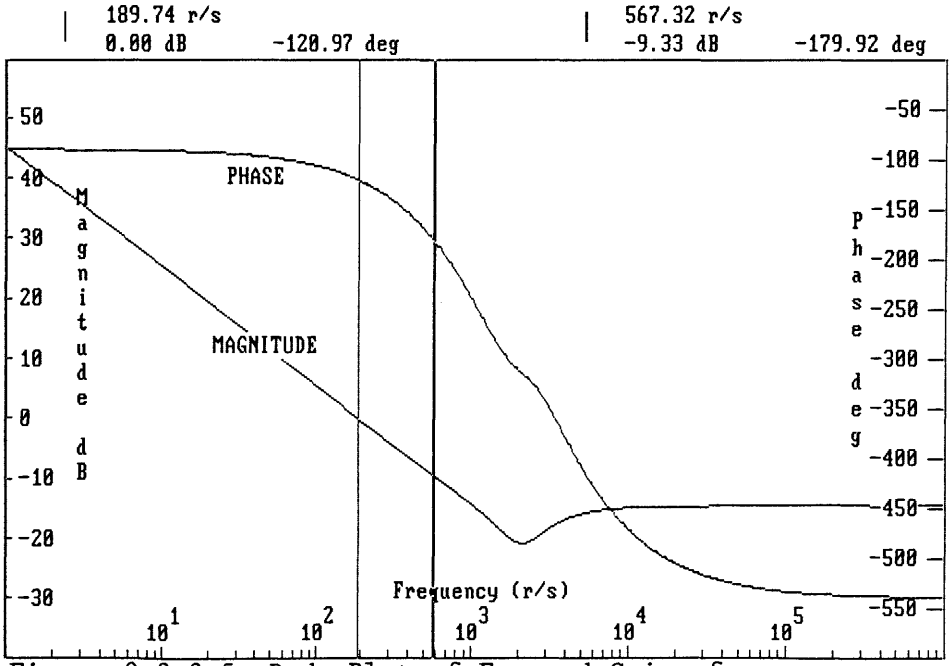

Figure 2.3.3-5 Bode Plot of Forward Gain of Compensated TCA Loop

7816. A Bode plot of the forward gain of the compensated loop is shown in Figure 2.3.3-5.

2.3.4 Keeping the Loops Decoupled

The loops have been designed as separate single-input single-output loops because the system is nominally decoupled. This decoupling is accomplished by finding the set of desired outputs which are pointing errors for each of the actuators. However, under certain conditions, the loops can cross-couple. Since the control system was designed to consist of three uncoupled loops, the stability and performance of the system depends on keeping the loops decoupled. There are two ways in which the loops can become cross-coupled. These are through measurement error due to sensor non-linearities, and through an error in the magnification factor of the telescope used to calculate the desired outputs.

Figure 2.3.4-1 shows a block diagram of the closed loop tracker. Here, the value M' is the telescope magnification factor which is used by the controller to decouple the loops, and is not exactly the same as the telescope magnification factor M. The functions α_1, α_2, and α_3 are the non-linearities of the sensor, and are functions of the positions of the spots. Without sensor noise, it can be seen from the figure that

$$y_{D1} = 2\theta_{TCA}(\alpha_1 - \alpha_3) - M\alpha_1(\theta_{TEL} - \theta_{TARG}) \qquad (2.3.4\text{-}1)$$

$$y_{D2} = 2\theta_{TCA}(\alpha_1 - \alpha_3) - M\alpha_1(\theta_{TEL} - \theta_{TARG}) - M'\alpha_2(\theta_{AIRU} - \theta_{TEL}) \qquad (2.3.4\text{-}2)$$

$$y_{D3} = 2\alpha_3\theta_{TCA} - M'\alpha_2(\theta_{AIRU} - \theta_{TEL}) \qquad (2.3.4\text{-}3)$$

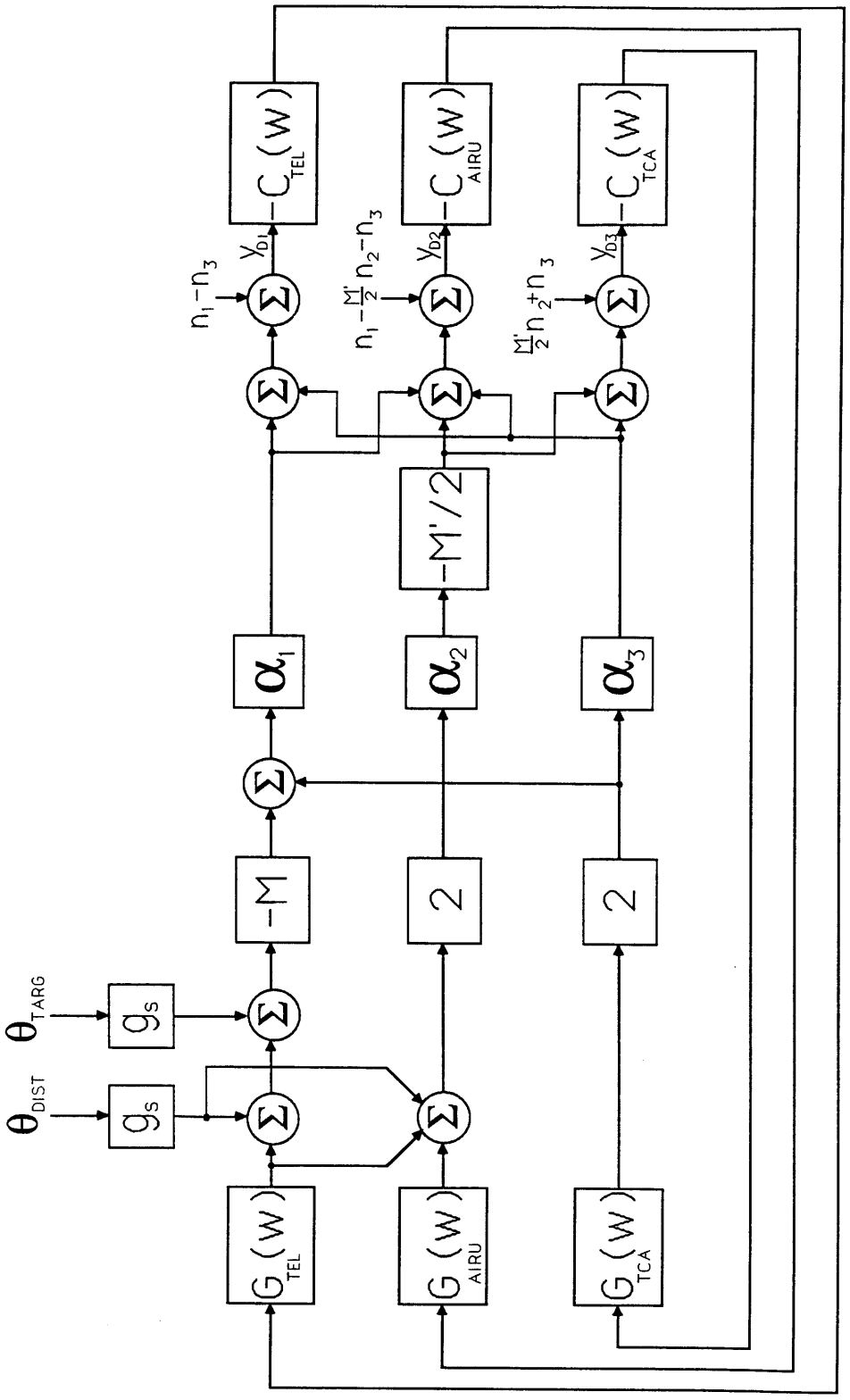

Figure 2.3.4-1 Block Diagram of SATE, Showing Loop Coupling Factors

These outputs cause the dynamics of the loops to couple. That is, y_{D1} depends upon θ_{TCA} as well as θ_{TEL}, y_{D2} depends upon all three actuator angles, and y_{D3} also depends upon all three actuator angles. If the sensor non-linearities are linearized so that all α_i are constant, such as by keeping the physical outputs near the center of a pixel, then the desired outputs become

$$y_{D1} = -M(\theta_{TEL} - \theta_{TARG}) \qquad (2.3.4\text{-}4)$$

$$y_{D2} = -M(\theta_{TEL} - \theta_{TARG}) - M'(\theta_{AIRU} - \theta_{TEL}) \qquad (2.3.4\text{-}5)$$

$$y_{D3} = 2\theta_{TCA} - M'(\theta_{AIRU} - \theta_{TEL}) \qquad (2.3.4\text{-}6)$$

In this case, the loops do not become coupled, but the system performance is hurt because the TCA is not compensating for the correct disturbance on the target spot. Because the TCA will allow the target spot to move on the sensor because of disturbances, the target spot will move to a region of the sensor which is less linear, resulting in cross-coupling.

Although it is not possible to see how sensitive the closed loop system is to sensor non-linearities and to telescope magnification factor error, this short study does show where cross coupling can occur, and what factors must be changed in order to eliminate any coupling which may occur in a working system. In particular, cross coupling can occur only when sensor non-linearities are present. However, the telescope magnification factor error can cause the cross-coupling to be worse by allowing the physical outputs to move away from the center of a pixel.

2.3.5 Implementing the Controller With Integer Arithmetic

A problem with attempting to implement a controller with a microprocessor which does not have an arithmetic coprocessor is that arithmetic operations are limited to integer operations. It is possible to implement floating point arithmetic in software, but the calculations would be prohibitively slow. This means that gains which are not integers must either be rounded or scaled so that they can be implemented. Of particular interest is the telescope magnification factor M = 3.8 which is needed to calculate the desired outputs. This factor must be represented as accurately as possible in order to avoid the coupling problem discussed in Section 2.3.4.

Figure 2.3.5-1 shows a block diagram of the parts of the closed loop system which must be implemented in the computer. The blocks labelled AVG perform the averaging function which is necessary to convert from the fast sampling rate to the slow sampling rate. The figure shows that only four gains must be represented in the controller. In Figure 2.3.5-2, the block diagram has been modified to show only the gains which are part of the controller. Here, the control gain of the TCA and AIRU actuators have been scaled and descaled. This is done because the integrator stages of the TCA and AIRU actuators saturate very quickly when driven by such large control gains. So, the control gains are divided down, and the gain of the TCA and AIRU amplifiers are increased by a factor of 100 and a factor of 10 respectively. This gives the actuators an increased dynamic range.

In Figure 2.3.5-3, the actual values of the control gains are labelled. Because the system will not be very sensitive to rounding the TCA control gain from 78.16 to 80.0 this gain will be changed with negligible effect on the bandwidth of the loop; the gain change will make the TCA loop faster by 2%. Now, the physical outputs can be scaled up by a factor of 10, and the control gains can be scaled down by a factor of 10. Figure 2.3.5-4 is the resulting block diagram. Now all of the

control gains are integers, and the telescope magnification factor was not disturbed.

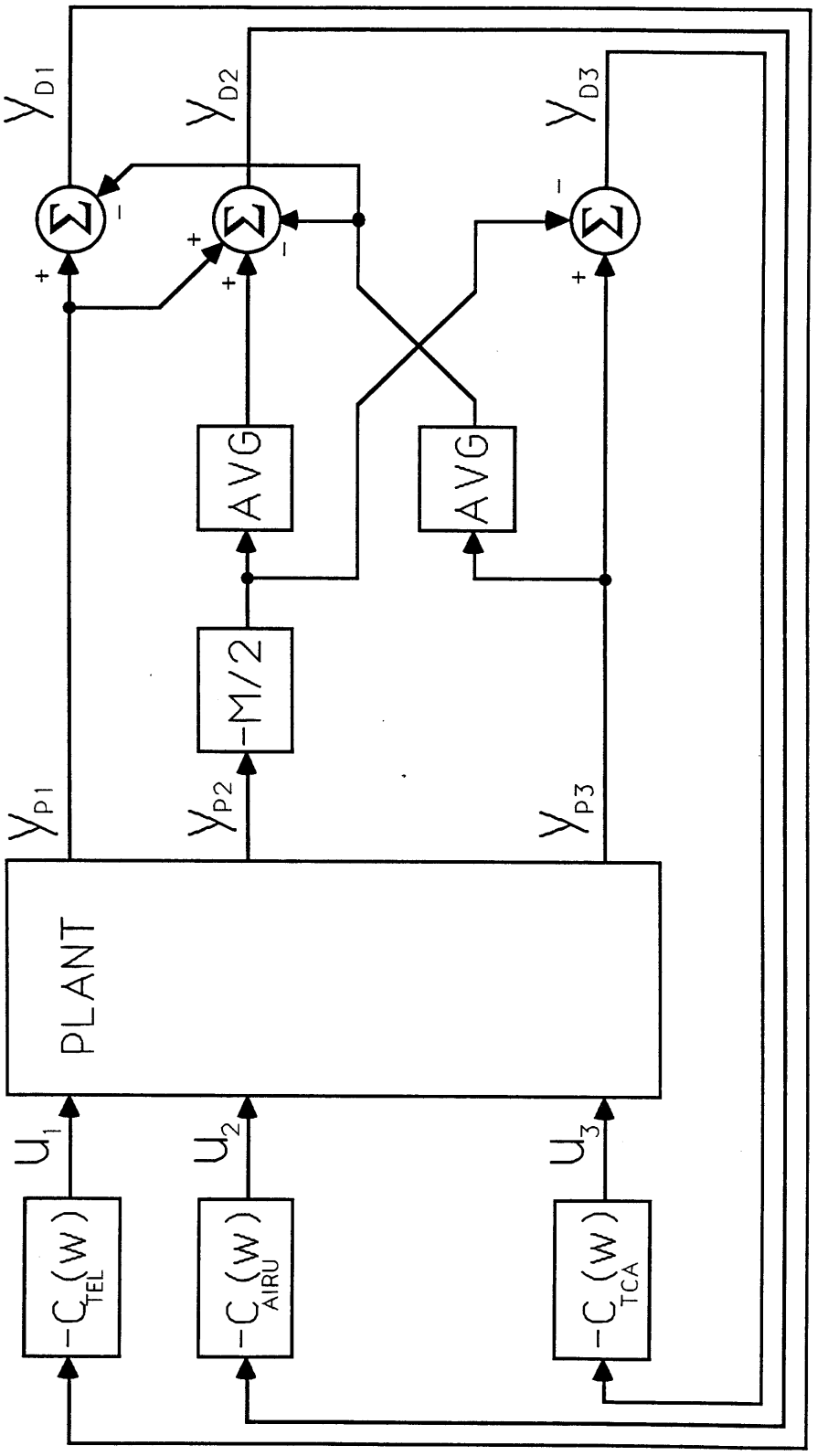

Figure 2.3.5-1 Block Diagram of SATE, Showing Controller Topology

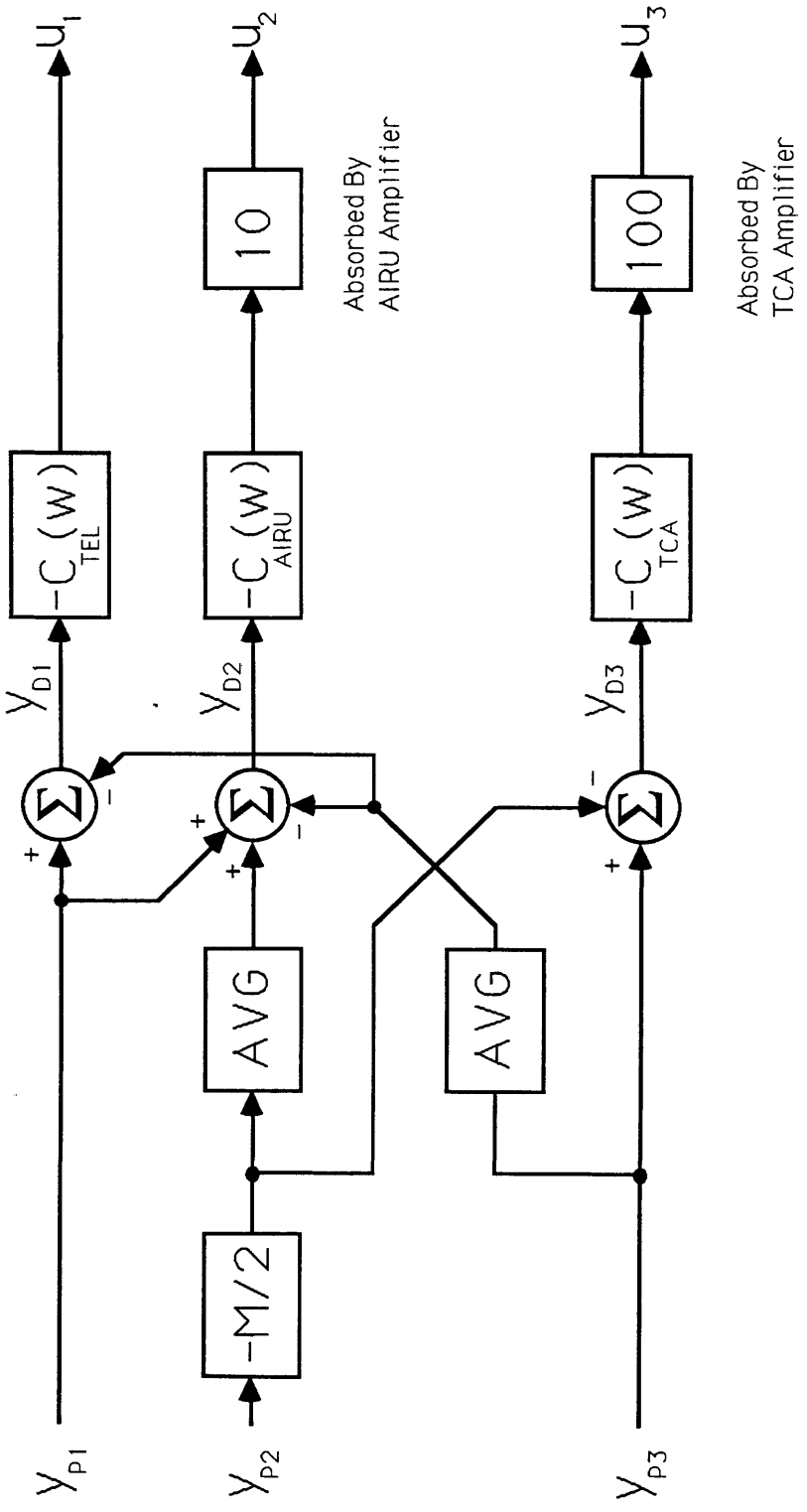

Figure 2.3.5-2 Block Diagram of Controller, with TCA and AIRU Control Gains Partially Implemented By Adjusting the Actuator Amplifier Gains

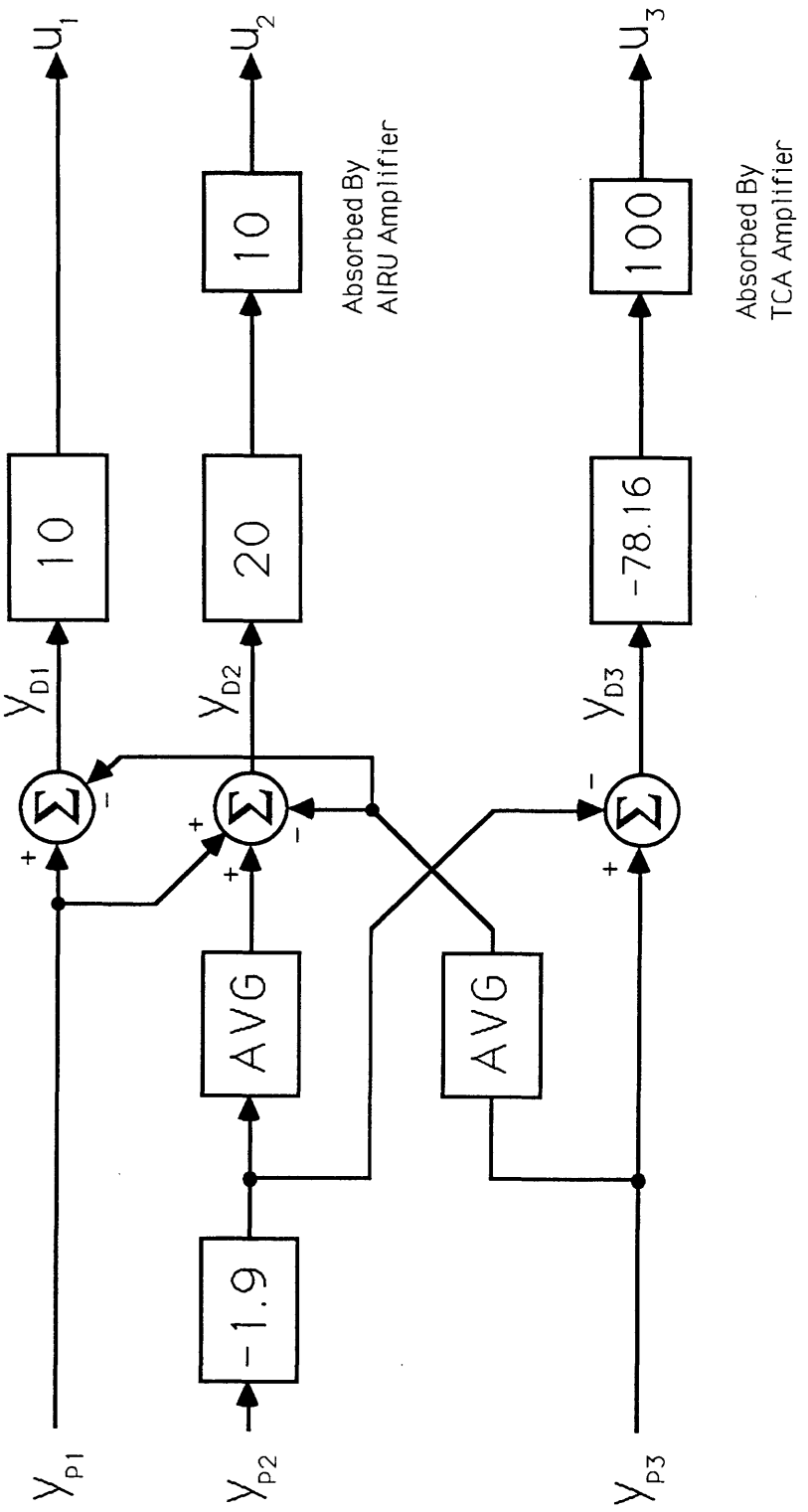

Figure 2.3.5-3 Block Diagram of Controller With Numerical Gain Values

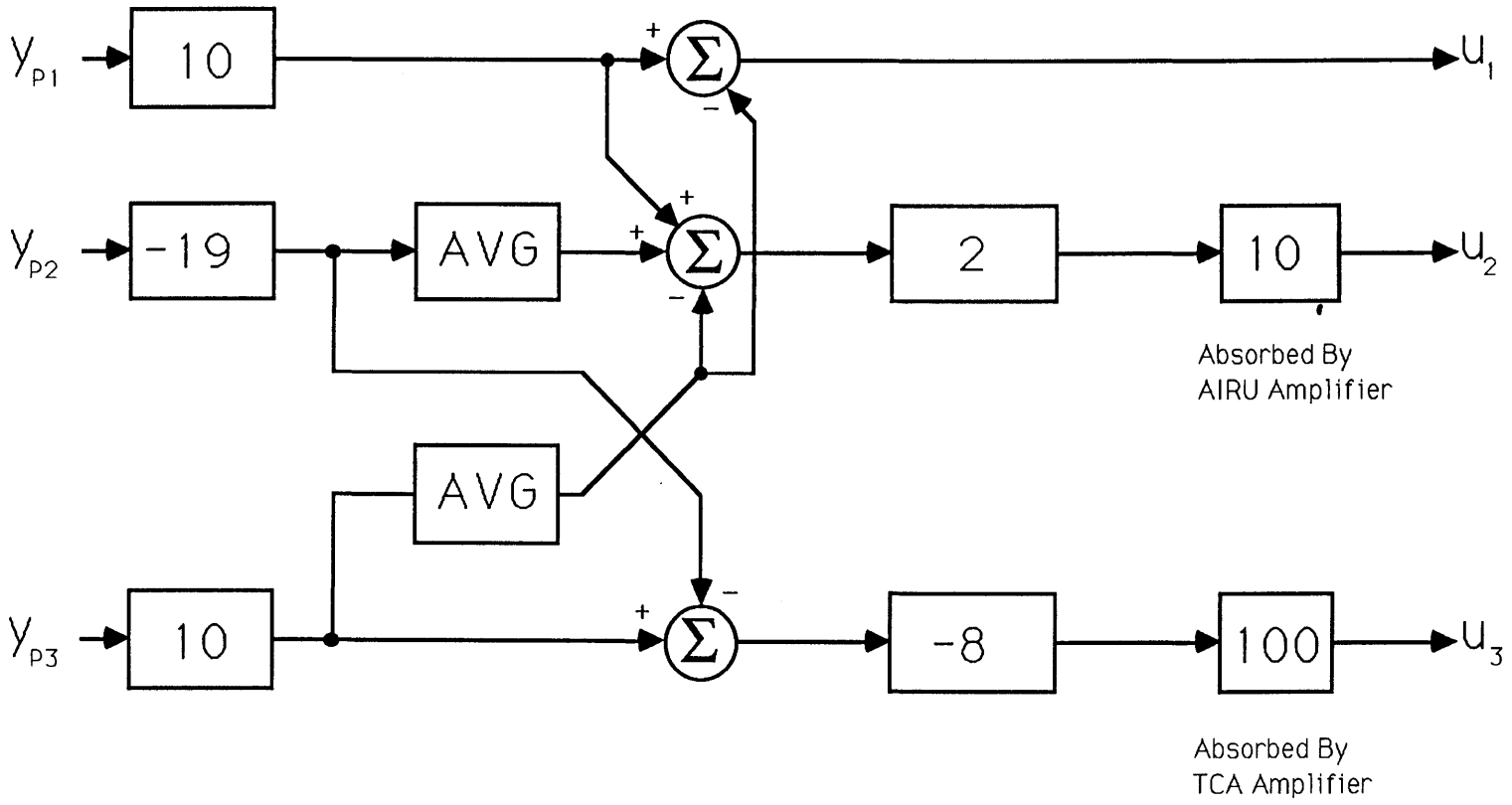

Figure 2.3.5-4 Block Diagram of Controller Implemented Using Integer Arithmetic

CHAPTER 3
SCALED SYSTEM LABORATORY EXPERIMENT

3.0 INTRODUCTION

In Chapter 2, a scaled version of a tracker employing the direct pseudo star projection method was designed. In this chapter, the scaled system is tested in the laboratory. This chapter begins with a description of the laboratory hardware which is involved in testing the design, and then describes the experiments which are performed. Finally, the results of the experiments are presented.

3.1 HARDWARE DESCRIPTION

3.1.0 Introduction

To allow the reader to visualize the system which was designed in Chapter 2, this section will describe the hardware which is used to implement the direct projection method tracker. First, the system optics are described, and then the electronics are described.

3.1.1 System Optics

The most prominent component of the system optics is the

telescope. This is a reflecting beam compressor with an entrance aperture of 4 inches, and a compression ratio of 3.8. The photograph in Figure 3.1.1-1 shows the telescope with the sensor platform attached, mounted on a motorized mirror mount. The two large black cables which lead to the mount are for the stepper motors which allow the mount to be turned. Only the motor which turns the telescope horizontally is used in this system. In the foreground of the photograph are two amplifier circuits for the TCA and AIRU actuators, separated by a threshold circuit for the sensor. At the lower right are the power supplies for the amplifiers, and at lower left can be seen part of the rack which holds the UNIDEX stepper motor controller and a VME bus. The VME bus is a standard bus made by Motorola.

Figure 3.1.1-2 shows a more detailed view of the sensor platform. The board containing the electronics is the MATE sensor analog board, which holds the optical sensor. This assembly is mounted on the sensor platform. Mounted on the post at the far left is the AIRU actuator. On the sensor platform are the alignment laser, the focussing lens, three beam splitters, a mirror at the top right corner of the sensor platform, and at the lower right corner of the sensor platform is the TCA fast steering mirror.

The last section of the system optics is the target. The target will be modelled using a HeNe laser. The beam from the laser will be expanded by a factor of three, and then directed into the front aperture of the telescope by a series of mirrors. Along the path of the target beam, neutral density filters can be inserted across the beam to adjust the intensity of the target image.

3.1.2 Electronics Support

There are four primary electronics systems which support the optics for the laboratory tests. These are the MATE sensor, a VME bus, a UNIDEX stepper motor controller, and an IBM PC-XT. The MATE sensor is the

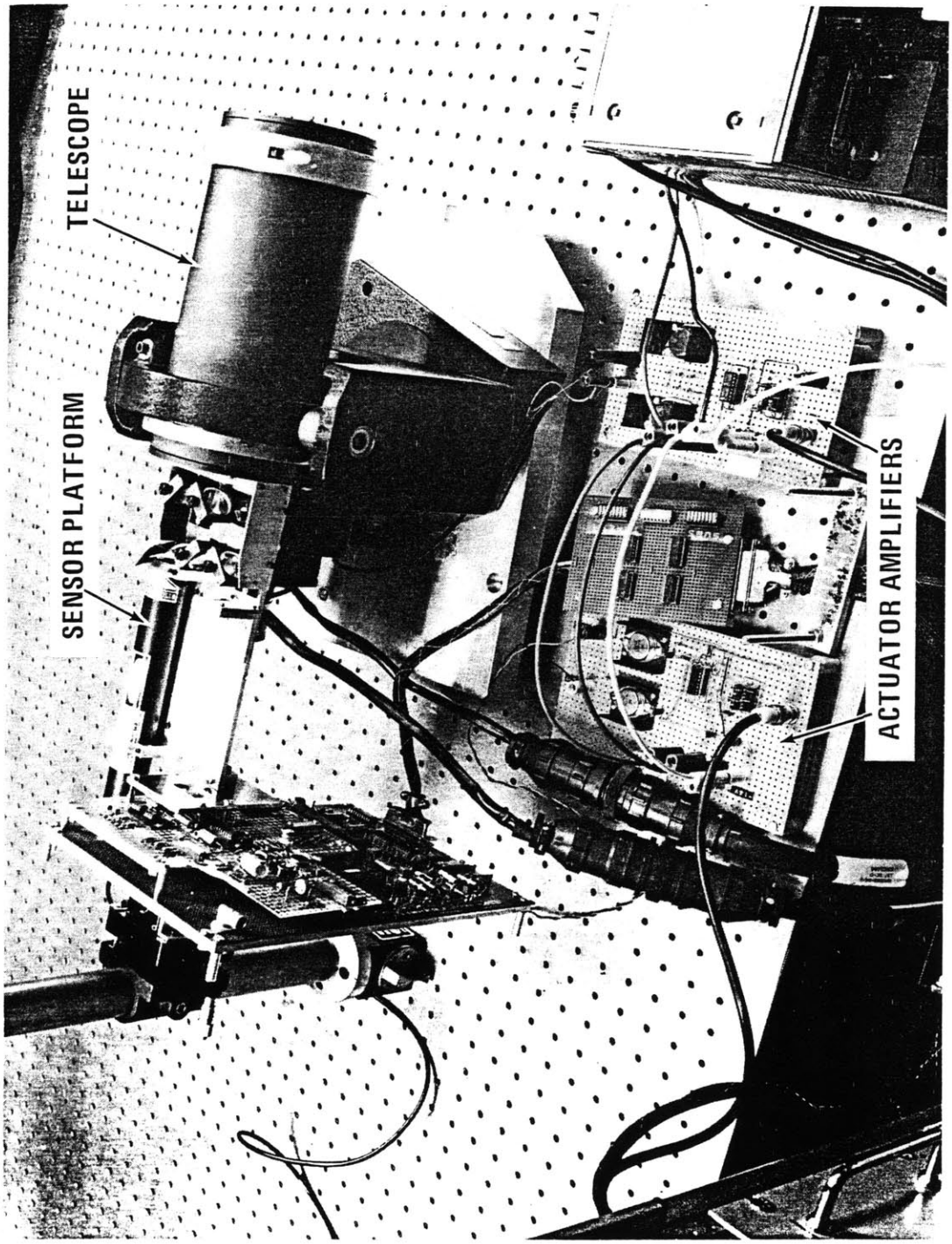

Figure 3.1.1-1 Photograph of Scaled Alignment Transfer System

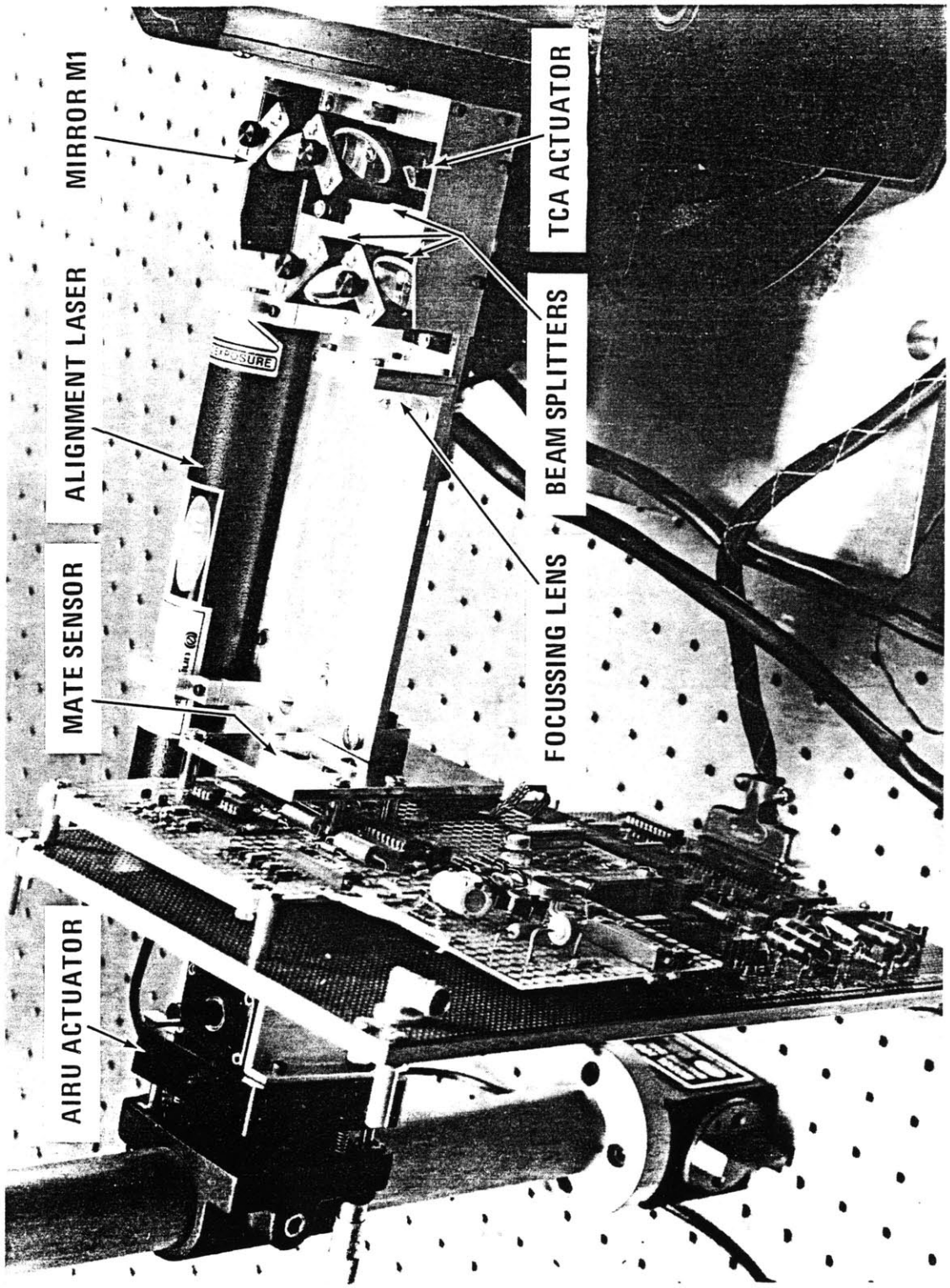

Figure 3.1.1-2 Photograph of the Sensor Platform of the Scaled System

optical sensor which is used for tracking the three spots generated by the optics [11]. It consists of a mosaic array sensor, a timing and analog-to-digital conversion board, and a card for the VME bus. The card for the VME bus allows sensor data to be accessed by other VME cards as if it were in memory on the bus.

Besides the MATE sensor card, the VME bus contains two VME110 cards, which are single board microcomputers with MC68000 microprocessors, an MVME410 parallel port, an MVME605 digital-to-analog converter (DAC) board, 64k bytes of global RAM, and the UNIDEX Controller Controller (UCC), a board built by the author. One of the MC68000 boards, the centroiding computer, will be used to read data from the MATE sensor, calculate centroids for the three spots, and send the centroids to locations in global memory. The second MC68000 board is the controller computer, which will read centroids from global memory, calculate the control signals for each of the actuators, and send the controls to their corresponding actuator. To control the AIRU and TCA, the control words from the controller computer are sent to the appropriate channels of the DAC board, which will drive the actuators. The telescope actuator control path is somewhat more complicated. The controller computer writes a 2 byte word to the parallel port, which sends the word to the UCC. The UCC accepts the word, and uses it as an input to a Delta-Sigma-Modulator (DSM) which was designed by Peter Welling of The Charles Stark Draper Laboratory. The two output lines of the DSM are a direction line, and a clock, and these are sent to the joystick port on the UNIDEX controller. The UNIDEX controller commands the stepper motor on the telescope mount according to the direction and the number of clock pulses it receives from the UCC. The assembly code for the controller computer appears in Appendix C.

An IBM PC-XT is used to write and assemble assembly language programs for the centroiding and controller computers, and is used as an I/O device for the two computers. It also allows data such as error measurements to be dumped from the controller computer into files for external processing and plot generation.

3.2 Experiments

3.2.0 Introduction

There are two things which must be accomplished in the experiments which are performed in this section. The first is that each of the loops designed in Section 2.3 must be closed individually and shown to perform as they were designed. Second, when the three loops are closed together, the control system must be shown to be stable. The experiments also attempt to measure the performance of the system.

3.2.1 Telescope Loop Bandwidth

In order to test the telescope loop, the other two loops are opened, and a step response is measured, To set up the step response, the telescope is first turned so that the target spot moves away from its null position on the sensor. Measurements of the target spot position are taken for a short time without controlling the telescope to establish the starting position of the target spot. The control loop is then closed for a longer time until the telescope has settled. If the target spot measurements are plotted versus time, a step response due to a step in target spot null position results.

The response of the actual closed telescope loop in this experiment is shown in Figures 3.2.1-1 and 3.2.1-2. The first figure shows the response of the telescope loop to a large step, where the target spot moves from the center of one pixel at centroid position 544, across an adjacent pixel with boundaries at 512 and 488, to the null position at the center of a third pixel at 416.

The large step response does not look at all linear, but this is

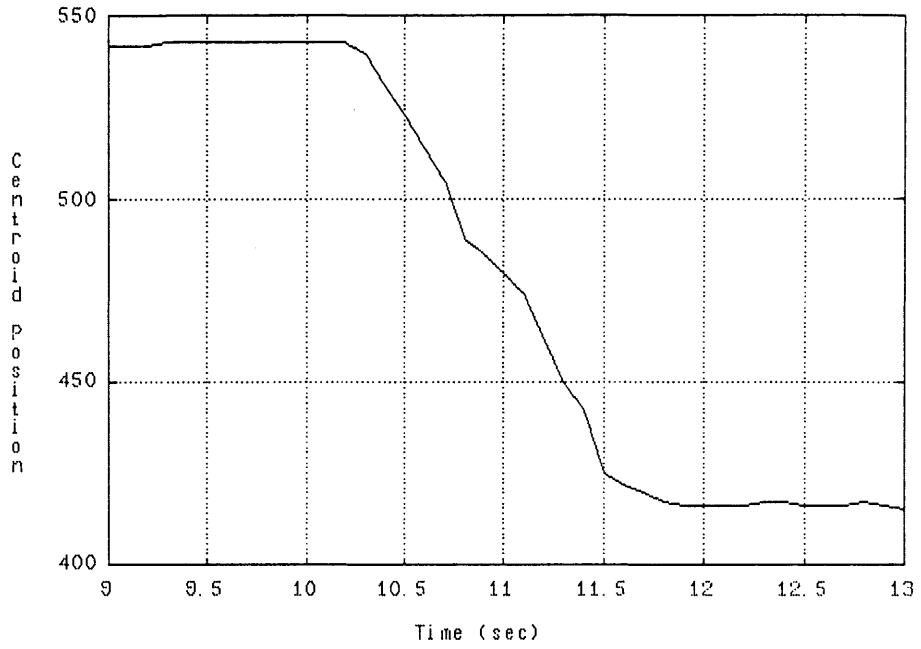

Figure 3.2.1-1 Telescope Loop Large Step Response

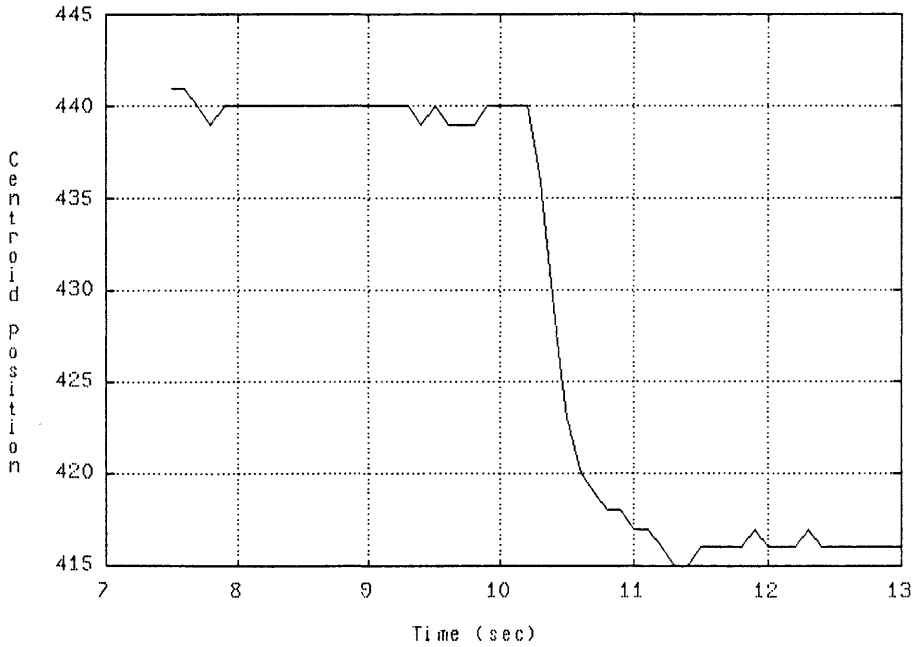

Figure 3.2.1-2 Telescope Loop Small Step Response

expected. It is jagged at the pixel boundaries due to the non-linearities of the sensor, as described in Chapter 2. Also, the telescope actuator is slew limited in this response, causing the response to look more like a ramp than an exponential. Because the large step response is so non-linear, it cannot be used to estimate the bandwidth of the loop thereby verifying the control loop design. However, it is comforting to know that the loop is stable even though the target spot crosses pixel boundaries on the sensor.

In order to verify the controller design, a small step response is measured, where the target spot position is kept within a single pixel. This response looks much more like the exponential which is expected from the single pole loop designed in Section 2.3.1. This response, however, is not quite a linear response. Until the target spot gets to position 429, which is within 13 centroid LSBs of its null position, the telescope actuator will be slew limited. If the time constant is estimated from the time where the target spot reaches 429, the time constant is 0.167 seconds. This time constant corresponds with a crossover frequency of 6 radians/sec, which is the crossover frequency for which the loop was designed.

3.2.2 AIRU Loop Bandwidth

The telescope loop step response is measured by moving the telescope away from the target, and then the loop is closed to drive the target spot to its null position. A similar technique is used to test the step response of the AIRU loop. However, since the AIRU plant contains an integrator, the system can never be driven open loop for very long.

To get the step response of the loop without driving it open loop, the loop is closed so that the pseudo star spot is driven to its null position on the sensor. After ten seconds, the null position is changed,

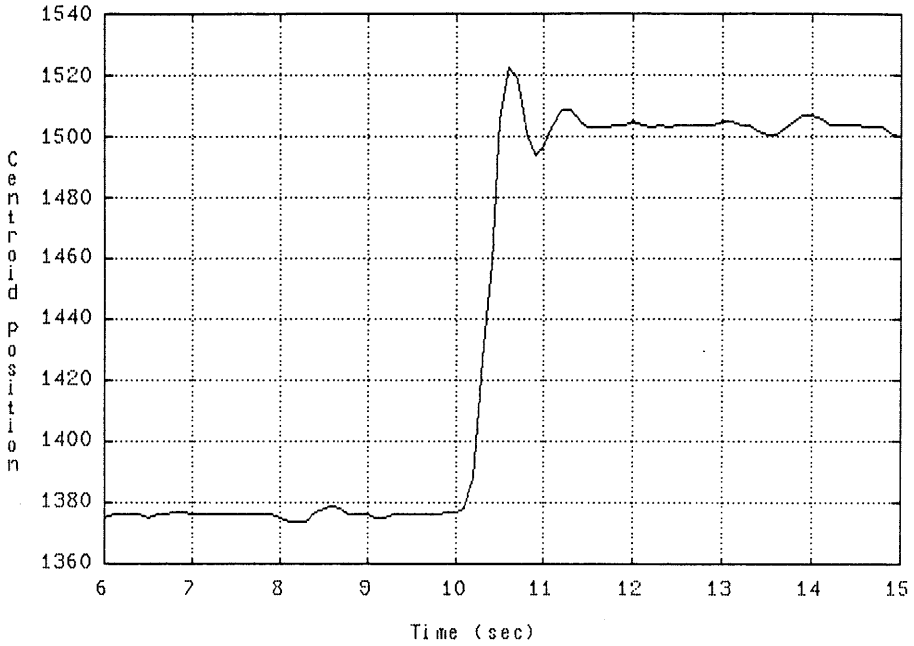

Figure 3.2.2-1 AIRU Loop Large Step Response

and the loop drives the pseudo star spot to the new null position. The motion of the pseudo star determines the step response of the AIRU loop.

The response of the AIRU loop to a large step is shown in Figure 3.2.2-1. In this figure, the initial null position is 1376, and the final null position is 1504. This drives the pseudo star from the center of one pixel, across two pixel boundaries located at 1408 and 1472, to the center of another pixel. The response can be seen to overshoot the final null position, and settle quickly in what appears to be a second order response.

From the figure, the rise time of the response can be measured to be

$$t_r = 0.27 \text{ sec} \qquad (3.2.2\text{-}1)$$

and the peak overshoot is

$$P_o = 1.15 \qquad (3.2.2\text{-}2)$$

From the rise time and the peak overshoot, the half power frequency ω_h and the damping ratio ζ of the closed loop can be calculated according to [7]

$$\zeta \approx \frac{2.2}{t_r} \qquad (3.2.2\text{-}3)$$

$$\zeta = \frac{1}{\left[\left(\frac{\pi}{\ln (P_o - 1)} \right)^2 + 1 \right]^{1/2}} \qquad (3.2.2\text{-}4)$$

So, the half power frequency and damping ratio are

$$\omega_h = 8.15 \text{ rad/sec} \qquad (3.2.2\text{-}5)$$

$$\zeta = 0.517 \qquad (3.2.2\text{-}6)$$

The last parameter needed to characterize this second order response is the natural frequency ω_n. This can be found from the half power frequency and damping ratio using

$$\zeta = \frac{\omega_h}{\left[1 - 2\zeta^2 + (2 - 4\zeta^2 + 4\zeta^4)^{1/2} \right]^{1/2}} \qquad (3.2.2\text{-}7)$$

The natural frequency of the response in the figure is

$$\omega_n = 6.5 \text{ rad/sec} \qquad (3.2.2\text{-}8)$$

Because the step response of the closed AIRU loop appears to be second order, the phase margin and crossover frequency can be estimated according to the curves given on page 157 of Reference [7]. From these curves, the crossover frequency ω_c and the phase margin Φ_m are

$$\omega_c = 5.1 \text{ rad/sec} \qquad (3.2.2\text{-}9)$$

$$\Phi_m = 52^\circ \qquad (3.2.2\text{-}10)$$

When the loop was designed in Section 2.2.1, it was designed to cross over at $\omega = 6.3$ rad/sec, with a phase margin of 47°. According to the Bode plot of the designed loop (see Figure 2.2.1-9), if crossover were forced to be $\omega = 5.1$ rad/sec, the phase margin would be 51.3°.

It is somewhat surprising that the large step response so closely matches the model developed in Chapter 2. The severe non-linearities of the sensor do not seem to have changed the response much from the expected linear response. Upon close inspection of the large step response, the envelope of the ringing seems to indicate that the system behaves as a second order system only after the spot reaches 1460. The rise time

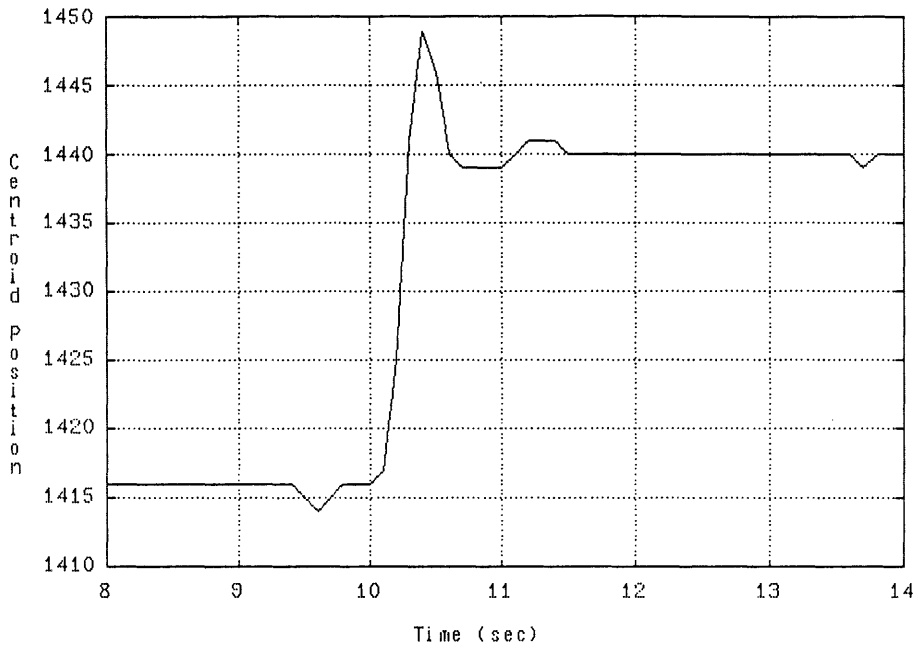

Figure 3.2.2-2 AIRU Loop Small Step Response

measured for this response may be slow due to a slew limit at the beginning of the response. To see if the sensor non-linearities or the slew limit of the loop have any serious effect on the performance of the loop, a small step response must be examined.

Figure 3.2.2-2 shows the small step response of the AIRU loop, where the entire response is kept within a single pixel. The initial null position is at 1416, and the final null is at 1440. Like the large step response, the small step response also exhibits an overshoot. The rise time and peak overshoot for this response are

$$t_r = 0.21 \text{ sec} \qquad (3.2.2\text{-}11)$$

$$P_o = 1.375 \qquad (3.2.2\text{-}12)$$

The faster rise time and higher peak overshoot indicate that the system is faster and less damped than the response of the first figure. The damping ratio, half power frequency, and natural frequency, are

$$\zeta = 0.298 \qquad (3.2.2\text{-}13)$$

$$\omega_h = 10.5 \text{ rad/sec} \qquad (3.2.2\text{-}15)$$

$$\omega_n = 7.2 \text{ rad/sec} \qquad (3.2.2\text{-}16)$$

From the curves on page 157 of Reference [7], the crossover frequency and phase margin of the response are

$$\omega_c = 6.5 \text{ rad/sec} \qquad (3.2.2\text{-}16)$$

$$\Phi_m = 35° \qquad (3.2.2\text{-}17)$$

Although the crossover frequency of the response is very close to the crossover frequency for which the loop was designed, the phase margin is 12° less than the designed phase margin. This response does not match the model as well as the large step response. However, the large step response was not a linear response, and is probably not very accurate. It is possible that sensor noise on the measurement of the small step response is causing the system to appear to have less phase margin than it actually has.

To see whether sensor noise may have caused the small step response to indicate that the system is "less stable" than it was designed to be, several more small step responses are taken with step sizes identical to the first one. Figure 3.2.2-3 shows one of the other

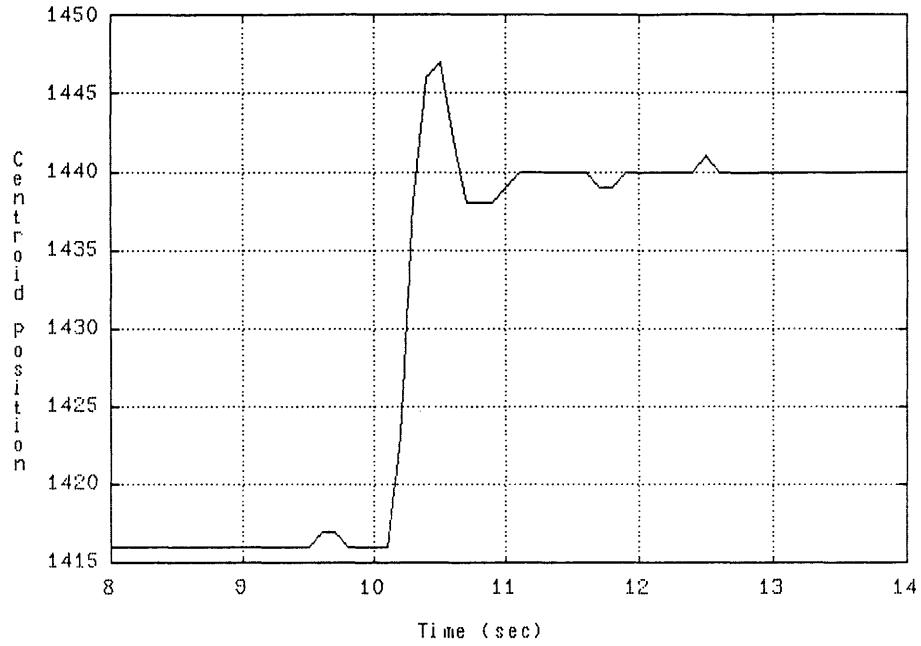

Figure 3.2.2-3 Rerun of AIRU Loop Small Step Response

responses. The crossover frequency and phase margins indicated by this response are

$$\omega_c = 8.0 \text{ rad/sec} \qquad (3.2.2\text{-}18)$$

$$\Phi_m = 40° \qquad (3.2.2\text{-}19)$$

If the loop designed in Chapter 2 were forced to cross over at 8 rad/sec, it would have a phase margin of 42°. Because the large step response and the rerun of the small step response agree quite closely with the model developed in Chapter 2, it seems likely that the model was good, and the the actual crossover frequency falls somewhere between 5 rad/sec and 8 rad/sec.

It is interesting to see what happens if the pseudo star spot is driven to a null position which is very close to a pixel boundary. Figure

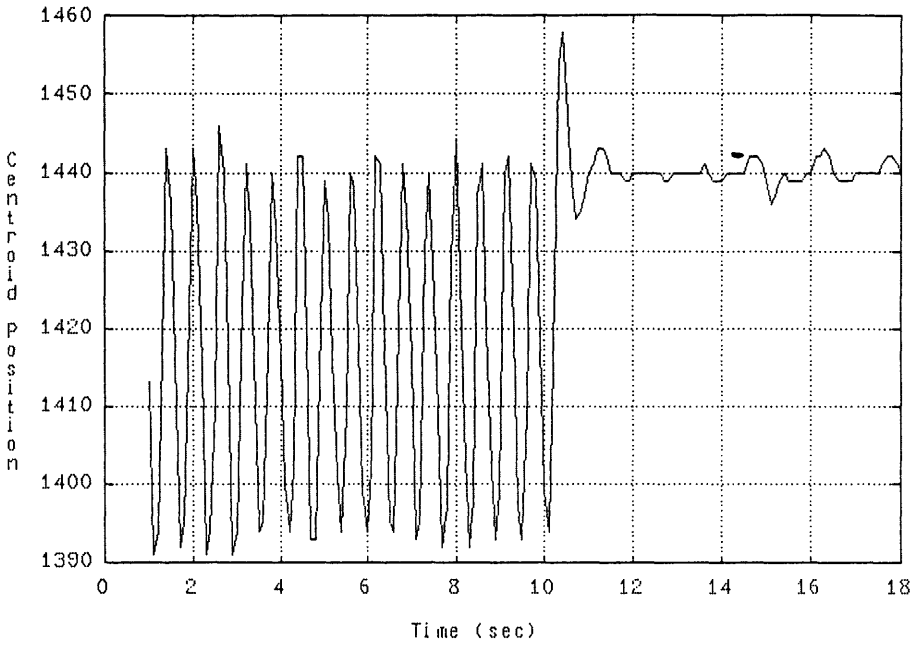

Figure 3.2.2-4 Limit Cycling Due to Driving the Pseudo Star Spot to a Null Position Which Is Too Close to a Pixel Boundary

3.2.2-4 shows a small step response with the same null positions as were used in Figures 3.2.2-2 and 3.2.2-3. As seen in Figure 2.2.1-2, the sensor has a very high gain at pixel boundaries, and also has hysteresis between pixels. If the pseudo star spot is ever driven across the pixel boundary such as by overshooting the null position or by sensor noise, then the limit cycling exhibited in the figure may occur. The effect is similar to attempting to drive the output of a Schmitt trigger to a value near zero.

The step responses of the AIRU loop agree closely with the expected responses of the loop which was designed. However, the limit cycling exhibited in the last figure may cause problems when more than one loop is closed at a time. Before multiple loops can be closed, however, the third loop must be closed around the TCA.

3.2.3 TCA Loop Bandwidth

The bandwidth of the TCA loop is measured in exactly the same way as the bandwidth of the AIRU loop. That is, the loop is closed so that the reference spot is driven to an initial null position on the sensor. Then, after a delay of 0.091 seconds, the null position is changed. The motion of the reference spot on the sensor determines the step response of the TCA loop.

The response of the TCA loop to a large step is shown in Figure 3.2.3-1. In this response, the initial null position of the reference spot is at 1056, and the final null position of the reference spot is at 1184. This drives the reference spot from the center of one pixel, across two pixel boundaries located at 1088 and 1152, to the center of another pixel. The figure shows that there is a small amount of overshoot in the large step response, however it is unclear whether the overshoot is due to the step response of the actuator, or due to the large jumps which the spot seems to take when it crosses pixel boundaries. The figure also shows that the rise time for this response is about 30 ms. This would imply that the half power frequency ω_h is approximately 33 rad/sec, which is alarmingly slow for a loop which is supposed to cross unity gain at ω_c = 190 rad/sec. The reason it is so slow is that the saturation limit on the DAC has been reached, and the response represents the slew limit of the loop. Although the pixel non-linearities and the slew limit make a bandwidth measurement impossible for this response, it is comforting to know that the loop is stable when the reference spot is driven across pixel boundaries.

Figure 3.2.3-2 shows a small step response, with the same step size as was used to characterize the AIRU loop in Figures 3.2.2-2 and 3.2.2-3. Like the large step response, this response also has a long rise time t_r = 7.9 ms, which means that the half power frequency ω_h is 126.1 rad/sec. This is still much lower than expected if the loop has a crossover frequency of 190 rad/sec. The reason for this is that for the

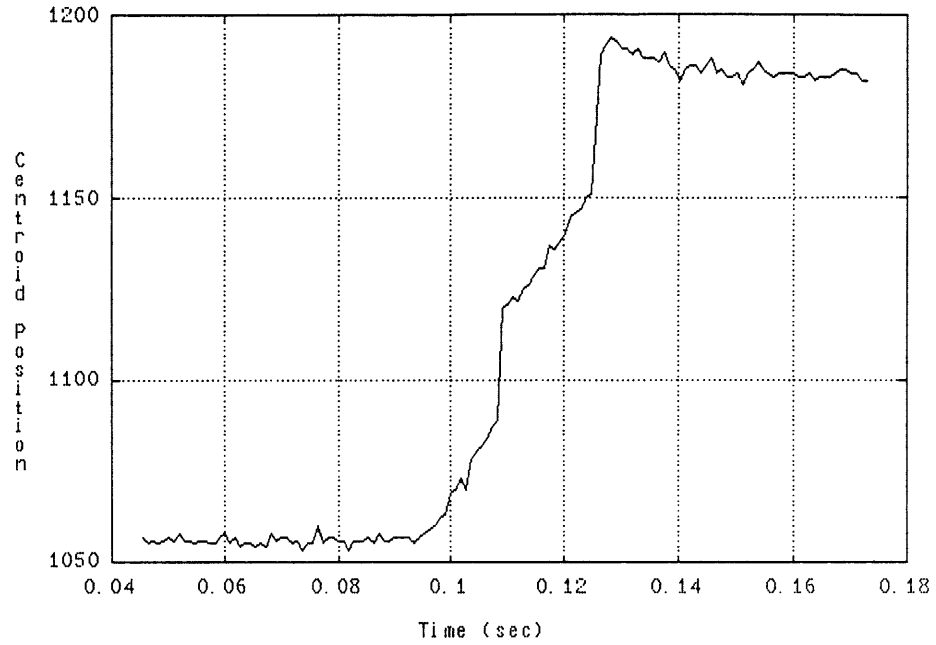

Figure 3.2.3-1 TCA Loop Large Step Response

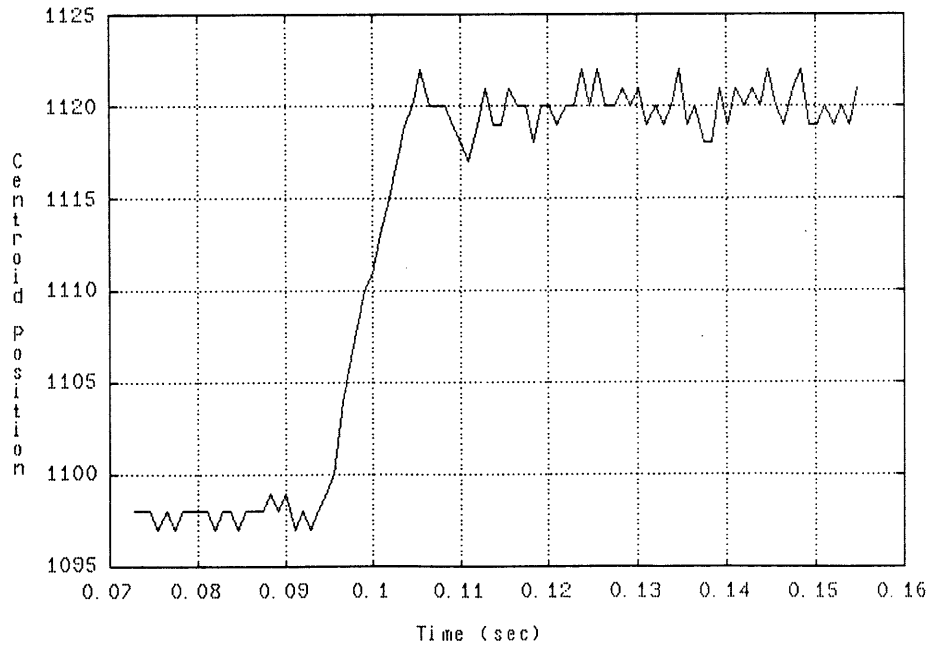

Figure 3.2.3-2 TCA Loop Small Step Response With DAC Saturation

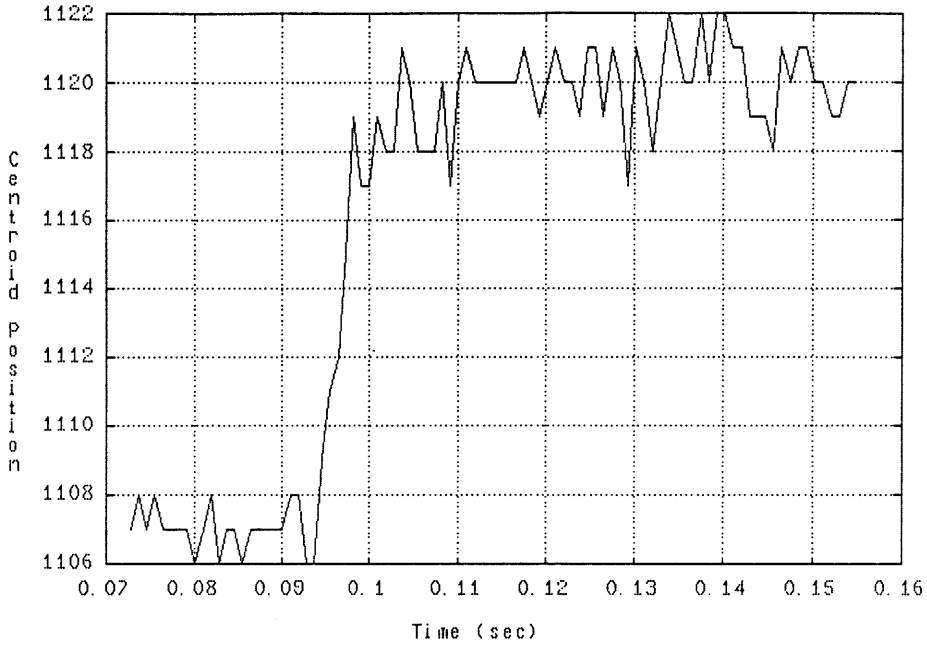

Figure 3.2.3-3 TCA Loop Linear Small Step Response

gain used to compensate the TCA loop, a tracking error of greater than 13 will cause the DAC to saturate. Here, the reference spot is said to be tracking the null position. So, for almost half of the step in the figure, the DAC is saturated, which means that the response is slew limited.

In Figure 3.2.3-3 the step size has been reduced to 13. Its initial null position is 1107, and its final null position is 1120, which means that the DAC is saturated only for the first sample after the step occurs. The rise time and half power frequency for this response are

$$t_r = 3.8 \text{ ms} \qquad (3.2.3\text{-}1)$$

$$\omega_h = 263.6 \text{ rad/sec} \qquad (3.2.3\text{-}2)$$

The noisy measurement of the reference spot position precludes

making a measurement of the peak overshoot of the response. However, it does not appear to have any overshoot at all. The lack of any perceivable overshoot in the response suggests that the damping ratio is

$$\zeta \geq 0.7 \qquad (3.2.3\text{-}3)$$

The noisy measurements make it necessary to confirm this damping ratio.

The TCA loop was originally designed to have a phase margin of 60°. When this phase margin was calculated, the TCA was modelled with two sampling periods of delay for calculations. One sample delay is used to calculate the centroids of the spots, and one sample delay is used to calculate the control signals. When the controller is implemented, the full delay which is allowed for the controller calculations is not used. Instead, approximately one half sample delay is used for the controller calculations in order to give the TCA loop as much phase margin as possible. By saving a half sample delay in the loop, another 5° is added to the phase margin, bringing the phase margin up to 65°.

From Reference [7] page 157, a phase margin of 65° results in a damping ratio of

$$\zeta = 0.7 \qquad (3.2.3\text{-}4)$$

If this damping ratio is used with the half power frequency, the natural frequency of the closed loop system can be found from Equation (3.2.2-7) to be

$$\omega_n = 268.9 \text{ rad/sec} \qquad (3.2.3\text{-}5)$$

The curves on page 157 of Reference [7] can be used to find the crossover frequency of the loop

$$\omega_c = 279.3 \text{ rad/sec} \qquad (3.2.3\text{-}6)$$

or

$$f_c = 28.5 \text{ Hz} \qquad (3.2.3\text{-}5)$$

This agrees with the designed crossover frequency of the loop to within 6%. However, it is based upon the empirical calculation of the damping ratio, which was not accurately measured in the response.

3.2.4 All Three Loops Closed

Now that all three loops have been closed individually, and have been shown to behave as they were designed, they must all be closed at once. The purpose of this experiment is to see if the system is stable with all three loops closed, and to see if the control system drives the three spots to the correct null positions on the sensor. Since the sensor is very non-linear near the pixel boundaries, the null positions for the spots will be in the center of pixels. As was mentioned in Section 2.3.4, nulling the spots at the center of pixels should minimize coupling between the loops.

Figures 3.2.4-1, 3.2.4-2, and 3.2.4-3 show the response of all of the spots when the controller is turned on. The null position for the target spot is at 416, the pseudo star is driven to 1440, and the

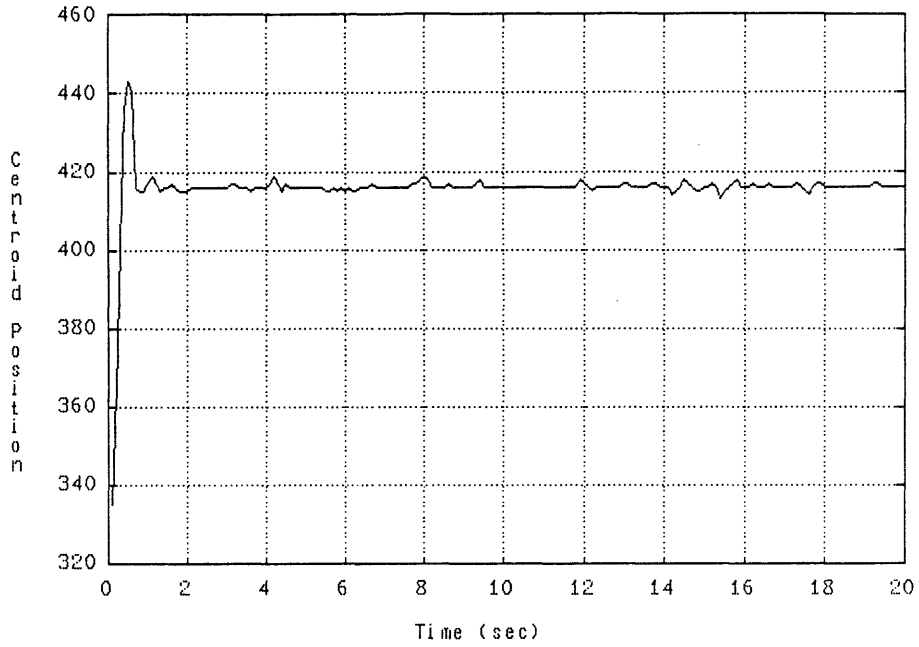

Figure 3.2.4-1 Acquisition of the Target Spot With All Three Loops Closed

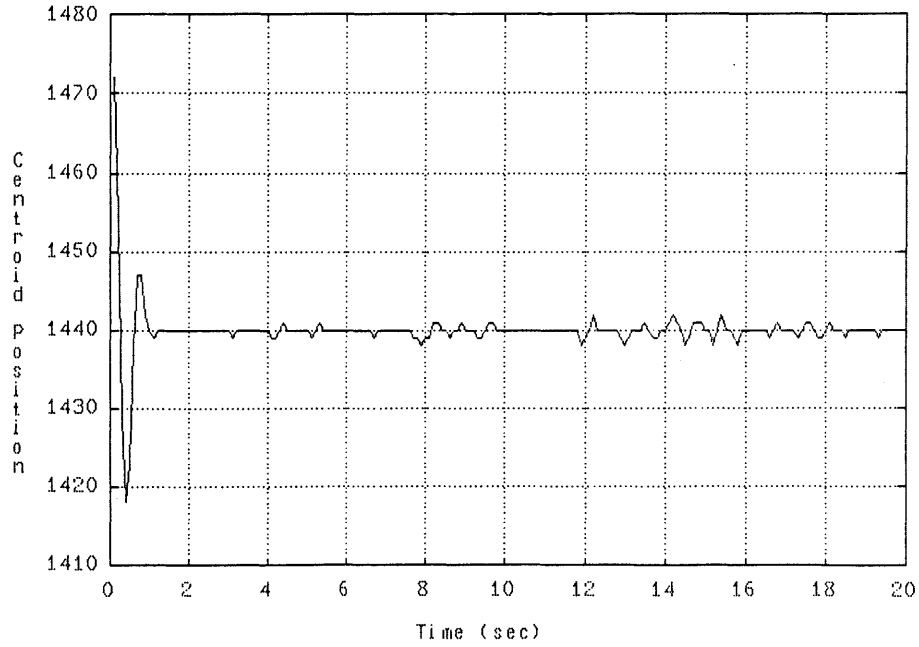

Figure 3.2.4-2 Acquisition of the Pseudo Star Spot With All Three Loops Closed

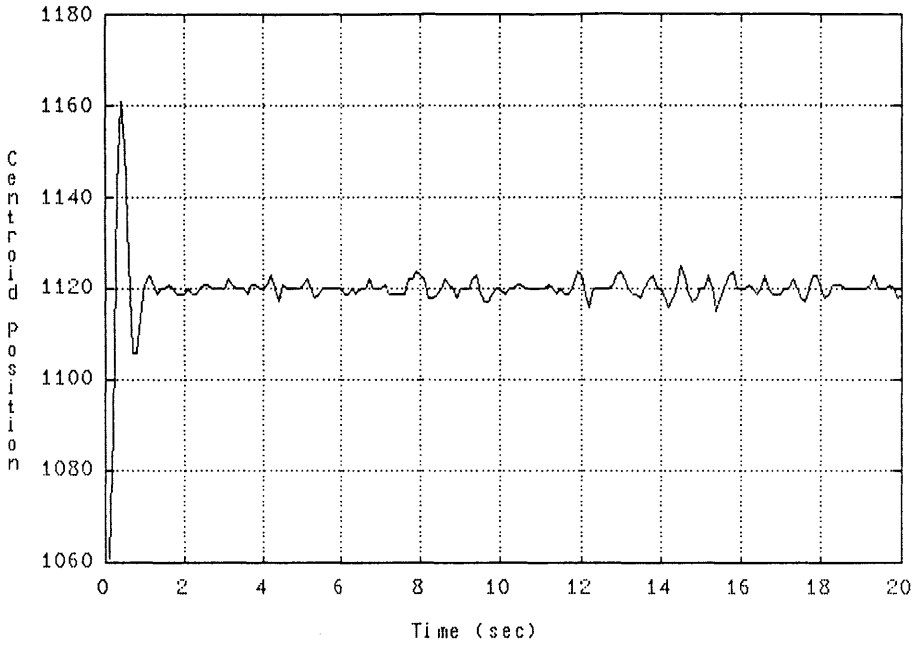

Figure 3.2.4-3 Acquisition of the Reference Spot With All Three Loops Closed

reference spot is to be nulled at 1120. The target spot can be seen to start a little more than one pixel from its null position. It has some overshoot (about 35%), and settles to its null position within one second. Once it is at its null position, it is held there to within ±3 LSBs for the remainder of the 20 second experiment. The accuracy to which motions of the target can be seen is interesting to note. If the target spot can be held constant to within ±3 LSBs, then target spot motions on the order of ±3 LSBs can be seen on the sensor. The pixels have a center-to-center spacing of 4 mils, and there are 64 LSBs per pixel. So, the smallest detectable motion of the target spot will be ±0.2 mils on the sensor. The focussing lens has a focal length of 7 inches, which means that the smallest detectable angle of target motion will be ±27 μrad at the point where light from the target reaches the focussing lens. Because of the magnification of the telescope, this means that target motions on the order of ±7 μrad can be detected by the system. This figure is somewhat misleading as a system accuracy specification, because the target used in this experiment is bright and stationary, and there are no disturbances on

the sensor platform. It is thus a best case figure of merit.

The accuracy of the system actually complicates measuring the control system response. This is because it is accurate enough to track motions of the target which are due to air currents in the laboratory. The results in the three figures were obtained with the air conditioners turned off and no one else in the laboratory.

The response of the pseudo star spot is similar to the response of the target spot, except that it takes a little longer to settle, and its overshoot is about 69%. The pseudo star spot is held at its null position to within ±2 LSBs after the transient settles. It is not clear, however, whether the larger errors are due to sensor platform disturbances, target motion due to air turbulence, or sensor noise.

The reference spot response is almost exactly a scaled version of the pseudo star response. The TCA loop is doing a very good job of causing the reference spot to track the pseudo star spot.

It is clear from the figures that the closed loop system is indeed stable, and does a good job of driving the three spots to their null positions on the sensor. However, it is not clear whether the loops are totally decoupled as they were designed to be, and it is not yet clear how quickly the system would react to a step in target position.

3.2.5 Response To A Step In Target Position

Although the time it takes to acquire all three spots and move them to their null positions gives some indication of the speed of the tracking system, acquisition is not a maneuver which is performed very often in a real tracking system. More likely, a system will acquire a new target when the alignment spots are already at their null positions. To see the response of the system to a change in targets, a step response is taken. In this experiment, the step is implemented by changing the null

position of the target spot, and waiting for the target spot to settle at the new null position.

Figures 3.2.5-1, 3.2.5-2, and 3.2.5-3 show the response of the system to a step in target spot null position. The first figure shows the response of the target spot, where the null position was stepped from 352, which is the center of one pixel, to 416, which is the center of an adjacent pixel. This response has a long settling time of about three seconds, and a large overshoot of about 109%. The long settling time means that the system will not be able to acquire new targets very quickly.

The three second settling time is very slow for a system whose slowest loop is about 1 Hz. Also, the ring and the large overshoot indicate that the system is much less stable than any of the individual loops. This indicates that the loops are coupled somewhat, changing the dynamics of the system.

In Chapter 2, the two ways in which the loops could become coupled were discussed. These are that the telescope magnification factor used in the controller could be wrong, or the sensor non-linearities could be causing the loops to couple. The telescope magnification factor was measured in Chapter 2, and there is little more that can be done about an error in this factor other than just trying a different number and seeing what happens to the loop. This was, in fact, attempted, and Figure 3.2.5-4 shows the response of the target spot when a factor of 4.0 is used. This response is a repeat of the experiment in Section 3.2.4, and there is no step in the null position of the target spot. The oscillations due to the error in the telescope magnification factor have an amplitude of approximately 20 LSBs peak-to-peak, and a frequency which is almost identical to the damped oscillations in the step response. This is evidence that telescope magnification factor error cause the loops to couple, thus undermining the stability of the system. Unfortunately, the integer arithmetic to which the controller computer is limited will not allow the magnification factor to be adjusted any closer to its actual value than the value of 3.8 used in the step response.

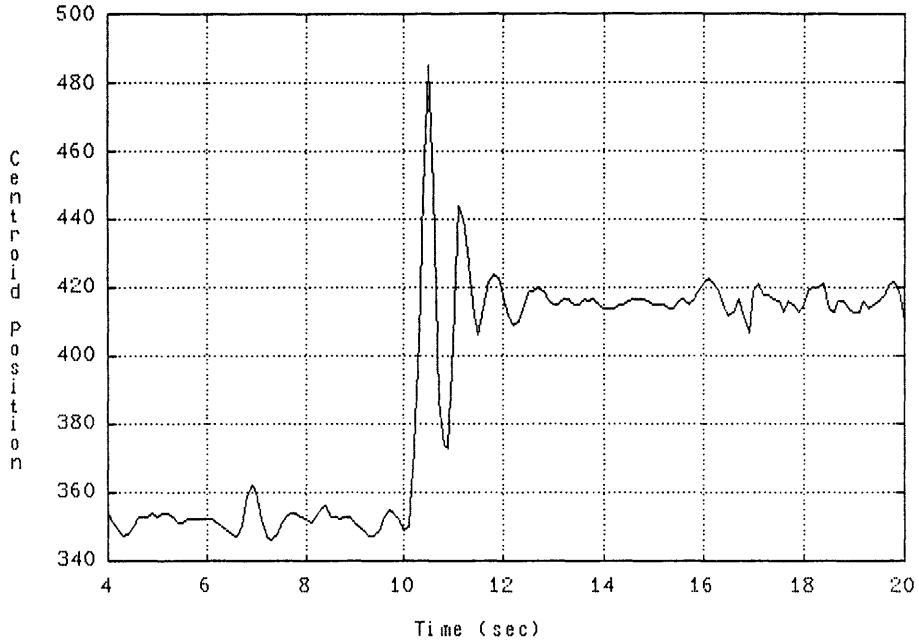

Figure 3.2.5-1 Response of the Target Spot to a Step In Target Position With All Three Loops Closed

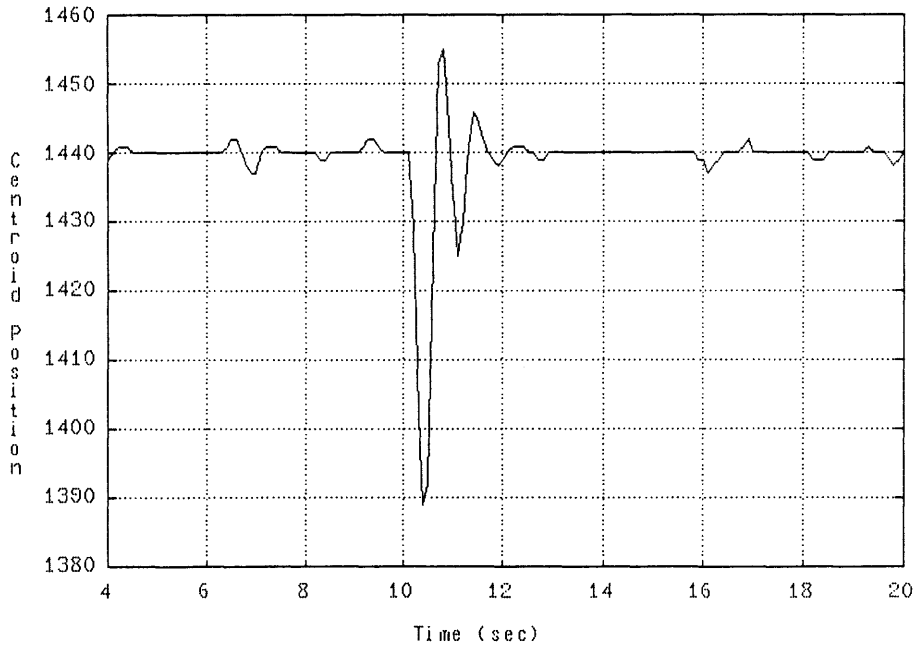

Figure 3.2.5-2 Response of the Pseudo Star Spot to a Step In Target Position With All Three Loops Closed

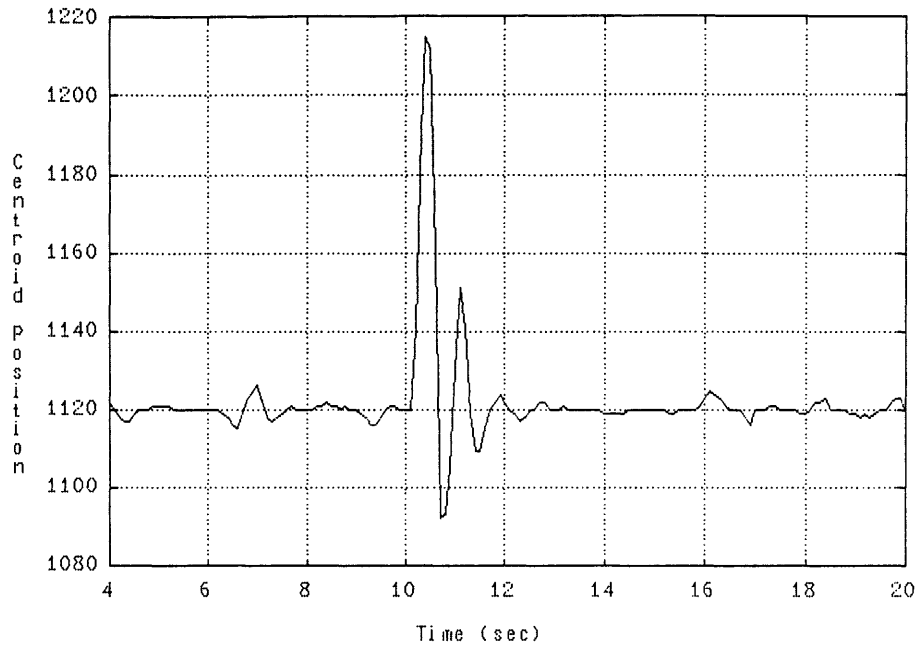

Figure 3.2.5-3 Response of the Reference Spot to a Step In Target Position With All Three Loops Closed

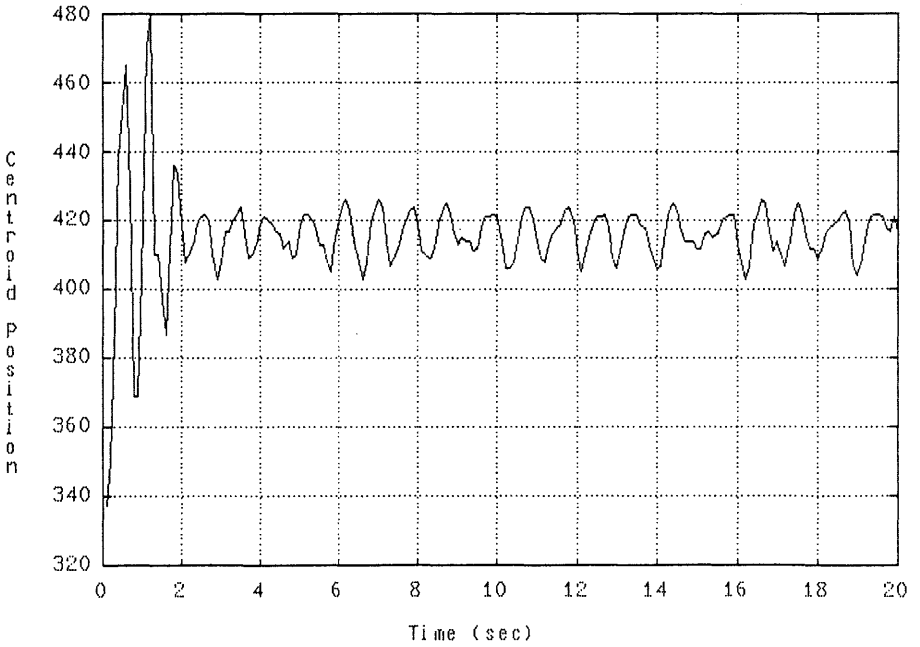

Figure 3.2.5-4 Target Spot Oscillations Due to Telescope Magnification Factor Measurement Error

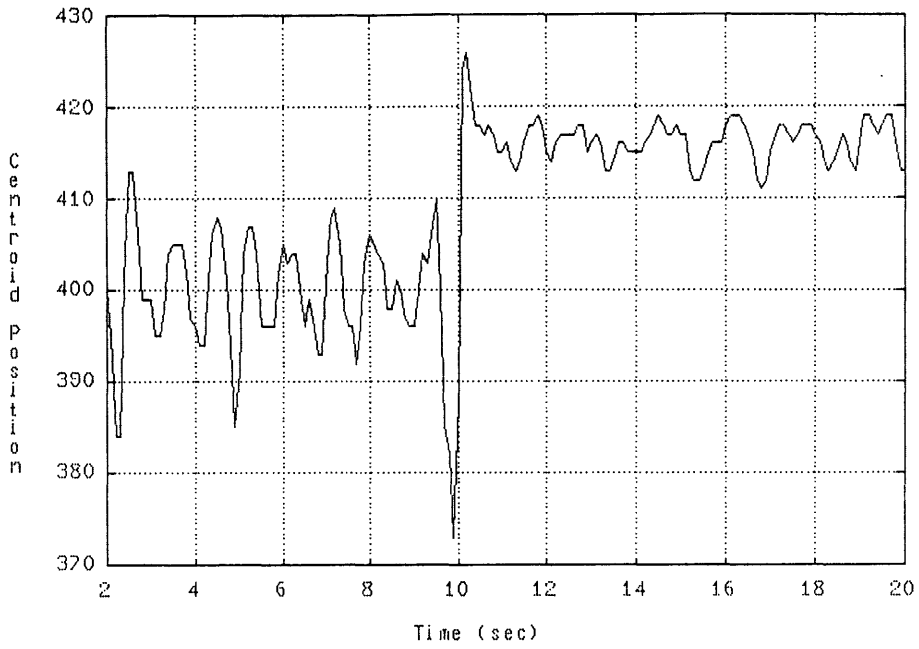

Figure 3.2.5-5 Target Spot Oscillations Due to Sensor Non-linearities

Because the oscillations in Figure 3.2.5-4 are neither growing nor decaying, there must be some non-linear process which keeps the oscillations at about a constant amplitude. The non-linear process is, of course, the non-linearities of the pixels in the sensor.

To see how sensitive the system is to the pixel non-linearities with the telescope magnification factor set to 3.8, another step response is shown in Figure 3.2.5-5. Here, the initial null position is at 400, which is half way between the pixel center and the edge of the pixel. The oscillations which occur during the first ten seconds of the response show that the system is very sensitive to pixel non-linearities.

It is difficult to tell exactly how each of the sources of coupling affect the closed loop system. One way to eliminate coupling due to telescope magnification error would be to have a telescope built very precisely with a known magnification factor. In a full scale system as described in Section 1.3, building such a precision telescope would be both feasible and necessary, but it is beyond both the scope and the budget of this thesis. In order to eliminate coupling due to sensor non-

linearities, the sensor could be linearized with a lookup table to the precision of the centroiding algorithm. However, this is also beyond the scope of this thesis.

3.2.6 Disturbance Rejection

Section 3.2 has presented five experiments to characterize the control system. The first three experiments characterized the bandwidths of the three individual loops, verifying the design process. Ideally, the first three experiments would have been enough to confirm the entire control system design, because the three loops are nominally decoupled. In Chapter 2, though, possible sources of loop cross-coupling were discussed, and it became necessary to check the stability of the entire closed loop system. By running experiments which kept the spots nulled at the center of pixels, it was determined that the system is indeed stable. However, when step responses were run, it was shown that the system exhibits some loop cross coupling which reduces the relative stability of the system. The step responses also showed that the system is very sensitive to sensor non-linearities and to errors in the telescope magnification factor used in the controller.

There is one experiment which is conspicuous in its absence from Section 3.2. That is, the disturbance rejection properties of the system should be characterized. Unfortunately, because of hardware constraints, this experiment cannot be performed in this thesis. In the interest of further research on this system, three ways in which this experiment may be performed are described below. It will be possible to perform these experiments only if the sensor is linearized and if the appropriate hardware is available.

The easiest way to simulate actual disturbances to the telescope/sensor platform assembly is to place the entire assembly on a

rotating table. Rotating the table through small angles with the control system turned off would allow the MATE sensor to measure the input disturbances. With the controller turned on, the motion of the target spot could be measured to allow the disturbance rejection characteristics of the system to be measured. This experiment was not run because a rotating table was not available for use with this thesis.

A second way to characterize the disturbance rejection properties of the system would be to disconnect the telescope loop, and drive the telescope with a disturbance signal. Since the TCA is supposed to compensate for disturbances independent of the telescope loop, this should be a satisfactory way to measure the disturbance rejection properties. Unfortunately, the sensor non-linearities limit the usefulness of this experiment. Because only two loops are closed, only two degrees of freedom exist to attempt to align the three spots on pixel centers. The two degrees of freedom will allow at most two of the spots to be held at pixel centers, and in actuality, only one spot will be moved to its null position. The sensor non-linearities then cause the two closed loops to couple, and system oscillations occur. This experiment might be made to work if the sensor is linearized.

A third way to see how well the system can reject disturbances is to simulate a step disturbance, similar to the way a step in target position was simulated in Section 3.2.5. If the null position of the target were changed by N pixels, and the null position of the pseudo star spot were changed by 2N/M pixels, where M is the magnification factor of the telescope, then this would appear to the system as a disturbance on the telescope of $-Ng_s/M$ radians. The problem with this experiment is once again the sensor non-linearities. Because 2N/M is not an integer when N is an integer less than 10M, which would cause the spots to move off of the sensor, these two spots cannot be simultaneously nulled at the center of pixels. Although if N is 2 pixels, the pseudo star spot would be centered fairly close to the center of a pixel and the reference spot would be moving over a range of two pixels, allowing sensor non-linearities to severely affect the disturbance rejection properties of the

system.

The overriding problem with attempting to measure the disturbance rejection capability of the system is with the sensor. If the system is close to its design capability, it should be able to attenuate disturbances by about 20 dB at 3 Hz. This means that in order to see a disturbance on the target spot with a peak amplitude of 3 LSBs with the controller turned on, the reference spot will be driven from one pixel boundary to another. Because the sensor is very non-linear at pixel boundaries, it is doubtful that the sensor would allow the disturbance rejection properties to be measured anywhere near the designed values. Before serious study of the disturbance rejection properties of this system can begin, the sensor must be linearized.

3.3 CONCLUSIONS

In this chapter the control system for SATE was tested in the laboratory. The results of the experiments showed that each of the individual loops worked almost exactly as was predicted in Chapter 2. When all three loops were closed at once, a minimum tracking error of ±2 LSBs, which corresponds with ±7 μrad of target position uncertainty, was recorded. The response of the system to a step in target position showed that there is some cross coupling between the loops in the system, which degrades the stability of the system.

With the exception of the loop cross coupling, the laboratory system worked very well. Operation with a linearized sensor to try to eliminate the cross coupling would be an immediate goal for future research.

CHAPTER 4
SUMMARY AND CONCLUSIONS

In this thesis, the problem of aligning a signal laser with a dim target was studied. The main focus of this thesis was the problem of tracking the target in the presence of vibrational disturbances on the sensor. Chapter 1 introduced the use of a pseudo star as an inertial reference, and the direct and indirect methods for projecting the pseudo star onto the sensor platform. The section describing the pseudo star showed the need for inertial reference to track the target line-of-sight so that the signal can be pointed ahead of the target. It also described the need for an inertial reference to detect sensor platform vibrations which could interfere with measurements of the target position. In addition, this section suggested two different ways in which the pseudo star could be implemented, namely with a laser on the IRU, or with a mirror on the IRU.

The indirect pseudo star projection method was described in the second section of Chapter 1. This method required an alignment laser to be mounted on the IRU so that a pseudo star beam could be directed into the front aperture of the tracking telescope via an extended corner cube. This allowed vibrations of the sensor platform to be sensed as position error of the pseudo star spot, and this error could be nulled out using the target control actuator. Two other spots, a second pseudo star and a signal beacon, were needed to allow the communication beam to be directed at the target satellite.

In the direct pseudo star projection method, which was described in the third section of Chapter 1, the pseudo star was implemented using a mirror on the IRU, and the alignment beam originated at a laser on the sensor platform. In this method, the sensor platform disturbances were

measured using the pseudo star, so that they could be subtracted from the target spot with the target control actuator. Three other spots, a spot to monitor secondary mirror motions, a spot to monitor TCA motions, and a signal beam, were needed to allow the communication beam to be directed at the target satellite.

After the full scale systems based on the two pseudo star projection methods were designed, one of the systems was chosen to be tested in the laboratory. The decision was based on which system could be best implemented in a full scale system. The indirect projection method suffered from two major problems. First, it required a laser to be mounted on the IRU, which may make the thermal design of the IRU unsolvable. Second, the aperture size mismatch between the pseudo star and the target spot caused the pseudo star to be 100 times larger than the target spot. The direct projection method also had two major problems. First, several unwanted spots reached the sensor, possibly interfering with the measurement of the other spots. The second problem was that the sensor platform disturbances were subtracted from the target spot rather than nulled, making the system more susceptible to sensor non-linearities than the indirect projection method. Because the problems with the direct projection method appeared more easily solved than the problems with the other method, the direct projection method was chosen to be implemented in the laboratory.

Chapter 2 began by scaling and simplifying the direct projection method tracker designed in Chapter 1. The system was simplified by removing the beacon spot and the secondary spot. The secondary spot was removed because the scaled system is small and not very accurate, so secondary mirror motions would not appreciably affect the system performance. The beacon spot was removed because it was argued that the pointing of the signal could be accomplished easily if the rest of the system could be made to work.

In the first section of Chapter 2, the scaled dynamics of the tracker were decoupled into three independent control loops using the appropriate choice of actuator pointing errors. This allowed the

controller to be designed using simple Bode techniques. In the second section of Chapter 2, control loops were designed around the three actuators, namely the telescope, the TCA, and the AIRU, using Bode techniques. The loops were to have large phase margins, and were to be made as simple as possible to allow the controller to run at high sampling rates. Because the sensor was determined to be very non-linear, sources of possible loop cross-coupling, including sensor non-linearities, were investigated. Finally, the controller was modified to be implemented using integer arithmetic.

Chapter 3 described the experimental portion of the thesis, in which the laboratory system was tested. Five experiments were run. The first three experiments tested each of the loops individually. Each loop had characteristics which were nearly identical to those expected from their design. That is, all of the loops were stable, exhibited at least 45° of phase margin, and had crossover frequencies almost exactly matching the designs. The fourth experiment closed all three loops together. Here a tracking error as low as ±7 μrad was recorded. The last experiment was the response of the system with three closed loops to a step change in target position. It was discovered that the loops did couple, resulting in lower relative stability of the system than was designed. The cross coupling was probably due to sensor non-linearities. Finally, this chapter suggested some additional experiments which should be performed to test the disturbance rejection properties of the system. These experiments require hardware which was not available for this thesis.

Further research is required to determine how well a full scale tracker using the direct projection method would work. The first step would be to perform the experiments suggested at the end of Chapter 3, to evaluate the disturbance rejection performance of the SATE system. Before the performance of the system could be improved much, however, the sensor must be linearized by using a lookup table or some equivalent means. The next step in improving the system would be to include vertical direction tracking. This would entail using two-degree-of-freedom actuators in place of each actuator in the SATE to allow the system to track targets

moving both vertically and horizontally. The spot position equations are very similar in the vertical direction to the horizontal direction, except that some of the signs change. Because all of the actuators can be made to decouple their vertical and horizontal motions, the control system for the vertical direction should be esily designed independently of the horizontal system. When a tracker which can track both vertically and horizontally is working, the beacon spot should be put back into the system. At this point, the system can be taken out of the laboratory and tested in the field.

Appendix A

CENTROID ERROR IN A DIM SPOT WITH A PERFECT SENSOR

It is interesting to see how large the error can be expected to be if an optical sensor is used to estimate the centroid of a dim spot. Aside from sensor noise, sensor fill factor and granularity, dark current noise, and round off errors, the accuracy to which the centroid of a spot on the sensor can be measured is limited by the number of photons which reach the sensor during a sampling interval.

To show the limitations of centroid calculations, it is first assumed that a gaussian spot of radius R (where the radius of the spot is defined to be the first standard deviation of the gaussian distribution) appears on the sensor centered at the origin of an x-y coordinate plane. That is, the i^{th} photon arrival will occur at the coordinates (x,y), and the center of the spot will be at (0,0). If the i^{th} photon arrival is expressed in polar coordinates, it arrives at (r_i,θ_i), where r_i has a zero mean gaussian distribution with variance R^2 and θ_i is evenly distributed over the range $[0,\pi)$ and is independent of r_i. The assumption that the radial distribution of the photon arrivals is gaussian is an approximation to the distribution of photon arrivals in the Airy disk of a focussed diffraction limited circular spot.

If the centroid of the spot is calculated after N statistically independent photon arrivals, the centroid will be

$$(x_{CN}, y_{CN}) = \left(\frac{\sum_{i=1}^{N} x_i}{N}, \frac{\sum_{i=1}^{N} y_i}{N} \right) \qquad \text{(A-1)}$$

where $x_i = r_i \cos \theta_i$

$y_i = r_i \sin \theta_i$

To get an idea of how far the calculated centroid would be from the center of the spot, it will be necessary to look at the RMS error.

To calculate this error the statistics for the coordinates of the centroid must be found.

$$\bar{x}_{CN} = E\left\{ \frac{\sum_{i=1}^{N} r_i \cos\theta_i}{N} \right\} = 0 \qquad \text{(A-2)}$$

$$\bar{y}_{CN} = E\left\{ \frac{\sum_{i=1}^{N} r_i \sin\theta_i}{N} \right\} = 0 \qquad \text{(A-3)}$$

$$\sigma^2_{x_{CN}} = E\left\{ \frac{\sum_{i=1}^{N}\sum_{i=1}^{N} r_i r_j \cos\theta_i \cos\theta_j}{N^2} \right\} - (\bar{x}_{CN})^2$$

$$= \frac{1}{N^2} \sum_{i=1}^{N}\sum_{i=1}^{N} E\{r_i r_j \cos\theta_i \cos\theta_j\} \qquad \text{(A-4)}$$

Because each arrival is independent of all other arrivals, the variance becomes

$$\sigma^2_{x_{CN}} = \frac{1}{N^2} \sum_{i=1}^{N} E\{r^2_i \cos^2\theta_i\} = \frac{1}{N} E\{r^2\cos^2\theta\} \qquad \text{(A-5)}$$

Similarly,

$$\sigma^2_{y_{CN}} = \frac{1}{N} E\{r^2\sin^2\theta\} \qquad \text{(A-6)}$$

The position of the centroid can be represented in vector form as

$$\underline{z}_{CN} = \begin{bmatrix} x_{CN} \\ y_{CN} \end{bmatrix}$$

So,

$$|\underline{z}_{CN}|^2 = [x_{CN} \;\; y_{CN}] \begin{bmatrix} x_{CN} \\ y_{CN} \end{bmatrix} = x^2_{CN} + y^2_{CN}$$

This means that the root mean squared error is

$$z_{RMS} = (\sigma^2_{x_{CN}} + \sigma^2_{y_{CN}})^{1/2} \qquad \text{(A-7)}$$

because x_{CN} and y_{CN} are uncorrelated and zero mean. By substituting (A-5) and (A-6) into (A-7), the RMS error can be calculated.

$$z_{RMS} = \frac{1}{\sqrt{N}} (E\{r^2\cos^2\theta\})^{1/2} + \frac{1}{\sqrt{N}} (E\{r^2\sin^2\theta\})^{1/2}$$

$$= \frac{1}{\sqrt{N}} E\{(r^2)^{1/2}\} = \frac{R}{\sqrt{N}} \qquad \text{(A-8)}$$

because the radial distribution is zero mean.

Appendix B

OBTAINING DESIRED OUTPUTS WITHOUT MEASURING THE DISTURBANCE

The statement was made in Section 1.3 that it is desirable to get the desired output vector $\underline{y}_D$ directly from the physical outputs, without explicitly measuring the disturbance vector $\underline{\theta}_D$. The reason for this is that the controller which will control the actuators in the system will get all of its information from the sensor. If the controller is to calculate the desired outputs, this calculation must require only the physical outputs.

In Section 1.3 it was stated that in order for the desired outputs to be calculated from the physical outputs, the relationship

$$C_2 C_1^{-1} L_1 = L_2$$

where

$$C_1 = \begin{bmatrix} -M & 0 & 2 & 2 & 0 \\ -2 & 2 & 0 & 0 & 0 \\ 0 & 0 & 2 & 0 & 0 \\ 0 & 0 & 0 & 2 & 0 \\ 0 & 0 & 0 & 0 & 2 \end{bmatrix}$$

$$L_1 = \begin{bmatrix} -M & M \\ -2 & 0 \\ 0 & 0 \\ 0 & 0 \\ 0 & 0 \end{bmatrix}$$

and C_2 and L_2 are as given in Equation (1.3.2-7), must be true for all $M \neq 0$. The inverse of C_1 is

Appendix B: Obtaining Desired Outputs Without Measuring the Disturbance

$$C_1^{-1} = \begin{bmatrix} \frac{-1}{M} & 0 & \frac{1}{M} & \frac{1}{M} & 0 \\ \frac{-1}{M} & \frac{1}{2} & \frac{1}{M} & \frac{1}{M} & 0 \\ 0 & 0 & \frac{1}{2} & 0 & 0 \\ 0 & 0 & 0 & \frac{1}{2} & 0 \\ 0 & 0 & 0 & 0 & \frac{1}{2} \end{bmatrix}$$

which can be verified by multiplication. So,

$$C_2C_1^{-1} = \begin{bmatrix} 1 & 0 & -1 & -1 & 0 \\ 1 & \frac{-M}{2} & -1 & -1 & 0 \\ 0 & \frac{M}{2} & 1 & 1 & 0 \\ 0 & 0 & 0 & 1 & 0 \\ 0 & \frac{-1}{2} & 0 & 0 & 1 \end{bmatrix}$$

$$C_2C_1^{-1}L_1 = \begin{bmatrix} -M & M \\ 0 & M \\ -M & 0 \\ 0 & 0 \\ 1 & 0 \end{bmatrix} = L_2$$

Thus, $C_2C_1^{-1}L_1 = L_2$ for all $M \neq 0$.

Appendix C

ASSEMBLY CODE FOR THE CONTROLLER COMPUTER

The following two assembly language programs were used to run the experiments described in Chapter 3. The first program is used to determine which experiment is to be run. For example, it is now set up to run a step in target position. This is done by using two loops LOOP1 and LOOP2, each of which run for ten seconds, where the target spot null position is changed after the first loop is finished. In each loop, the routines GET_CENT and CONTROL are called. GET_CENT gets the centroids from global memory, where they were placed by the centroiding computer. Code for the centroiding computer is not included here. The code for CONTROL is listed following the SATE Control Loop. CONTROL is the actual implementation of the controller.

```
;                                   SATE CONTROL LOOP
;
;
;
;       This program will be the control loop for controlling the three
;actuators in SATE.  This will allow the loops to be controlled and
;centroids to be stored in memory.

        XREF    CONTROL,SEND_AIRU,SEND_TCA,SEND_TEL,PS_AVG,RS_AVG
        XDEF    RS_NULL,PS_NULL,TS_NULL


TDELAY  EQU     $50000  ;DELAY FOR SUPERDRIVE (LONGER FOR HARD DISK)

PBUFFER EQU     $40000  ; POINTS TO THE BEGINNING OF THE BUFFER IN RAM
ENDBUFF EQU     PBUFFER+1200    ; (BUFFER GOES FROM $40000 TO $7FFFE)
CBUFFER EQU     $60000

STRBHI  EQU     $3C             ;VALUE WHICH SETS DATA STROBE HIGH
STRBLO  EQU     $34             ;VALUE WHICH SETS DATA STROBE LOW

PORTA   EQU     $FE6041         ;PARALLEL PORT A DATA ADDRESS
PSTATA  EQU     $FE6043         ;ADDRESS OF DATA STROBE

TCA_DAC0 EQU    $FE6201         ;DAC CHANNEL 1 LOW ORDER 8 BITS
TCA_DAC1 EQU    $FE6203         ;DAC CHANNEL 1 HIGH ORDER 4 BITS
AIRU_DAC0 EQU   $FE6205         ;DAC CHANNEL 2 LOW ORDER 8 BITS
AIRU_DAC1 EQU   $FE6207         ;DAC CHANNEL 2 HIGH ORDER 4 BITS

AV_CENTS EQU    109             ;NUMBER OF FAST SAMPLING INTERVALS IN
                                ;  A SINGLE SLOW SAMPLING INTERVAL

GLOBAL_COM EQU  $7FFFE          ; Start of Communication Space

RS_NULL1 EQU    $460            ;$460 IS CENTERED IN 17TH PIXEL
PS_NULL1 EQU    $5A0            ;$5A0 IS CENTERED IN 22ND PIXEL
TS_NULL1 EQU    $190            ;$1A0 IS CENTERED IN 6TH PIXEL
TS_NULL2 EQU    $1A0            ;$1A0 IS CENTERED IN 6TH PIXEL



        ORG $F80
RS_NULL: DC.W   1120            ;RS_NULL POSITION ON SENSOR = 1120 = $460
PS_NULL: DC.W   1440            ;PS_NULL POSITION ON SENSOR = 1440 = $5A0
```

```
TS_NULL: DC.W   416             ;TS_NULL POSITION ON SENSOR =  416 = $1A0

        ORG $1020


        LEA     PBUFFER,A3      ;A3 POINTS INTO MEMORY
        LEA     CBUFFER,A2      ;A2 POINTS INTO MEMORY

        LEA     STMSG,A5        ;PRINT A MESSAGE TO THE WORLD
        LEA     ESTMSG,A6
        TRAP    #15
        DC.W    2

        MOVE.L  A3,A5           ;WAIT FOR A CARRIAGE RETURN
        MOVE.L  A5,A6
        TRAP    #15
        DC.W    1

        LEA     RSMSG,A5        ;PRINT REFERENCE SPOT LOCATIONS
        LEA     ERSMSG,A6
        TRAP    #15
        DC.W    2

        CLR.L   D0
        CLR.L   D1
        CLR.L   D2
        CLR.L   D3              ;INIT COUNTER AND SUMMATION REGISTERS
CLR_REGS:
        CLR.L   D4
        CLR.L   D5
        CLR.L   D6
        CLR.L   D7

        CLR.L   PS_AVG
        CLR.L   RS_AVG

RS_PS_INIT:
        MOVE.W  #256,D7
RS_LOOP:
        BSR     GET_CENT
        ADD.L   D1,D4           ; ACCUMULATE REFERENCE SPOT
        ADD.L   D2,D5           ; ACCUMULATE PSEUDO-STAR SPOT
        SUBQ.W  #1,D7
        BGT     RS_LOOP

        ASR.L   #8,D4           ; AVERAGE REFERENCE SPOT
        ASR.L   #8,D5           ; AVERAGE PSEUDO-STAR SPOT
```

```
        LEA     PRNBUF,A4
        MOVE.L  A4,A5

        MOVE.W  D4,D1
        JSR     D1_PRT
        MOVE.W  D5,D1
        JSR     D1_PRT
        MOVE.W  D3,D1
        JSR     D1_PRT

        MOVE.L  A4,A6
        TRAP    #15
        DC.W    2               ; PRINT STARTING VALUES


PORT_INIT:
        MOVE.B  #$38,PSTATA     ;POINT AT DDRA
        MOVE.B  #$FF,PORTA      ;DDRA SETS PERPH DATA A OUTPUTS
        MOVE.B  #STRBHI,PSTATA  ;SETS DATA STROBE HIGH

INITDAC:
        MOVE.B  #0,TCA_DAC0     ;INITIAL TCA DAC = 0
        MOVE.B  #$08,TCA_DAC1
        MOVE.B  #0,AIRU_DAC0    ;INIITAL AIRU DAC = 0
        MOVE.B  #$08,AIRU_DAC1



        CLR.L   D0
        CLR.L   D1
        CLR.L   D2
        CLR.L   D3              ;INIT COUNTER AND SUMMATION REGISTERS
        CLR.L   D4
        CLR.L   D5
        CLR.L   D6
        CLR.L   D7

        LEA GLOBAL_COM,A6
        MOVE.W  #$00,(a6)       ;RESET DATA READY STROBE TO $00


        MOVE.W  #TS_NULL1,TS_NULL
LOOP1:
        BSR     GET_CENT

        SUB.W   RS_NULL,D1      ;SUBTRACT NULL FROM MEASURED RS POSIT
        SUB.W   PS_NULL,D2      ;SUBTRACT NULL FROM MEASURED PS POSIT
        SUB.W   TS_NULL,D3      ;SUBTRACT NULL FROM MEASURED TS POSIT
```

```
        BSR     CONTROL

        CMPI.W  #3,D0
        BLT     LOOP1

        ADDI.L  #$01,D7         ;INCREMENT COUNTER
        CMPI.L  #100,D7
        BNE     LOOP1



        CLR.L   D7
        MOVE.W  #TS_NULL2,TS_NULL

LOOP2:
        BSR     GET_CENT

        SUB.W   RS_NULL,D1      ;SUBTRACT NULL FROM MEASURED RS POSIT
        SUB.W   PS_NULL,D2      ;SUBTRACT NULL FROM MEASURED PS POSIT
        SUB.W   TS_NULL,D3      ;SUBTRACT NULL FROM MEASURED TS POSIT

        BSR     CONTROL

        CMPI.W  #3,D0
        BLT     LOOP2

        ADDI.L  #$01,D7         ;INCREMENT COUNTER
        CMPI.L  #100,D7
        BNE     LOOP2



        CLR.L   D3              ;CLEAR CONTROL OUTPUTS
        BSR     SEND_TEL
        MOVE.B  #0,TCA_DAC0     ;INITIAL TCA DAC = 0
        MOVE.B  #$08,TCA_DAC1

        MOVE.B  #0,AIRU_DAC0    ;INIITAL AIRU DAC = 0
        MOVE.B  #$08,AIRU_DAC1

        JMP     DUMP


GET_CENT:
                                ; DESTROYS REGISTERS D0,D6 A6
                                ; RETURNS CENTROID IN REGS D1, D2, AND D3
```

```
        LEA GLOBAL_COM,A6
        CLR.L   D1
        CLR.L   D2
        CLR.L   D3

WAIT:
        TST.W (A6)
        BEQ WAIT

        MOVE.W  (A6),D0         ;Move the no of centroids available to D0
        MOVE.W  #$00,(a6)       ;RESET DATA STROBE

        MOVE.W #10,d6
DELAY:
        SUBQ.W #1,d6
        BGT DELAY

        MOVE.W  -(a6),D6        ; GET SPOT CENTROID #1 (y)
        MOVE.W  -(A6),D2        ; (x)

        MOVE.W  -(a6),D6        ; GET SPOT CENTROID #2  (y)
        MOVE.W  -(A6),D1        ; (x)

        MOVE.W  -(a6),D6        ; GET SPOT CENTROID #3  (y)
        MOVE.W  -(A6),D3        ; (x)

        RTS


;
; DUMP SENDS THE DATA STORED IN THE BUFFER TO THE P.C.
; (THE FILE SPECIFIED IN THE VTERM SETUP SHOULD BE IN THE RAM DISK TO MAKE
; THIS GO FASTER)
;
DUMP:   LEA     PBUFFER,A3
        LEA     CBUFFER,A2
        LEA     PRNBUF,A4

        LEA     TRMSG,A5        ;TELL THE WORLD WE'RE READY
        LEA     ETRMSG,A6
        TRAP    #15
        DC.W    2

        MOVE.L  A4,A5           ;WAIT FOR A CARRIAGE RETURN
        MOVE.L  A4,A6
        TRAP    #15
        DC.W    1

DLOOP:  LEA     PRNBUF,A4
```

```
        MOVE.L  A4,A5
        JSR     STXY
        JSR     STXY
        JSR     STXY
        JSR     STXY
        JSR     STXY
        JSR     STXY
        JSR     STXY
        JSR     STXY            ; 8 PAIRS OF CENTROIDS
        MOVE.L  A4,A6
        TRAP    #15
        DC.W    2               ; PRINT A LINE

        CMPA.L  #ENDBUFF,A3
        BGT     QUIT

        move.l  #TDELAY,D0      ; WAIT FOR PC DISK DRIVE TO CATCH UP

DWAIT:  sub.l   #1,D0
        bge     DWAIT
        jmp     DLOOP

QUIT:   LEA     DMSG,A5
        LEA     EDMSG,A6
        TRAP    #15
        DC.W    2

        TRAP    #15
        DC.W    0

;
; STXY IS A SUBROUTINE THAT STORES AN X AND Y CENTROID IN MEMORY AT (A4)+

STXY:   JSR     XCENT
        MOVE.B  #' ',(A4)+      ;STORE A SINGLE SPACE BETWEEN XY ENTRIES
;       JSR     YCENT
;       MOVE.B  #' ',(A4)+
        MOVE.B  #' ',(A4)+      ;STORE TWO SPACES AT THE END
        RTS
;
;CENT IS A SUBROUTINE THAT STORES A CENTROID (GIVEN IN (A3)+) IN MEMORY AT
;  (A4)+ IN THE FORM OF A 3 DIGIT ASCII STRING.

XCENT:  MOVE.W  (A3)+,D1
D1_PRT: BGE     NO_SIGN_CH
        MOVE.B  #'-',(A4)+
        NEG.W   D1
        BRA     SKIP
NO_SIGN_CH:
```

```
        MOVE.B  #' ',(A4)+
SKIP:   move.W  D1,D0
        lsr.W   #8,D0
        JSR     LTR
        MOVE.W  D1,D0
        LSR.B   #4,D0
        JSR     LTR
        MOVE.W  D1,D0
        ANDI.B  #$0F,D0
        JSR     LTR
        RTS

YCENT:  MOVE.W  (A2)+,D1
        move.W  D1,D0
        lsr.W   #8,D0
        JSR     LTR
        MOVE.W  D1,D0
        LSR.B   #4,D0
        JSR     LTR
        MOVE.W  D1,D0
        ANDI.B  #$0F,D0
        JSR     LTR
        RTS

;
;LTR IS A SUBROUTINE THAT TURNS THE LOW ORDER 4 BITS OF DATA IN D0 TO HEX
;AND STORES IT IN (A4)+

LTR:    cmpi.b  #$0A,D0
        bge     LETR1
        addi.b  #$30,D0                 ; makes hex digits
        jmp     STCH1
LETR1:  addi.b  #$37,D0                 ; makes hex letters
STCH1:  move.b  D0,(A4)+                ; stores the first hex digit
        RTS


; HERE LIE THE VARIOUS MESSAGES THAT GET PRINTED OUT TO MAKE THINGS
; LOOK NICE
;
STMSG:  DC.B    'PRESS CARRIAGE RETURN TO BEGIN STORAGE OF CENTROIDS '
ESTMSG: DC.B    ' '

TRMSG:  DC.B    'READY TO TRANSFER DATA TO PC (HIT CARRIAGE RETURN)'
ETRMSG: DC.b    ' '

RSMSG:  DC.B    ' REFERENCE SPOT, PSEUDO-STAR SPOT, TARGET SPOT
CENTROIDS:'
ERSMSG: DC.B    ' '
```

```
DMSG:   DC.B    'STOP',$0D,$0A,'TRANSFER TO PC COMPLETE'
EDMSG:  DC.B    ' '

PRNBUF: DS.B    120                     ;TEMPORARY PRINT BUFFER

        END
```

```
;                               CONTROL
;
;
;       This program will be called as a subroutine by programs which want
;to control the Telescope, TCA, and AIRU actuators in the Scaled Alignment
;Transfer Experiment.  This routine will expect four arguments in
;registers D0-D3.  These arguments will be:  the number of arguments which
;are valid, (the Target Spot position will not be valid every time CONTROL
;is called) the RS error from its null position, PS error from null, and
;the TS position from null.


        XDEF    CONTROL,SEND_AIRU,SEND_TCA,SEND_TEL,PS_AVG,RS_AVG
        XREF    RS_NULL,PS_NULL,TS_NULL

STRBHI          EQU     $3C             ;VALUE WHICH SETS DATA STROBE HIGH
STRBLO          EQU     $34             ;VALUE WHICH SETS DATA STROBE LOW

PORTA           EQU     $FE6041         ;PARALLEL PORT A DATA ADDRESS
PSTATA          EQU     $FE6043         ;ADDRESS OF DATA STROBE

TCA_DAC0        EQU     $FE6201 ;DAC CHANNEL 1 LOW ORDER 8 BITS
TCA_DAC1        EQU     $FE6203 ;DAC CHANNEL 1 HIGH ORDER 4 BITS
AIRU_DAC0       EQU     $FE6205 ;DAC CHANNEL 2 LOW ORDER 8 BITS
AIRU_DAC1       EQU     $FE6207 ;DAC CHANNEL 2 HIGH ORDER 4 BITS

AV_CENTS        EQU     109             ;NUMBER OF FAST SAMPLING INTERVALS
                                        ;IN A SINGLE SLOW SAMPLING
INTERVAL
;TEL_MAG        EQU     3.8             ;TELESCOPE MAGNIFICATION FACTOR
TEL_GAIN        EQU     10              ;FIRST (ONLY) GAIN IN TELESCOPE
                                        ;COMPENSATION = 10
```

```
AIRU_GAIN1      EQU     19              ;FIRST AIRU GAIN IN COMPENSATION
                                        ;  IS 10*M/2 = 19
AIRU_GAIN2      EQU     2               ;SECOND AIRU GAIN IN COMPENSATION
                                        ;  IS 2*AIRU_COMP_GAIN/100, WHERE
                                        ;  THE FACTOR OF TWO WILL BE
                                        ;  DIVIDED OUT IN THE DAC GAIN,
                                        ;  AND A FACTOR OF 10 WILL BE
                                        ;  MULTIPLIED BY THE AIRU
                                        ;  ACTUATOR AMPLIFIER
TCA_GAIN1       EQU     10              ;FIRST GAIN IN TCA COMP = 10
TCA_GAIN2       EQU     8               ;SECOND GAIN IN TCA COMP IS
                                        ;  TCA_COMP_GAIN/1000, WHERE A
                                        ;  FACTOR OF 100 WILL BE
                                        ;  MULTIPLIED BACK BY
                                        ;  THE TCA AMPLIFIER

TEL_POS_BND     EQU     $0080           ;POSITIVE TELESCOPE CONTROL BOUND
                                        ;  IS $80
TEL_NEG_BND     EQU     $FFFFFF80       ;NEGATIVE TEL CONTROL BOUND=$FF80
AIRU_POS_BND    EQU     $0FFF
AIRU_NEG_BND    EQU     $0000

TCA_POS_BND     EQU     $07FF
TCA_NEG_BND     EQU     $0000


        ORG     $F00

PS_AVG: DC.L    $0
RS_AVG: DC.L    $0


        ORG     $1500


CONTROL:                        ; TS is in D3, PS in D2, and RS in D1
                                ; # of centroids available is in D0
                                ; D4 and D6 are temporary registers


        EXT.L   D1
        EXT.L   D2
        EXT.L   D3


TCA_CALC:
        MULS    #AIRU_GAIN1,D2  ; MULTIPLY PS BY FIRST_AIRU_GAIN
        MULS    #TCA_GAIN1,D1   ; MULTIPLY RS BY FIRST_TCA_GAIN
        ADD.L   D1,RS_AVG       ; ACCUMULATE RS MEASUREMENTS
```

```
        ADD.L   D2,PS_AVG       ; ACCUMULATE PS MEASUREMENTS

        ADD.L   D2,D1           ; ADD PS TO RS
        ASL.W   #3,D1           ; MULTIPLY BY SECOND_TCA_GAIN
        NEG.W   D1
        BSR     TCA_CONTROL     ; SEND TCA CONTROL

        CMPI.W  #3,D0           ; IF < 3 CENTROIDS AVALABLE, THEN DONE
        BLT     CONTROL_DONE


SLOW_CALCS:

        MOVE.W  D3,D4
        ADD.W   TS_NULL,D4
        MOVE.W  D4,(A3)+        ;STORE X COORD OF TS CENTROID IN PBUFFER

        MULS    #TEL_GAIN,D3    ; MULTIPLY TS BY TELESCOPE GAIN

        MOVE.L  PS_AVG,D2       ; CALCULATE PS AVERAGE
        DIVS    #AV_CENTS,D2


        MOVE.W  D2,D4
        EXT.L   D4
        DIVS    #AIRU_GAIN1,D4  ; DIVIDE PS AVERAGE BY FIRST_AIRU_GAIN
                                ;   BACK TO SENSOR COORDINATES FOR STORAGE
        ADD.W   PS_NULL,D4
        MOVE.W  D4,(A3)+        ;STORE X COORD OF PS AVERAGE IN PBUFFER


        MOVE.L  RS_AVG,D4       ; CALCULATE RS AVERAGE
        DIVS    #AV_CENTS,D4

        MOVE.W  D4,D1
        EXT.L   D1
        DIVS    #TCA_GAIN1,D1   ; DIVIDE RS AVERAGE BY FIRST_TCA_GAIN BACK
                                ;   TO SENSOR COORDINATES FOR STORAGE
        ADD.W   RS_NULL,D1
        MOVE.W  D1,(A3)+        ;STORE X COORD OF RS AVERAGE IN PBUFFER



        ADD.W   D4,D2
        SUB.W   D3,D2
        NEG.W   D2
        MULS    #AIRU_GAIN2,D2  ;MULTIPLY BY SECOND AIRU_GAIN

        SUB.W   D4,D3
```

```
        BSR     AIRU_CONTROL    ;SEND AIRU CONTROL
        BSR     TEL_CONTROL     ;SEND TELESCOPE CONTROL

        CLR.L   PS_AVG          ;CLEAR PS AVERAGE ACCUMULATOR
        CLR.L   RS_AVG          ;CLEAR RS AVERAGE ACCUMULATOR


CONTROL_DONE:
        RTS



; LIMIT TELESCOPE CONTROL SIGNAL, AND THEN SEND THE CONTROL TO THE UNIDEX

TEL_CONTROL:

        CMPI    #TEL_POS_BND,D3 ;CHECK FOR CONTROL PAST UPPER LIMIT
        BLE     TEL_NEG_CHK
        MOVE.L  #TEL_POS_BND,D3 ; LIMIT CONTROL IF PAST UPPER LIMIT
        JMP     SEND_TEL

TEL_NEG_CHK:
        CMPI.W  #TEL_NEG_BND,D3 ;CHECK FOR CONTROL PAST LOWER LIMIT
        BGE     SEND_TEL
        MOVE.L  #TEL_NEG_BND,D3 ; LIMIT CONTROL IF PAST LOWER LIMIT


SEND_TEL:                       ;SEND A WORD TO UNIDEX CONTROLLER
CONTROLLER
                                ;EXPECTS DATA IN REGISTER D3,
                                ;DESTROYS D4,D5

        MOVE.W  D3,(A2)+        ;STORE TELESCOPE CONTROL IN CBUFFER

        MOVE.W  D3,D4
        MOVE.W  D3,D5
        LSR.W   #8,D4

        MOVE.B  D4,PORTA        ;SEND MSB OF CONTROL TO PORT A BYTE 1
        MOVE.B  #STRBLO,PSTATA  ;MAKE DATA STROBE GO LOW
        MOVE.B  #STRBHI,PSTATA  ;MAKE DATA STROBE GO HIGH


        MOVE.B  D5,PORTA        ;SEND LSB OF CONTROL TO PORT A BYTE 2
        MOVE.B  #STRBLO,PSTATA  ;MAKE DATA STROBE GO LOW
        MOVE.B  #STRBHI,PSTATA  ;MAKE DATA STROBE GO HIGH
```

```
        RTS


; LIMIT AIRU CONTROL SIGNAL, AND THEN SEND THE CONTROL TO AIRU ACTUATOR

AIRU_CONTROL:

        ADDI.L  #$800,D2
        CMPI    #AIRU_POS_BND,D2 ;CHECK FOR CONTROL PAST UPPER LIMIT
        BLE     AIRU_NEG_CHK
        MOVE.L  #AIRU_POS_BND,D2 ; LIMIT CONTROL IF PAST UPPER LIMIT
        JMP     SEND_AIRU
AIRU_NEG_CHK:
        CMPI.W  #AIRU_NEG_BND,D2 ;CHECK FOR CONTROL PAST LOWER LIMIT
        BGE     SEND_AIRU
        MOVE.L  #AIRU_NEG_BND,D2 ; LIMIT CONTROL IF PAST LOWER LIMIT


SEND_AIRU:                      ;SEND A WORD TO AIRU CHANNEL OF DAC
                                ;EXPECTS DATA IN REGISTER D2, DESTROYS D4

        MOVE.L  D2,D4
;       LSL.W   #1,D4           ; RESCALE OUTPUT FOR D/A
        MOVE.B  D4,AIRU_DAC0
        LSR.W   #8,D4
        MOVE.B  D4,AIRU_DAC1

        RTS


; LIMIT TCA CONTROL SIGNAL, AND THEN SEND THE CONTROL TO TCA ACTUATOR

TCA_CONTROL:

        ADDI.L  #$400,D1
        CMPI    #TCA_POS_BND,D1   ;CHECK FOR CONTROL PAST UPPER LIMIT
        BLE     TCA_NEG_CHK
        MOVE.L  #TCA_POS_BND,D1   ; LIMIT CONTROL IF PAST UPPER LIMIT
        JMP     SEND_TCA
TCA_NEG_CHK:
        CMPI.W  #TCA_NEG_BND,D1   ;CHECK FOR CONTROL PAST LOWER LIMIT
        BGE     SEND_TCA
        MOVE.L  #TCA_NEG_BND,D1 ; LIMIT CONTROL IF PAST LOWER LIMIT
```

```
SEND_TCA:                          ;SEND A WORD TO TCA CHANNEL OF DAC
                                   ;EXPECTS DATA IN REGISTER D1, DESTROYS D4


        MOVE.L  D1,D4
        LSL.W   #1,D4              ; RESCALE OUTPUT FOR D/A
        MOVE.B  D4,TCA_DAC0
        LSR.W   #8,D4
        MOVE.B  D4,TCA_DAC1

        RTS

    END
```

REFERENCES

[1] Johnson, Donald O., "Advanced Inertial Reference Unit Technology Development Plan", The Charles Stark Draper Laboratory, Cambridge, MA, July 1983 (internal document CSDL-R-1649).

[2] "A Proposal for Ground Based Laser / Space Segment (GBL/SS) Technology Development in Advanced Inertial Reference Unit and Integrated Control", The Charles Stark Draper Laboratory, Cambridge, MA, July 1985 (internal document, Proposal No. 5-828).

[3] Johnson, William M., "Mechanical/Optical Error Sources for TABTIP Concept", The Charles Stark Draper Laboratory, Cambridge, MA, May 14, 1986 (internal document, 15K/WMJ-86-1583 REV. 01).

[4] Kieft, J., and Andrews, L., "Completion of Unit Test of Mosaic Array Centroiding in Scaled OAM Demonstration", The Charles Stark Draper Laboratory, Cambridge, MA, March 3, 1983 (internal document, ASD-83-2089).

[5] Kwakernaak, Huibert, and Sivan, Raphael, Linear Optimal Control Systems, Wiley-Interscience, a division of John Wiley & Sons, Inc. NY, 1972.

[6] Zak, R., "Computer Simulation of MATE Sensor Non-linearities", The Charles Stark Draper Laboratory, Cambridge, MA, July 22, 1985, (internal document, 87-15G-243).

[7] Roberge, James K., Operational Amplifiers: Theory and Practice, John Wiley & Sons, Inc., NY, 1975.

[8] Athans, Michael, Massachusetts Institute of Technology, Course notes for 6.233: Multivariable Control Theory I, November 7, 1985.

[9] Ogata, Katsuhiko, Discrete-Time Control Systems, Prentice-Hall, Inc., Englewood Cliffs, New Jersey, 1987.

[10] "Notes On Sampled Data Systems", Massachusetts Institute of Technology, Supplementary course notes for 6.302: Feedback Systems, 1986.

[11] Zak, R., "MATE Design Documentation", The Charles Stark Draper Laboratory, Cambridge, MA, July 3, 1985, (internal document, ASD-85-2303).